

UNIVERSITY OF OSLO
Department of Chemistry

**Thin films of multiferroic
BiCoO₃ by ALD**

Thesis for the Master of
Science degree in
Materials, Energy and
Nanotechnology

Knut Bjarne Gandrud

October 2009



Preface

This thesis concludes the work for the Master of Science degree in Nanotechnology under the program for Materials, Energy and Nanotechnology at the Department of Chemistry, University of Oslo. The experimental work was conducted at section B at the Chemistry Department in the time period from August 2007 to October 2009.

This thesis was written with the assumption that the reader has the equivalent of a bachelor degree in material science. The work carried out on the bismuth precursors and depositions of bismuth oxide was done in collaboration with Erik Østreng [1].

First I would like to thank my supervisors first amanuensis Ola Nilsen and professor Helmer Fjellvåg for challenges, guidance and giving me the opportunity to work on this project. I would also like to thank Oddvar Dyrli for teaching me how to operate the AFM, and Mohammed A. K. Ahmed for useful tips regarding precursor synthesis.

In addition, I would like to thank the people in the thin film group, Karina B. Klepper, Madeleine Diskus, Titta Aaltonen, Heidi Østbye Nilsen, Mari Endresen Alnes, and also Thomas Levy for the much needed climbing sessions.

I specially want to thank Kristoffer R. Haug, Erik Østreng, Jon E. Bratvold and Per-Anders Hansen for two enjoyable years in the office and the many, both relevant and not so relevant, discussions.

Finally, I would like to express my gratitude to my family for their never-ending support. Without them I most likely never would have found the strength to finish this work, as my father had to give up on a yearlong struggle against brain cancer in December 2007.

University of Oslo, September 09

Knut Bjarne Gandrud

Abstract

This work presents the first reported thin film deposition of α - Bi_2O_3 by ALD (Atomic Layer Deposition). In addition, thin films of Co_3O_4 and CoO are for the first time reported deposited by ALD from the respective novel precursor combinations $\text{Co}(\text{thd})_3/\text{O}_3$ and $\text{Co}(\text{thd})_2/\text{H}_2\text{O}$ ($\text{thd} = 2,2,6,6$ -tetramethyl-3,5-heptanedionate). Finally, BiPh_3 ($\text{Ph} = \text{phenyl}$), $\text{Bi}(\text{t-OBu})_3$ ($\text{t-OBu} = \text{tert-butoxide}$) and $\text{Bi}(\text{thd})_3$ were all investigated for potential use as bismuth precursors in the ALD process.

Thin films of Co_3O_4 deposited from the novel precursor combination $\text{Co}(\text{thd})_3/\text{O}_3$ was investigated and a comparison to the already well investigated precursor combination $\text{Co}(\text{thd})_2/\text{O}_3$ is given.

It was found that BiPh_3 can be used as a bismuth precursor for deposition in the Bi-Co-O system by ALD, although the concentration of bismuth, with respect to the metal content, was limited to a maximum of 22.8 at.%. $\text{Bi}(\text{t-OBu})_3$ was synthesized and investigated for the potential use as an ALD precursor, however, it was found that this compound has too low thermal stability to be applicable in the ALD processes.

$\text{Bi}(\text{thd})_3$ was synthesized and investigated for use as precursor in the ALD process. It was found that uniform films of α - Bi_2O_3 could be deposited from the $\text{Bi}(\text{thd})_3/\text{H}_2\text{O}$ precursor combination, however, in-situ QCM measurements indicated a non-ideal ALD growth behavior. It is suggested that a surface controlled reaction occurs between $\text{Bi}(\text{thd})_3 \cdot n(\text{H}_2\text{O})$ and its own crystal water. In addition, a suggestion for a new and yet unreported phase of $\text{Bi}(\text{thd})_3$ is given.

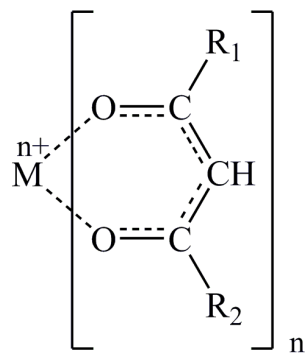
Deposition and investigation of thin films in the Bi-Co-O system are also presented. However, an etching process was observed between the $\text{Bi}(\text{thd})_3$ precursors and the Co_3O_4 surface. A possible mechanism is presented. Thin films of composition near 50:50 at.% of Bi and Co has been obtained. Mild heat-treatment under oxygen atmosphere resulted in the formation of multiple phases such as Co_3O_4 and a sillenite phase, with the proposed composition $\text{Bi}_{3.43}\text{Co}_{0.57}\text{O}_{5.90}$.

Abbreviations

| | |
|---------|--|
| ALD | Atomic Layer Deposition |
| ALCVD | Atomic Layer Chemical Vapor Deposition |
| ALE | Atomic Layer Epitaxy |
| CVD | Chemical Vapor Deposition |
| XRD | X-ray Diffraction |
| GIXRD | Grazing Incidence X-ray Diffraction |
| XRR | X-ray Reflectometry |
| In-situ | Lat. <i>in the place</i> , the experiment is carried out while deposition occurs |
| AFM | Atomic Force Microscopy |
| RMS | Root Mean Square |
| FT-IR | Fourier Transform Infrared Spectroscopy |
| MS | Mass Spectrometry |
| TGA | Thermogravimetric Analysis |

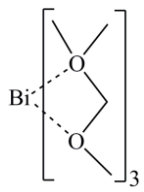
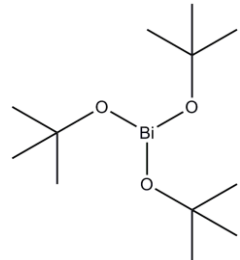
List of precursors

β -diketonato complexes

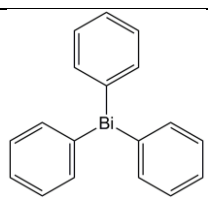
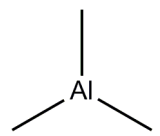
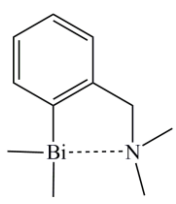


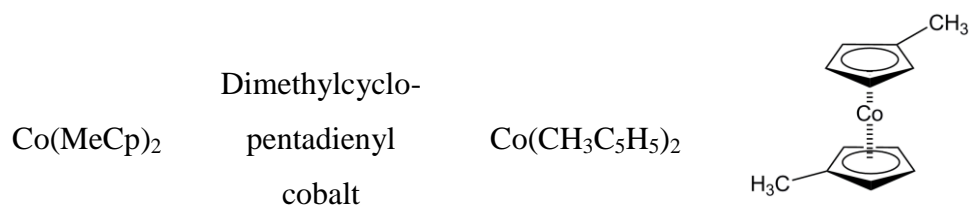
| Abbreviation | Name | R_1 | R_2 |
|---------------------------------|--|-------------|-------------|
| acac | Pentane-2,4-dionate (acetylacetonate) | CH_3 | CH_3 |
| tfac | 1,1,1-trifluoropentane-2,4- dionate (trifluoroacetylacetonate) | CH_3 | CF_3 |
| hfac | 1,1,1,5,5,5-hexafluoropentane- 2,4-dionate (hexafluoroacetylacetonate) | CF_3 | CF_3 |
| thd (also called dpm) | 2,2,6,6-tetramethylheptane-3,5- dionate (dipivaloylmethanate) | $C(CH_3)_3$ | $C(CH_3)_3$ |

Alkoxides [M-(OR)_x]

| Abbreviation | Name | Chemical formula | Structure |
|------------------------|---|---|--|
| Bi(mmp) ₃ | tris(1-methoxy-2-methyl-2-propoxy)bismuth | Bi(O ₂ C ₅ H ₁₁) ₃ |  |
| Bi(t-OBu) ₃ | bismuth tert-butoxide | Bi(OC ₄ H ₉) ₃ |  |

Organometallic [M-(R)_x]

| Abbreviation | Name | Chemical formula | Structure |
|-------------------------|---|--|--|
| BiPh ₃ | triphenyl bismuth | Bi(C ₆ H ₅) ₃ |  |
| TMA | Trimethyl aluminium | Al(CH ₃) ₃ |  |
| BiMe ₂ (dmp) | dimethyl(2-N,N-dimethylamino methylphenyl)bismuth | Bi[(CH ₃) ₂ -(2-(CH ₃) ₂ NCH ₂ C ₆ H ₄)] |  |



Amines

| Abbreviation | Name | Chemical formula | Structure |
|--------------------------------------|--|--|-----------|
| $\text{Co}(\text{}^i\text{PrAMD})_2$ | bis(<i>N,N'</i> - diisopropyl- acetamidinato) cobalt(II) | $\text{Co}(\text{CN}_2(\text{C}_3\text{H}_7)_2)_2$ | |

Contents

| | | |
|-------|--|----|
| 1 | Background..... | 1 |
| 1.1 | Aim, motivation and approach..... | 1 |
| 1.2 | Prior art | 2 |
| 1.2.1 | Bulk studies of the Bi-Co-O system | 2 |
| 1.2.2 | Thin films | 8 |
| 1.2.3 | Physical properties of BiCoO ₃ | 14 |
| 1.3 | Multiferroics: Magnetic and electric properties..... | 15 |
| 1.3.1 | Magnetism | 15 |
| 1.3.2 | Ferroelectrics | 20 |
| 1.3.3 | Multiferroics | 23 |
| 2 | Methods | 29 |
| 2.1 | Synthesis | 29 |
| 2.1.1 | The ALD technique | 29 |
| 2.1.2 | Synthesis of metalorganic precursors for ALD | 48 |
| 2.2 | Characterization techniques | 60 |
| 2.2.1 | X-ray diffraction (XRD)..... | 60 |
| 2.2.2 | Spectroscopy..... | 68 |
| 2.2.3 | Microscopy | 70 |
| 2.2.4 | Characterization of precursors..... | 73 |
| 3 | Experimental work | 77 |
| 3.1 | Precursor synthesis | 77 |
| 3.1.1 | Synthesis of Co(thd) ₂ | 77 |

| | | |
|-------|---|-----|
| 3.1.2 | Synthesis of $\text{Co}(\text{thd})_3$ | 78 |
| 3.1.3 | Synthesis of $\text{Bi}(\text{thd})_3$ | 78 |
| 3.1.4 | Synthesis of $\text{Bi}(\text{t-OBu})_3$ | 79 |
| 3.2 | The ALD reactor | 80 |
| 3.2.1 | The reaction chamber | 82 |
| 3.2.2 | Transport gas | 82 |
| 3.2.3 | Growth parameters for deposition of thin films | 83 |
| 3.3 | Substrates | 83 |
| 3.4 | Precursors..... | 84 |
| 3.5 | Characterization equipment | 85 |
| 3.5.1 | X-ray based methods | 85 |
| 3.5.2 | FT-IR | 86 |
| 3.5.3 | AFM | 86 |
| 3.5.4 | Equipment used for characterization of precursors | 86 |
| 3.6 | Heat treatment of the deposited thin films..... | 87 |
| 4 | Results | 89 |
| 4.1 | Synthesis and investigation of precursors..... | 89 |
| 4.1.1 | $\text{Co}(\text{thd})_2$ | 89 |
| 4.1.2 | $\text{Co}(\text{thd})_3$ | 91 |
| 4.1.3 | BiPh_3 | 94 |
| 4.1.4 | $\text{Bi}(\text{t-OBu})_3$ | 96 |
| 4.1.5 | $\text{Bi}(\text{thd})_3$ | 97 |
| 4.2 | Thin films in the Co-O and Bi-O systems | 109 |

| | | |
|-------|---|-----|
| 4.2.1 | Thin films based on $\text{Co}(\text{thd})_2$ and O_3 | 109 |
| 4.2.2 | Thin films based on $\text{Co}(\text{thd})_3$ and O_3 | 114 |
| 4.2.3 | Thin films based on $\text{Co}(\text{thd})_3$ and H_2O | 124 |
| 4.2.4 | Thin films based on $\text{Co}(\text{thd})_2$ and H_2O | 124 |
| 4.2.5 | Thin films based on $\text{BiPh}_3 + \text{H}_2\text{O}/\text{O}_3$ | 128 |
| 4.2.6 | Thin films based on $\text{Bi}(\text{thd})_3 + \text{H}_2\text{O}$ | 129 |
| 4.3 | Thin films in the Bi-Co-O system..... | 136 |
| 4.3.1 | Thin films based on BiPh_3 | 136 |
| 4.3.2 | Thin films based on $\text{Bi}(\text{thd})_3 / \text{H}_2\text{O}$ and $\text{Co}(\text{thd})_2 / \text{O}_3$ | 142 |
| 5 | Discussion..... | 153 |
| 5.1 | Cobalt precursors | 153 |
| 5.2 | Bismuth precursors | 161 |
| 5.3 | Etching of Co_3O_4 by $\text{Bi}(\text{thd})_3$ | 167 |
| 5.4 | The Bi-Co-O films | 170 |
| 6 | Conclusion..... | 171 |
| 7 | Further work | 173 |
| 8 | References | 177 |
| 9 | Appendix | 187 |
| 9.1 | $\text{Bi}(\text{thd})_3$ synthesis sample names | 187 |
| 9.2 | KBG1117 | 188 |
| 9.3 | TEM of KBG1008 | 192 |

Dedicated to
my Father

Ove Gandrud

04.07.1948 – 16.12.2007

*Thank you for opening my eyes
to all the wonders in this world.*

1 Background

This chapter describes the motivation for synthesis of thin films of BiCoO_3 , and how this challenge was approached. Prior work for bulk and in thin films synthesis in the Bi-Co-O system will be presented together with work performed on both cobalt and bismuth oxides with ALD (Atomic Layer Deposition). Finally theory for the magnetic and electric properties of the multiferroic material BiCoO_3 will be given, together with some potential applications.

1.1 Aim, motivation and approach

The aim of this work was to synthesize thin films in the Bi-Co-O system using the ALD technique, with main focus on the multiferroic phase BiCoO_3 . Multiferroic materials, which are rare in nature [2], have received renewed interest in the recent years [3], because obtaining a better understanding of these materials is of high fundamental and technological importance [4-7]. The first and maybe greatest challenge for deposition of BiCoO_3 with ALD is to find a suitable bismuth precursor for deposition of bismuth oxide (Bi_2O_3) films. There have been several attempts to deposit thin films of bismuth oxide with ALD, however none have yet succeeded [8-11]. It may seem that finding a suitable bismuth precursor is notorious more difficult than for most other elements. As many functional materials such as ferroelectrics contain bismuth, it is not due to lack of interest that there still are so few suitable bismuth precursors for the ALD process.

The initial plan was to begin with a literature survey on suitable bismuth precursors before reattempting to obtain control over thin film deposition of bismuth oxide with ALD, thereafter, binary films of bismuth and cobalt

oxide would be deposited to investigate the Bi-Co-O system. Finally thin films of the BiCoO₃ phase would be tried deposited by utilizing strain engineering on various substrates. The precursor for deposition of cobalt oxide was already well investigated in our group [12-15]. However, a search for a better cobalt precursor would be investigated as well.

1.2 Prior art

The Bi-Co-O system is relatively unexplored in the scientific literature; therefore in the following overview a complete presentation of all the work previously performed on this system, both in bulk form and as thin films, will be attempted given. A complete Bi-Co-O phase diagram is difficult to obtain in the available literature [16], however, both phase diagrams for the Bi₂O₃ – CoO and Bi₂O₃ – Co₃O₄ systems will be presented in the following, and some work on a few closely related systems will also be mentioned. Thereafter work on deposition of thin films consisting of cobalt and bismuth oxide by ALD will be covered, and finally the predicted physical properties of BiCoO₃, by DFT (density functional theory) calculations, will be presented.

1.2.1 Bulk studies of the Bi-Co-O system

BiCoO₃ is only stable at high-pressures and thus to be regarded as metastable under ambient conditions [17].

The first reported study on BiCoO₃ is provided by Tomashpol'Skii et al. in 1969 [18] where BiCoO₃ was obtained as bulk material by high-pressure synthesis at 6 GPa and 700 °C. They reported that BiCoO₃ prepared at 700 °C at atmospheric pressure by the solid state reaction of the corresponding oxides had a defect pyrochlore structure with $a = 10.52 \text{ \AA}$,

while BiCoO_3 prepared at 6 GPa and 700 °C had a cubic structure with $a = 4,228 \text{ \AA}$.

Vasudevan et al. reported in 1978 a study on BiCoO_3 synthesized by high temperature solid state reaction at atmospheric pressure [19]. This resulted in a compound with a bcc structure (Im3) and $a \approx 10.2 \text{ \AA}$. They also reported that the BiCoO_3 samples prepared from the mixed oxides showed a few additional reflections in the X-ray patterns, which could be indexed taking basis in a primitive cubic (Pn3) structure with $a \approx 10.2 \text{ \AA}$. Magnetic measurements performed on BiCoO_3 samples proved them to be paramagnetic in the range -173 to 572 °C, with a magnetic moment of 2.3 μ_B per cobalt ion. They emphasize that this magnetic moment is much lower than what expected for high-spin Co^{3+} ($S=2$) ions which should be 4.0 μ_B . They postulate that this could be explained by the coexistence of both high- and low-spin ($S=0$) in preferred sites or due to partial antiferromagnetic alignment of the high-spin ions. An equal population of low- and high-spin ions would indeed result in a magnetic moment of 2.3 μ_B [19]. In addition, it was not possible to identify any Néel temperature in the investigated temperature range, and they suggested therefore that T_N is below -173 °C. Further, they report that BiCoO_3 is an insulator at room temperature, where the activation energy for conduction in the region 127 – 327 °C is ~0.4 eV while at still higher temperatures it is ~1 eV. It should be mentioned that as the synthesis was carried out under ambient pressure, it is highly unlikely that the BiCoO_3 phase was obtained in this study.

In 1979 Rozaj-Brvar et al. reported a study of reactions of Bi_2O_3 with CoO in argon in mixtures of compositions up to 20 mol % CoO [20]. A compound with a bcc sillenite-type structure, $a = 10.206 \text{ \AA}$, melting incongruently at 790 °C and presumably having the composition $\text{Bi}_{24}\text{CoO}_{37}$ ($12\text{Bi}_2\text{O}_3:1\text{CoO}$) was detected. In addition a eutectic in the Bi_2O_3 -CoO system was found to be at 720 °C and at 15 mol % CoO. Samples with

increasing CoO content up to 80 mol % CoO were found to be two-phase mixtures, which showed increasing amounts of the CoO phase. The phase diagram is shown in *Figure 1-1*.

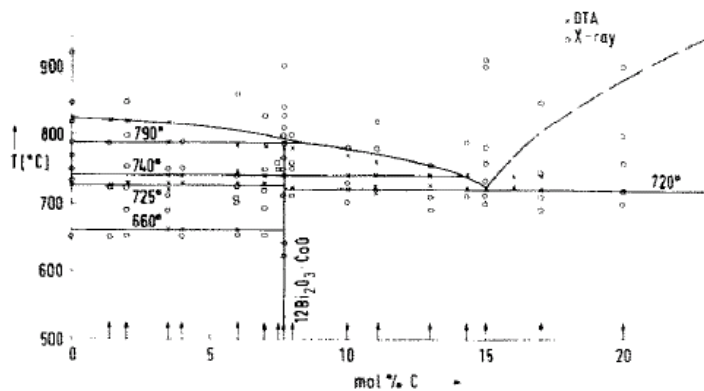


Figure 1-1. The Bi_2O_3 -rich part of the Bi_2O_3 – CoO system [20].

A study of reactions between Bi_2O_3 and Co_3O_4 was reported by Ramanan et al. in 1981 [21]. The resulting ternary oxide had the general formula $\text{Bi}_{26-x}\text{Co}_x\text{O}_{40-y}$ and exhibited a bcc structure related to α - Bi_2O_3 . They found that the cobalt ion replaced bismuth randomly at the octahedral 24r sites (space group 123).

In 1982 Dance et al. performed an ESR (electron spin resonance) study that implied the presence of Co^{3+} in the tetrahedral sites of the sillenite phase $\text{Bi}_{12}[\text{Co}^{3+}_{1/2}\text{Bi}^{5+}_{1/2}]\text{O}_{20}$, which was prepared in air at 797 °C from Bi_2O_3 and Co_3O_4 [22].

A phase diagram of Bi_2O_3 - Co_2O_3 mixtures in the range from 0 to 16 mol % Co_2O_3 was published in 1985 by Gorashchenko et al. [23]. The region of two-sided solid solutions based on the sillenite compound $12\text{Bi}_2\text{O}_3:1\text{Co}_2\text{O}_3$, which melts congruently at 780 °C, is mapped in this diagram. The oxidation number of cobalt after the synthesis was neither

checked in that work, nor was the unit cell parameter of the resulting phase reported.

J. Gopalakrishnan reported a study on some oxides of bismuth in 1986 [24]. He suggested that two sillenite phases occurs in the Bi-Co-O system, namely $\text{Bi}_{25}\text{CoO}_{40}$ and $\text{Bi}_{10}\text{Co}_{16}\text{O}_{40-\delta}$. He also believed that in $\text{Bi}_{26-x}\text{Co}_x\text{O}_{40-\delta}$ sillenites, bismuth atoms can be substituted for cobalt atoms in the tetrahedral Co positions at $x < 2$ to form $(\text{Bi}^{5+}\text{Co}^{3+})[\text{Bi}_{24}^{3+}]\text{O}_{40}$, and cobalt atoms can substitute for bismuth atoms in the 24f positions at $x > 2$ to form $((\text{Co}^{2+})_2[\text{Bi}_{10}^{3+}\text{Co}_{14}^{3+}]\text{O}_{38})$.

In 1996 Mary et al. reported a study [25] on single crystal X-ray diffraction refinements of the sillenite phase $\text{Bi}_{12.7}\text{CoO}_{0.3}\text{O}_{19.35}$ crystallized from the melt of composition $3\text{Bi}_2\text{O}_3:1\text{Co}_3\text{O}_4$. They found that the compound is cubic (I23) and $a = 10.172 \text{ \AA}$. The structure consists of five coordinated Bi atoms at the 24f site and a mixture of Co and Bi at the tetrahedral 2a site. Bi atoms at the tetrahedral sites are apparently displaced toward vacant O sites leading to a typical lone pair environment for Bi.

A new study on reactions of Bi_2O_3 with cobalt oxides in air and in vacuum was reported in 1998 by Kargin et al. [26]. This report presents phase diagrams of $\text{Bi}_2\text{O}_3\text{-CoO}$ (Figure 1-2) and a $\text{Bi}_2\text{O}_3\text{-Co}_3\text{O}_4$ (Figure 1-3). Two sillenite compounds with the composition $44\text{Bi}_2\text{O}_3:1\text{Co}_3\text{O}_4$ ($a = 10.200 \text{ \AA}$) and $19\text{Bi}_2\text{O}_3:1\text{CoO}$ ($a = 10.185 \text{ \AA}$) were prepared in air and *in vacuo*, respectively.

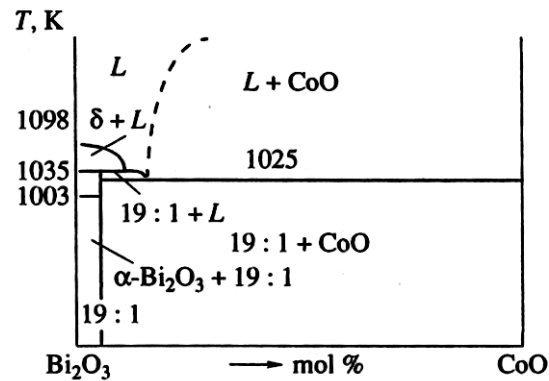


Figure 1-2. The phase diagram for $\text{Bi}_2\text{O}_3\text{-CoO}$ mixtures in argon. The composition at the eutectic point approximates 16 mol % CoO [26].

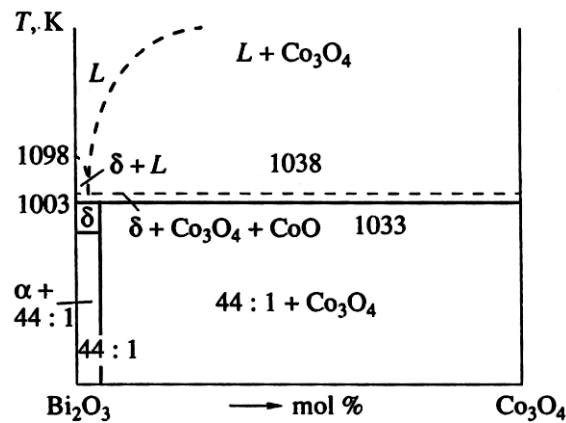


Figure 1-3. The phase diagram for $\text{Bi}_2\text{O}_3\text{-Co}_3\text{O}_4$ mixtures in air in a temperature range from 25 to 852 °C [26].

The synthesis in vacuum ($p = 0.0267$ Pa) from Bi_2O_3 and CoO resulted in the sillenite phase $19\text{Bi}_2\text{O}_3:1\text{CoO}$ ($\text{Bi}_{38}\text{CoO}_{58}$), with $a = 10.185$ Å, which melted incongruently at 780 °C. From the data obtained they suggest that the type of sillenite compound formed – either with Co^{2+} ($19\text{Bi}_2\text{O}_3:1\text{CoO}$) or with Co_3O_4 ($44\text{Bi}_2\text{O}_3:1\text{Co}_3\text{O}_4$) – is a function of synthesis variables (temperature and oxygen partial pressure). They also establish that the Bi-Co-O system in air does not form any compounds with the Co_2O_3 phase. This observation contradicts earlier work carried out in Ref. [23].

A. Belik et al. reported in 2006 a new high pressure synthesis of bulk BiCoO_3 at 6 GPa and 970 °C [27]. The crystal- and magnetic structures of polycrystalline BiCoO_3 was determined from data obtained by neutron diffraction in the temperature range -268 to 247 °C, and they report it to have antiferromagnetic long-range order below $T_N = 197$ °C. They proposed a model for the antiferromagnetic order where the magnetic moments of the Co^{3+} ions are parallel to the c -axis and align antiferromagnetically in the ab plane. The antiferromagnetic ab layers stack ferromagnetically along the c -axis, forming a C-type antiferromagnetic (C-AFM) structure. They found from the obtained data that the refined magnetic moments at -268 and 27 °C are $3.24(2) \mu_B$ and $2.93(2) \mu_B$, respectively. In addition they report that BiCoO_3 has the space group $P4mm$, $a = 3.72937(7) \text{ \AA}$ and $c = 4.72382(15) \text{ \AA}$ at room temperature, the tetragonality (c/a) is 1.267, and that BiCoO_3 is an insulator with resistivity of about $10^5 \Omega\text{cm}$ at 127 °C. They suggested that BiCoO_3 should be considered as a pyroelectric material rather than a ferroelectric, since the measured resistivity is too low for the application of a large electric field. However they did find a noticeable amount of impurities in the sample, grains of Co_3O_4 were embedded into grains of BiCoO_3 , and $\text{Bi}_2\text{O}_2\text{-CO}_3$ was found as separate particles. This could have influenced the electrical measurements, as Co_3O_4 is a p-type semiconductor [28]. They also report that BiCoO_3 decompose in air to form Co_3O_4 and a sillenite-like $\text{Bi}_{25}\text{CoO}_{39}$ at 447 °C, and if the sample was heated to 327 °C the oxygen content of the sample slightly changed.

Another high pressure synthesis of bulk BiCoO_3 was reported by T. Oguchi et al. in 2007, to support first-principles calculations. However, they report no measured properties and provide no parameters [29].

1.2.1.1 Bulk study on the Bi-Fe-Co-O system

A $(1-x)\text{BiCoO}_3-x\text{BiFeO}_3$ solid solution have also been reported synthesized by high-pressure by Azuma et al. in 2008 [30]. They reported a $\text{BiCo}_{1-x}\text{Fe}_x\text{O}_3$ phase diagram, see *Figure 1-4*.

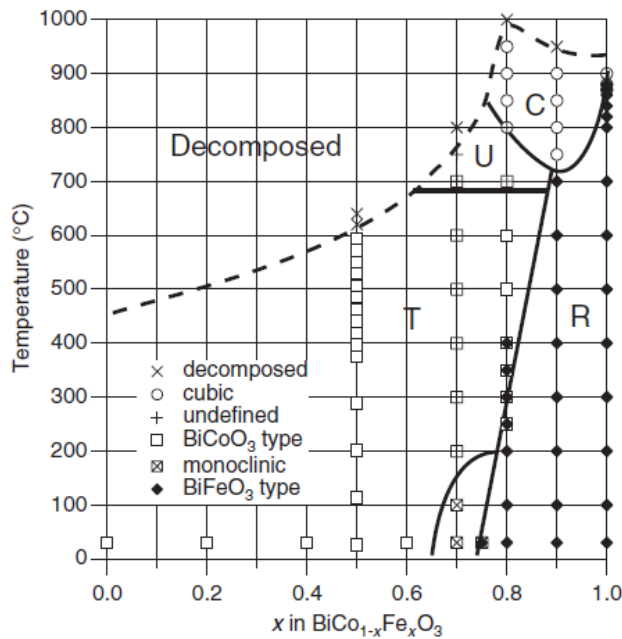


Figure 1-4. A composition-temperature phase diagram for the $\text{BiCo}_{1-x}\text{Fe}_x\text{O}_3$ system. In the figure C, T and R stands for the cubic, tetragonal and rhombohedral phases, respectively [30].

1.2.2 Thin films

BiCoO_3 has previously been synthesized as thin films in a $(1-x)\text{BiCoO}_3-x\text{BiFeO}_3$ solid solution system by MOCVD [17, 31]. The precursors used for deposition of BiCoO_3 with MOCVD was $\text{Bi}[(\text{CH}_3)_2-(2-(\text{CH}_3)_2\text{NCH}_2\text{C}_6\text{H}_4)]$ and $\text{Co}(\text{MeCp})_2$ together with oxygen (O_2). In both studies, the deposition temperature was $700\text{ }^\circ\text{C}$ and $(100)\text{SrTiO}_3$ was used as substrate.

As mentioned earlier depositions of BiCoO_3 by the ALD technique has not previously been reported, probably due to lack of suitable bismuth precursor for the ALD process [10].

1.2.2.1 Cobalt

Thin films of Co_3O_4 films have been reported deposited by ALD using $\text{Co}(\text{thd})_2$ and ozone (O_3) [12, 32], CoI_2 and oxygen (O_2) [33], $\text{Co}(\text{acac})_2$ and O_2 [34, 35] as well as $\text{Co}(\text{acac})_3$ and O_2 [34-41]. Thin films of CoO have been reported deposited using $\text{Co}(\text{PrAMD})_2$ and water (H_2O) [42].

$\text{Co}(\text{thd})_2$ was used in Ref. [32] as precursor for depositions on corning glass in the temperature range 200 – 400 °C, the sublimation temperature of the precursor was 100 °C and the applied pulse and purge parameters was 1.8s and 2.5s, respectively for $\text{Co}(\text{thd})_2$, and 1.0s and 3.0s respectively for O_3 . Films containing the Co_3O_4 phase and a mixture of the two phases $\text{Co}_3\text{O}_4/\text{CoO}$ were obtained at the temperatures 200 – 300 °C and 350 – 400 °C, respectively. An upper deposition temperature of 400 °C was used due to decomposition of $\text{Co}(\text{thd})_2$.

Klepper et al. report in Ref. [12] deposition from $\text{Co}(\text{thd})_2$ in the temperature range 138 – 283 °C, with an growth rate of 21 pm/cycle. The pulse and purge parameters employed for the deposition were 1.5s pulse of $\text{Co}(\text{thd})_2$, 1.0s purge, 6.0s pulse of ozone and 1.5s purge. The as deposited films were found to have a epitaxial growth of the cubic Co_3O_4 phase, on $\text{MgO}(100)$, $\alpha\text{-Al}_2\text{O}_3(001)$ and $\text{SrTiO}_3(100)$.

CoI_2 and O_2 was used for deposition in the temperature range from 450 – 700 °C in Ref. [33]. The growth rate was shown to be heavily influenced by the deposition temperature. On $\text{SiO}_2/\text{Si}(100)$ substrates, a growth rate of 200 pm/cycle was observed at 450 °C, decreasing to 4 pm/cycle at 700 °C. On $\text{MgO}(001)$ substrates the growth rates were found to

be 120 pm/cycle at 475 °C, while no growth could be detected at 700 °C. The as deposited films were observed to grow as the cubic Co₃O₄ phase throughout the temperature range 475 – 700 °C, polycrystalline on SiO₂/Si(100), and epitaxial on MgO(100).

Both Co(acac)₂ [34, 35] and Co(acac)₃ [34-41] have been used with O₂ for deposition of metallic cobalt for catalytic purposes by ALD. The Co₃O₄ phase was identified by X-ray diffraction. Typically a source temperature around 170 – 180 °C was used for sublimation of the Co(acac)₂ and Co(acac)₃ precursors.

CoO is reported deposited at 250 °C with a growth rate of 40 pm/cycle by Lim et al. in Ref. [42] using Co(ⁱPrAMD)₂ and H₂O.

Cobalt is also a constituent in deposition of (Co_{1-x}Fe_x)₃O₄ with ALD using Co(thd)₂, Fe(thd)₃ and O₃ in Ref. [15]. The pulse/purge parameters for Co(thd)₂ was the same as used in Ref. [12], the temperature range for deposition was 185 – 310 °C.

Co(thd)₂ has also been used together with La(thd)₃ and O₃ to deposit LaCoO₃ in the temperature range 200 – 400 °C [32].

1.2.2.2 Bismuth

Previously, there have been some attempts to deposit films of binary bismuth oxide using ALD. In 2000 Schuisky et al. reported an unsuccessful attempt to deposit bismuth oxide using BiPh₃ and H₂O [8]. The report unfortunately lacked descriptions about observations and parameters.

Different bismuth precursors for the ALD-technique was investigated by Vehkamäki et al. in 2004 [9]. They studied silylamides Bi(N(SiMe₃)₂)₃, Bi(N(SiMe₂Et)₂)₃ and Bi(N(SiMe₂Buⁿ)₂)₃, alkylamides Bi(NEt₂)₃ and Bi(NPrⁱ)₃, donor functionalized alkylamide Bi(Bu^tNC₂H₄NMe₂)₃ and thioamidate Bi(SC(Me)NPrⁱ)₃. Among the studied

compounds they found that with regards to volatility and thermal stability, $\text{Bi}(\text{N}(\text{SiMe}_3)_2)_3$ seemed to be the most potential precursor for ALD. By using $\text{Bi}(\text{N}(\text{SiMe}_3)_2)_3$ and H_2O as precursors, they were able to deposit films of BiO_x on silicon and borosilicate glass substrates at temperatures 190 – 200 °C. Uniform, amorphous BiO_x films were deposited with growth rates between 15 – 23 pm/cycle, although the reproducibility of these results were poor. Further, they reported that the precursor decomposed above 200 °C, and that BiO_x formation also were observed at 170 – 190 °C, but this temperature range was not studied any further as the pulse and purge lengths for the different precursors was too long. They suggested that a possible explanation for the poor reproducibility of the BiO_x films were due to reduction of bismuth to metallic form when no other metal oxides are present in the film, leading to termination of the growth. And that in ALD, the periodic exposures to low vapor pressures of H_2O in a flow type reactor may not be effective enough to fully oxidize bismuth. As support they point to a study done by Schuisky et al. in [8], where they observed metallic bismuth in their as deposited films of Bi-Ti-O systems. However, the metallic bismuth in the as deposited films grown by Schuisky et al. was probably caused by using a higher deposition temperature than the decomposing temperature for the bismuth precursor utilized, BiPh_3 .

In 2006 Vehkamäki et al. reported again an attempt to deposit bismuth oxide using $\text{Bi}(\text{N}(\text{SiMe}_3)_2)_3$ and H_2O as precursors at 190 °C [10]. They now report a growth rate of 8 pm/cycle which is lower than the growth rate previously reported, and the result was an amorphous BiO_x film with large grains with radius of about 30 nm that were uniformly distributed over the film. As a possible explanation of the observed morphology and also for the variations in the BiO_x growth, it is suggested that bismuth was reduced to metallic form during the metal precursor pulse or the purging steps. The metallic bismuth would diffuse on the surface, coalesce and form small

islands. It is mentioned that Terajima and Fujiwara have previously reported an average diffusion length for bismuth of 5 – 13 nm on mica surfaces at 175 °C during bismuth film deposition by evaporating in a high-vacuum system, and that bismuth re-evaporation was considered to take place [43]. It is also mentioned that Hwang et al. considered evaporation of bismuth during ALD as the cause of decrease in bismuth content in their films as they increased the deposition temperature from 225 to 300 °C in their $\text{Bi}_2\text{Ti}_2\text{O}_7$ process [44]. Further they report an attempt to anneal the amorphous bismuth film containing the 30 nm grains distributed on the surface. Since metallic bismuth melts at 271.3 °C, they annealed the sample for 1 hour at 300 °C in N_2 atmosphere. Since no change could be observed in the annealed sample, they suggested it is likely that if reduction of bismuth indeed takes place on the surface of the growing film, it seems likely that reoxidation has followed during further deposition cycles.

An attempt to grow binary bismuth oxide using BiPh_3 and O_3 as precursors was reported by Harjuoja et al. in 2006 [11]. This resulted in visually dark and patchy films with a steep thickness profile, indicating poor ALD growth. They did, however, not report any of the parameters used for this deposition.

Bismuth has been deposited together with titanium by ALD in the Bi-Ti-O system using $\text{Bi}(\text{mmp})_3$ and O_3 [45], and H_2O [44] as precursors. In Ref. [44] Hwang et al. varied the deposition temperature from 225 – 300 °C, and observed that the bismuth concentration in the film decreased with increasing growth temperature. This decrease could anyhow be controlled within a certain range by increasing the bismuth pulse at a given temperature. The as grown $\text{Bi}_2\text{Ti}_2\text{O}_7$ films were amorphous and contained metallic bismuth at high growth temperatures and high bismuth concentrations. They reported a growth rate of 75 pm/cycle at 225 °C which decreased to 55 pm/cycle at 300 °C.

Cho et al. used ALD with direct liquid injection (DLI) method to deposit films in the Bi-Ti-O system in Ref. [45], with the $\text{Bi}(\text{mmp})_3/\text{O}_3$ precursor combination. They reported an ALD window in the temperature range of 250 – 350 °C, and that the bismuth concentration in the films decreased above 425 °C, which is a higher temperature than reported by Hwang et al. in Ref. [44] for the same decrease in bismuth concentrations. They also found that the as deposited films at 300 °C were amorphous. However they observed no metallic bismuth incorporated in the deposited films as Hwang et al. did, probably due to the use of O_3 which is a stronger oxidizing precursor than H_2O .

BiPh_3 has also been reported used as precursor with H_2O as the oxygen source [8], for depositions together with TiCl_4 in the Bi-Ti-O system. Schuisky et al. reports in [8] that at 260 °C the growth rate is about 20 pm/cycle. With an increasing number of BiPh_3 pulses, the growth rate drops, and they suggest that the previously as-deposited TiO_x layer acts as a catalyst which enhance the reactivity of the BiPh_3 precursor, and thus with increasing bismuth pulses this catalytic effect is suppressed as the TiO_x layer becomes covered with increasing amounts of BiO_x . However, for the films deposited at 260 °C, bismuth was incorporated in a metallic form rather than as an oxide. This is, as mentioned earlier, probably due to the use of a deposition temperature above the decomposition temperature of BiPh_3 (see results in section 4.1.3.2 on page 95). They were also unsuccessful in obtaining bismuth titanates with higher Bi to Ti ratios than 0.61 due to the difficulties with the decreasing growth rate for subsequent bismuth pulses.

Thin films in the Ba-Ti-O system have also been deposited using BiPh_3 and O_3 , together with the precursor pair $\text{T}(\text{O}^i\text{Pr})_4/\text{H}_2\text{O}$ [11]. In Ref. [11] Harjuoja et al. reported good control of the film stoichiometry at the deposition temperature of 250 °C, and that the as deposited films were amorphous. Annealing in N_2 at temperatures from 700 to 1000 °C resulted

in crystalline films, however, the total bismuth content was significantly reduced by the annealing procedure. This effect was most notable for the samples with high bismuth contents after annealing at 1000 °C. By reference to the phase diagrams in *Figure 1-2* and *Figure 1-3* on page 6, it is evident that pure Bi₂O₃ melts below 825 °C. Stoichiometric loss due to the volatile nature and the high vapor pressure of low melting point oxides, such as Bi₂O₃, is according to Ref. [46] well-known in the literature. Hence evaporation of bismuth oxide could therefore be a possible explanation of the observed decrease in bismuth content during the annealing.

Bi(CH₂SiMe₃)₃ and O₃ as precursor pairs have been used to deposit thin films in the Bi-Si-O system [47]. In Ref. [47] Harjuoja et al. reports that in the temperature range 250 – 350 °C they managed to deposit amorphous films in the Bi-Si-O system with a constant growth rate of 40 pm/cycle.

Harjuoja et al. further report in Ref. [11] that the bismuth content in the Bi-Si-O thin films was successfully controlled by adding BiPh₃/O₃ ALD cycles into the Bi(CH₂SiMe₃)₃/O₃ process at 250 °C, and the as-deposited films were amorphous.

1.2.3 Physical properties of BiCoO₃

The magnetoelectric properties of BiCoO₃ are rather unexplored. This is mainly due to the difficulties in preparing high quality samples [48]. No such measurements have previously been reported for thin film samples. The expected magnetoelectric properties of this material are based on ab-initio calculations performed on BiCoO₃ using DFT (density functional theory) [48-50].

Uratani et al. predicted that BiCoO₃ has an insulating and antiferromagnetic (G or C-type) ground state in Ref. [49]. They also predicted a giant electric polarization of 179 μC cm⁻² in BiCoO₃.

In Ref. [50] Cai et al. reports that the C-AFM structure is lowest in energy and thus more stable than other possible configurations, in addition they predict a band gap of 2.11 eV in the insulating ground state of the C-AFM ordering.

A giant magnetoelectric coupling in BiCoO_3 is predicted by Ravindran et al. in Ref. [48], which means that the magnetic state of the cobalt atom can be switched between a magnetic high spin state (HS, $S=2$) and a nonmagnetic low spin state (LS, $S=0$) by an electric field. They also predict a giant electric polarization of $170 \mu\text{C cm}^{-2}$ in good agreement with Ref. [49]. Their calculations also show that the magnetic ground state for the ferroelectric phase of BiCoO_3 will be C-AFM which is in agreement with Ref. [27, 50]. In addition they report a calculated total moment of $3.10 \mu_{\text{B}}$, which is comparable with $3.24 \mu_{\text{B}}$ as measured from neutron diffraction measurements at $-268 \text{ }^\circ\text{C}$ in Ref. [27].

1.3 Multiferroics: Magnetic and electric properties

This chapter gives a short and general description of magnetic and electric properties which can be found in multiferroic materials. The term multiferroic is also explained, together with why there are so few multiferroic materials.

1.3.1 Magnetism

Materials with magnetic dipoles can be divided into four different fundamental configurations: ferro-, antiferro-, ferri- and paramagnetic. *Figure 1-5* shows a principal sketch of how the magnetic dipoles (spins) are ordered in these four different cases.

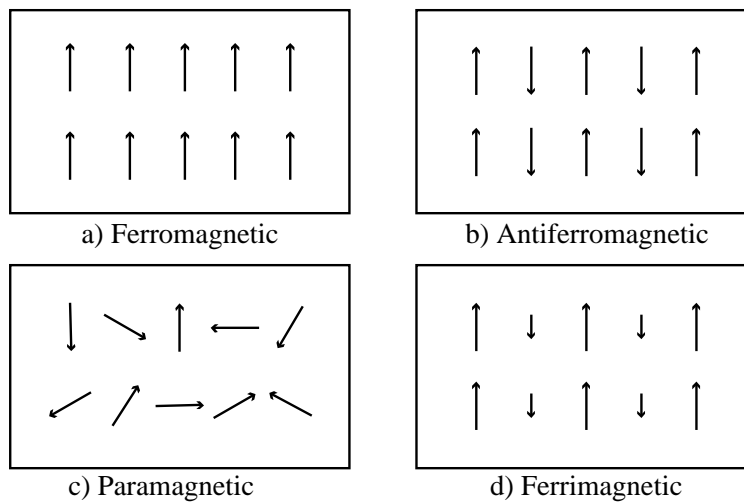


Figure 1-5. The different alignments of magnetic dipoles for a) ferromagnetic-, b) antiferromagnetic-, c) paramagnetic- and d) ferrimagnetic material.

As mentioned earlier, BiCoO_3 is reported to have an antiferromagnetic ordering [27], thus this configuration is explained more in detail together with ferromagnetism. Ferrimagnetism is not possible in such compounds, as it requires two subsets of magnetic moments [51], and will therefore not be discussed any further.

1.3.1.1 Ferro- and antiferromagnetism

This subchapter elaborates on the origin of ferromagnetism and antiferromagnetism and how such materials behave in an external magnetic field.

1.3.1.1.1 Origin of ferromagnetism

There are only nine crystals of pure elements which are ferromagnetic: three 3d metals, Fe, Co, and Ni, and six 4f metals, Gd, Dy, Tb, Ho, Er, and Tm [52]. However the number of ferromagnetic alloys and compounds is

practically unlimited. A material that undergoes changes from a random distribution of its magnetic dipoles (*Figure 1-5 c*) to an ordered parallel magnetic structure (*Figure 1-5 a*), below a certain temperature, called the Curie temperature T_C , is called ferromagnetic. The Curie-Weiss law which describes this transition is given in *Eq. 1-1* [51];

$$\chi = \frac{C}{T - T_C} \qquad \text{Eq. 1-1}$$

where χ is the magnetic susceptibility, C is the Curie constant, T is the absolute temperature and T_C is explained above. The driving force for ferromagnetic ordering is the exchange energy, which gives the system a gain in free energy by ordering the magnetic moments (electron spins) parallel.

However, when the atom is introduced into a solid or a molecule another interaction, chemical bonding, is important. In general, the bonding energy is greater than the exchange energy, however the d- and f-orbitals are localized and do not extend far from the atomic nucleus, hence the bonding energy between these orbitals are weak. As a consequence they are strongly influenced by the exchange energy and ferromagnetic properties can therefore occur in materials with incompletely filled d- or f-orbitals.

1.3.1.1.2 Properties of ferromagnets in magnetic fields

When an external magnetic field \mathbf{H} is applied to a ferromagnet an internal magnetic field \mathbf{M} will be created. The total magnetization \mathbf{B} given by *Eq. 1-2*, and the resulting magnetization curve $\mathbf{B}(\mathbf{H})$, shown in *Figure 1-6*, is a distinguishing feature of a ferromagnet.

$$\mathbf{B} = \mu_0(\mathbf{H} + \mathbf{M}) \quad \text{Eq. 1-2}$$

where \mathbf{B} , \mathbf{H} and \mathbf{M} is described above and μ_0 is the vacuum permeability.

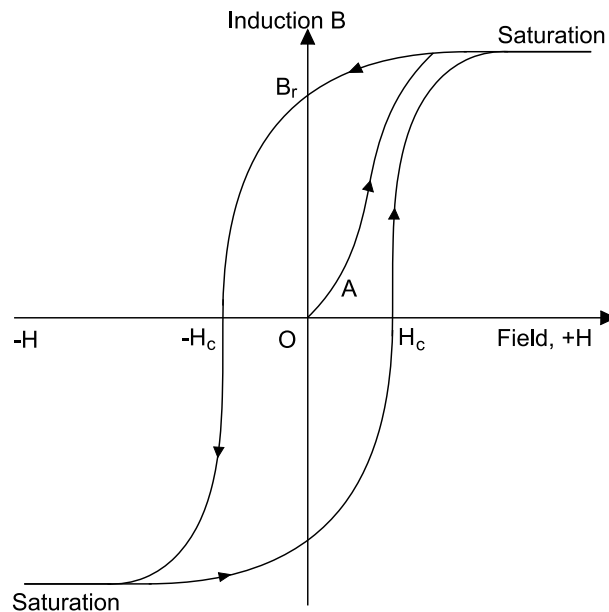


Figure 1-6. The magnetization curve $B(H)$ for a ferromagnetic material.

As *Figure 1-6* shows in the absence of a field ($\mathbf{H}=0$) there is no magnetization ($\mathbf{B}=0$), meaning there is no resultant magnetization of the sample in the initial state (O). With an increase in the external field some of the domains start to align themselves with the external field. As the field is increased further the domains that are aligned with the external field will grow at the expense of those domains that are poorly aligned, until saturation is reached. At this point all the magnetic domains are aligned parallel with the external field. When the external field is removed a large amount of these domains remain locked in this alignment, and the magnetization \mathbf{B} will drop to $\mathbf{B}_r = \mu_0\mathbf{M}$, which is called the remanent magnetization, giving rise to a net magnetization of the sample. As the

external field is set in reverse the magnetization of the sample decreases until a critical field is reached ($-H_c$), which is called the coercive field. At this point the net magnetization of the sample is back to zero. A further increase in the external field leads again to a saturation with a net magnetic moment for the sample.

1.3.1.1.3 Origin of antiferromagnetism

As mentioned earlier the d- and f-orbitals on the magnetic atom in a ferromagnet do only participate in weak bonding, however, for an antiferromagnet this is not the case. In an antiferromagnet, the transition metal ions are separated by a nonmetal such as oxygen, and the d orbitals on the metal ions participate in the bonding. And this interaction of the d orbitals on the cations via the intermediate anion is called superexchange, leading to a long range ordering of antiparallel spins on the metal ion. A schematic illustration of this antiparallel spin ordering, due to overlap of the metal d orbitals with the oxygen p orbitals, is shown in *Figure 1-7*.

For an antiferromagnetic material the temperature at which the material undergoes a transition from paramagnetic to antiferromagnetic is called the Néel temperature, T_N .

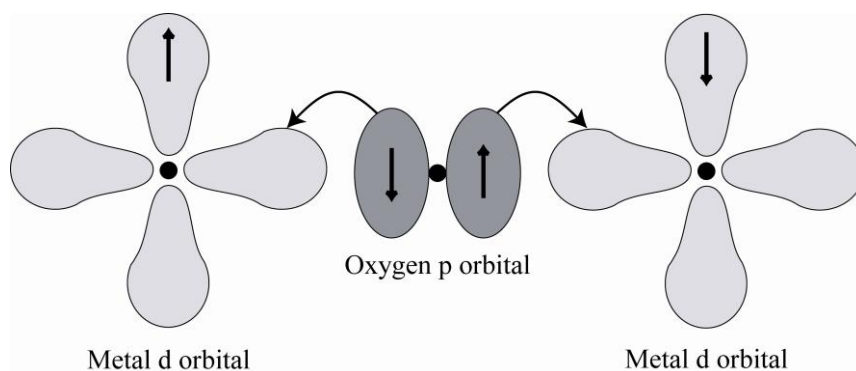


Figure 1-7. Schematic illustration of superexchange leading to antiferromagnetic alignment of spins on metal cations.

1.3.2 Ferroelectrics

Ferroelectric materials are characterized by a spontaneous polarization in absence of an electric field. Thus a ferroelectric material has to be an insulator; otherwise any polarization in the material would be canceled out by mobile electrons. Insulating materials are often referred to as dielectrics and one of the most important parameters used to describe an insulator is its dielectric constant, properly called the relative permittivity, ϵ_r . The relative permittivity describes the response of a solid to an electric field. As an example, the ferroelectric crystallographic polymorph of barium titanate (BaTiO_3) has a relative permittivity in the order of $1 \cdot 10^4$ [51], while silicon (Si) has a relative permittivity of 11.8 [53]. Materials with high dielectric constant can be used in a capacitor, where an increased permittivity allows the same charge to be stored with a smaller electric field (and thus a smaller voltage), leading to an increased capacitance.

1.3.2.1 The origin of ferroelectricity

The ferroelectric phase is obtained below a critical temperature called the Curie temperature. There are several different mechanisms which results in ferroelectricity, however, only the two that are relevant for the work in this thesis will be presented here. The first mechanism is often found in perovskites, having an ABO_3 formula, where the B-atom has a d^0 electronic configuration. In typical ferroelectrics as BaTiO_3 and lead titanate (PbTiO_3) the titanium cation is situated in an off-centre position in the oxygen octahedron. It is shown for BaTiO_3 that the hybridization between the empty Ti 3d orbitals and O 2p orbitals stabilizes the off-centering of the Ti atom [54, 55]. As a consequence the center of gravity of the anion array will now not coincide with the positive cation, and each unit cell in the structure now contains a dipole. As a centre of symmetry in the structure would force the

generated dipole moment to be canceled out by symmetry, a ferroelectric material must therefore be non-centrosymmetric. In perovskite ferroelectrics this cation displacement is bi-stable with respect to the center, meaning that the displacement can take place in more than one direction, making it possible to switch the polarization by applying an external electric field.

As ferroelectricity exists in BiCoO_3 and other materials which do not have d^0 electronic configuration on the B atom, there must be another mechanism for the origin of ferroelectricity in these materials. In fact the lone pair electrons of some main group elements (Tl^+ , Pb^{2+} , Sn^{2+} , Sb^{3+} , Bi^{3+} , Se^{4+} , Te^{4+}) is known to be stereochemically active. It is shown that the Bi lone pair ($6s^2$) instead of remaining spherical mix with the Bi 6p states and creates a space-filling localized lobe, which in turn pushes away its neighboring atoms causing a structural distortion [56-58]. This distortion stabilizes the polarization of the material, and it is also reported in the case of BiCoO_3 that Bi-O hybridization plays an important role in increasing and further stabilizing this polarization [48, 50]. Thus, in the perovskite structure, the properties of the A-atom can also significantly influence the formation of a ferroelectric phase in a material.

1.3.2.2 Properties of ferroelectrics in electric fields

A ferroelectric material in an electric field behaves much like a ferromagnetic material in a magnetic field. In general the polarization of a ferroelectric crystal will be zero, as the crystal is composed of an equal number of domains oriented in all the equivalent directions allowed by the symmetry. If a small electric field, \mathbf{E} , is applied the crystal will behave like a normal dielectric. This corresponds to the segment O-A in *Figure 1-8*. As \mathbf{E} increases, domains will gradually change orientation and the observed polarization will increase rapidly. Ultimately all the dipoles will be aligned

parallel; this is the state of saturation. Extrapolation of the linear portion at saturation to $\mathbf{E} = 0$ gives the value of the spontaneous polarization \mathbf{P}_s . The most important characteristic of a ferroelectric is that the spontaneous polarization can be reversed by the application of a suitably oriented electric field. As the field is removed, the polarization will drop to \mathbf{P}_r , which is called the remanent polarization. Reversal of the field, will cause a reversal of the dipole direction, and at a field value called the coercive field, \mathbf{E}_c the sample has again no net polarization. Further reversal of the field will again lead to saturation, and the spontaneous polarization has been switched.

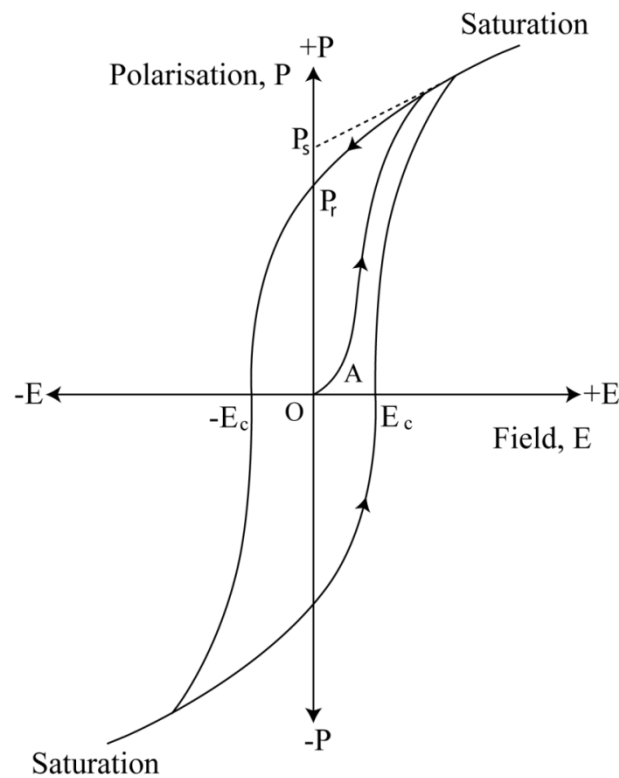


Figure 1-8. Hysteresis behavior of the polarization, P , in relation to the applied electric field, E , for a ferroelectric crystal.

1.3.3 Multiferroics

This subchapter will first explain the term multiferroics, followed by an explanation for why these materials are so rare in nature. Then an explanation will be given on how the different mechanisms, resulting in antiferromagnetic and ferroelectric properties in BiCoO_3 , can be combined together. Finally its predicted properties will be mentioned, together with some possible applications for multiferroic materials.

Materials in which two or all three of the properties ferroelectricity, ferromagnetism, and ferroelasticity occur in the same phase are called multiferroic [59]. Only multiferroic materials, which also are magnetoelectric, will be discussed in this work. By definition, a magnetoelectric multiferroic must be simultaneously both ferromagnetic and ferroelectric [60], see *Figure 1-9*, therefore ferroelastic materials will not be discussed any further. In a magnetoelectric materials there is also often a coupling between the two order parameters, which can give induction of magnetization by an electric field or polarization by a magnetic field [3]. The promise of coupling between the magnetic and electronic order parameters and the potential to manipulate one through the other has captured the imagination of researchers worldwide.

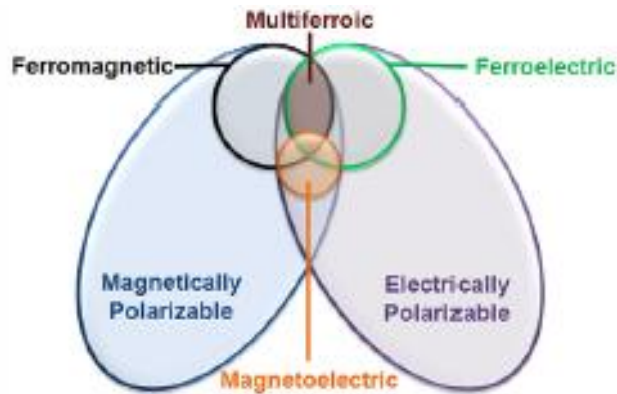


Figure 1-9. Relationship between multiferroic and magnetoelectric materials. The requirements to achieve both in a material is illustrated [61].

It should be noted, however, that the current trend is to extend the definition of multiferroics to include materials possessing two or more of any of the ferroic or corresponding antiferroic properties such as antiferroelectricity and antiferromagnetism, and it is this definition that will be used in this thesis.

Apart from that there is only 13 point groups that can give rise to multiferroic behavior, the scarcity of multiferroics can be explained by:

- I. A ferroelectric material must by definition be an insulator, and as earlier pointed out many ferroelectric materials have d^0 electronic configuration.
- II. Many ferromagnets are metals, and magnetic ordering is only possible due to the presence of d-electrons.

Thus from point *I* and *II* there seem to exist a mutually exclusion between the conventional mechanism of off-centering in a ferroelectric and the formation of magnetic order, which explains why multiferroic materials are rare in nature.

As stated earlier the origin of ferroelectricity in BiCoO_3 is a result of the lone-pair on the Bi^{3+} ion, which hybridize with the O 2p orbital to stabilize a polarization of the structure. Resulting in a tetragonal structure with a c/a ratio of 1.27 which is remarkably large compared with ordinary perovskite-type oxides (for example, 1.06 for tetragonal PbTiO_3) [49]. And the calculated polarization of $179 \mu\text{C cm}^{-2}$ for BiCoO_3 is the largest among the multiferroic materials identified so far [48].

The four unpaired electrons on the Co^{3+} ion is the origin of the magnetic properties, which by superexchange results in an (C-AFM) antiferromagnetic ordering [27], see *Figure 1-10*. The calculated value of $3.10 \mu_{\text{B}}$ is less than the expected value of $4.00 \mu_{\text{B}}$, due to strong hybridization between Co 3d and O 2p states [49].

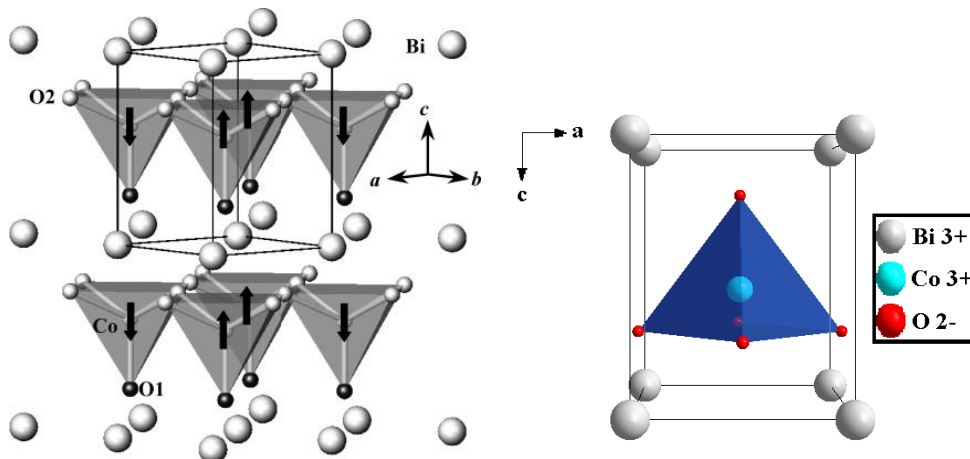


Figure 1-10. (Left picture) Crystal structure of BiCoO_3 with solid lines displaying the chemical cell. Arrows at the Co atoms indicate the C-type spin ordering below $T_N = 197^\circ\text{C}$ [27]. (Right picture) The unit cell of BiCoO_3 seen along the b-axis.

Given the unique magnetic and electric properties of multiferroic materials, one can easily think of many different applications. First, the ability to couple the two order parameters together allows an additional degree of freedom in the design of conventional actuators, transducers, and storage

devices [62]. Other applications include multiple state memory elements, in which data is stored both in the electric and magnetic polarization, or novel memory media, which might allow writing of a ferroelectric data bit, and reading of the magnetic field generated by association.

In the literature it is stated that the ultimate goal for device functionality would be a single phase multiferroic with strong coupling between ferroelectric and ferromagnetic order parameters making for simple control over the magnetic nature of the material with an applied electric field at room temperature [61]. In fact, as mentioned earlier, BiCoO_3 is to this date the only material shown to be able to exhibit such strong coupling [48]. Where BiCoO_3 transforms from the high spin state to a nonmagnetic low spin state with 5% volume compression, which can be done by an external electric field, see *Figure 1-11*.

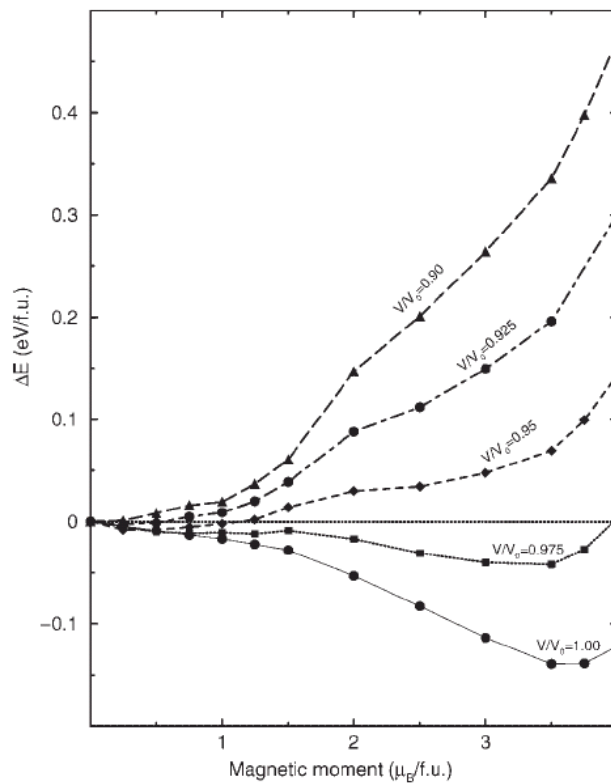


Figure 1-11. Variation of total energy with magnetic moment for BiCoO_3 for different volumes [48].

However, BiCoO_3 is an antiferromagnet and today the technological applications of antiferromagnets are rather limited. They are used in spin valves, where an antiferromagnet is used as a pinning layer for the magnetic spins on a ferromagnet [63]. However, aside from the potential applications, the fundamental physics of multiferroic materials are rather rich and fascinating.

2 Methods

In this chapter a general introduction will be given on the different methods utilized in this work. The chapter is divided in two main parts, the first part goes through the methods used for synthesis of both thin films and precursors. The second part describes the methods used for characterization of the synthesized thin films and precursors.

2.1 Synthesis

As extensive work has been done on synthesis of metalorganic compounds in this work, this subchapter is divided in two main parts, synthesis of thin films by ALD and synthesis in inert atmosphere using Schlenk line and glove box.

2.1.1 The ALD technique

In this section first a short review of the history of the ALD technique will be given, followed by a description of the theoretical aspects.

2.1.1.1 History

ALD is a chemical gas phase thin film deposition technique based on alternating self-limiting gas-to-surface reactions. This approach makes it extremely easy to control the thickness and the stoichiometry of the deposited films.

The motivation behind the development of this technique was the desire to produce thin films electroluminescent flat panel displays (TFEL). This is a demanding application as it requires thin films with high dielectric strength, low pin-hole density and uniformity over large-area substrates.

Nevertheless thin films deposited by ALD managed to meet these requirements. The technique was developed and introduced as atomic layer epitaxy (ALE) in the late 1970s by Suntola and his co-workers in Finland [64, 65], and was patented already in 1977 [66]. Shortly after the successful introduction of ALE, the method was investigated for its ability to grow epitaxial semiconductors based on the III-V compounds [67, 68]. Though there were reported many outstanding results, the method has had a limited successes in this field with no reported commercial applications. Meanwhile, depositions for nonepitaxial applications where slowly but steadily taken into investigation, some of the areas examined were solar cells, optics, protective coatings and gas-sensors.

In the 1990s the interest towards ALD increased, mainly due to the fact that the silicon-based microelectronics started to look for new thin film deposition methods. Their present deposition techniques were foreseen to meet major problems with conformality in its next years, due to the ever decreasing device dimensions with also increased aspect ratios.

2.1.1.2 Alternative names

The technique has been given many different names since its introduction in 1977. As mentioned earlier the method was initially introduced as ALE, where the word “epitaxy” translated from Greek means “arranged on”. Epitaxial growth is today commonly used to describe the growth of a single crystalline film on a single crystalline substrate with a well-defined structural relationship between the two. The term epitaxy was in the case of ALE used to emphasize the sequentially controlled surface reactions upon the previously deposited layer [64, 69]. However this use of the term has led to unfortunate confusion when describing growth of amorphous or polycrystalline films by ALE. The ALE name is presently limited to

depositions where epitaxial growth occurs and the most common name today is Atomic Layer Deposition (ALD), which therefore is the chosen name in this thesis. However, in a transition period, the name *Atomic Layer Chemical Vapor Deposition* (ALCVD) was used. This name emphasizes its relationship with the Chemical Vapor Deposition (CVD) technique. Further names for this technique are: *Molecular Layer Epitaxy* (MLE) which highlight the use of molecular precursors, *Digital Layer Epitaxy* (DLE) which emphasizes digital control of the thickness and *Molecular Layering* (ML) which comes from old Russian literature [70, 71].

2.1.1.3 The ALD-cycle

The main characteristic feature of the ALD-technique is the altering self-limiting gas-to-surface reactions obtain by sequential pulsing of the precursors below their decomposition temperatures. The individual precursor pulses are separated by pulses of inert gas to remove excess reactants. This eliminates gas phase reactions between the different precursors as they never meet in the gas phase. In the simplest case, where only two different precursors are used, one ALD cycle will consist of four steps:

- I) Precursor 1 is pulsed into the reaction chamber.
- II) The reaction chamber is purged with an inert gas to remove any surplus of precursor 1.
- III) Precursor 2 is pulsed in to the reaction chamber.
- IV) The reaction chamber is purged with an inert gas again.

This is repeated until the desired thickness of the deposited film is reached. The deposition rate for one cycle depend on the type of precursors used and can vary between 10-1200 pm per cycle [72]. *Figure 2-1* shows the

principles behind one ALD-cycle for the deposition of alumina (Al_2O_3) from trimethylaluminium (TMA, $\text{Al}[(\text{CH}_3)_3]$) and H_2O .

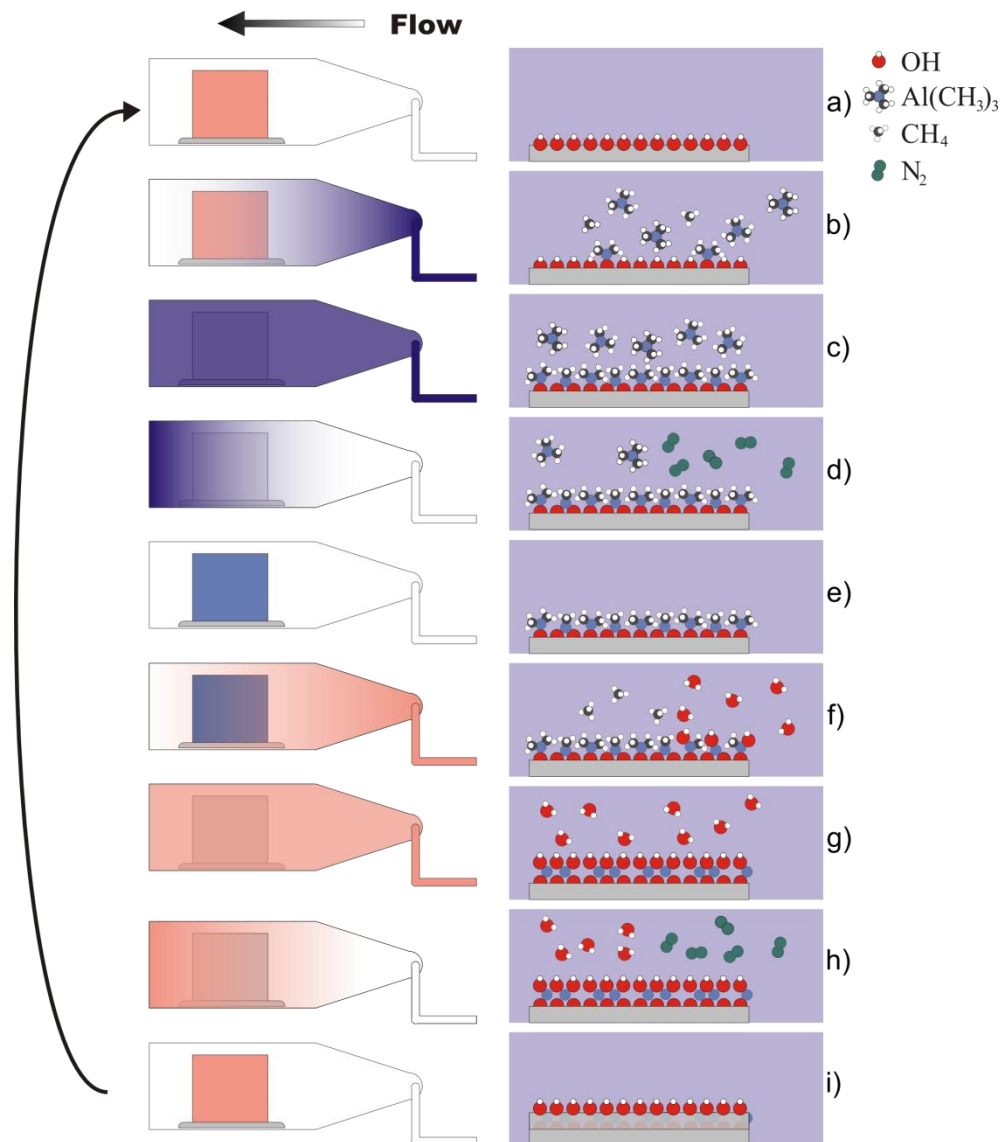


Figure 2-1. A principle sketch of the ALD-process for deposition of Al_2O_3 from TMA and H_2O [73].

In *Figure 2-1*, TMA is first pulsed into the reaction chamber (*Figure 2-1 b*) where it reacts with the available OH-groups on the surfaces present. The result is formation of methane and an aluminum complex chemically

bonded to the surface. The reaction ceases when all available OH-groups have reacted, and a monolayer of aluminum complexes are formed on the surface (*Figure 2-1 c*). At this point the excess TMA molecules will only be physisorbed to the already chemically bonded monolayer on the surface. Due to the weak van der Waal forces involved in the physisorption process this process is fast and reversible. The previous chemical adsorption process is often connected with an activation energy and require thus a certain temperature to proceed. This may therefore be a limiting factor for growth at lower temperatures [70, 74]. The surplus of the TMA precursor, including any physisorbed TMA and byproducts is purged away by an inert gas, in this case N₂ (*Figure 2-1 d*). As mentioned earlier, this purge step is a decisive factor that separates the ALD-technique from other gas phase deposition methods. By purging, unwanted gas phase reactions between the different precursors are avoided. After this purging step the surface is now terminated by methyl groups (*Figure 2-1 e*). When water is pulsed in (*Figure 2-1 f*), the water molecules react chemically with the adsorbed monolayer of aluminium complexes. The reaction again ceases upon completion where there are no more methyl-groups available for reaction with water. Surplus water is then purged away with an inert gas (*Figure 2-1 h*) whereupon the surface again is terminated by OH-groups (*Figure 2-1 i*). The cycle is thereafter repeated until the desired thickness is obtained. This growth mechanism also makes the ALD technique able to perfectly cover surfaces with a complex geometry [70].

2.1.1.4 Demands for the ALD-process

To obtain the characteristics of an ALD process there are some conditions that has to be met. These conditions will be discussed in this section as well as their effect on the quality of the deposited film.

2.1.1.4.1 Precursors

A range of different precursors can be used in the ALD processes such as pure elements, halides, organometallics, metalorganics and pure organic compounds. However a usable precursor must meet some requirements. Probably the most important is that the precursor must be volatile enough to enable transport to the reaction chamber through the gas phase. A rough limit for a suitable vapor pressure is 0.1 mbar at the source temperature used [70]. In order to maintain a self limiting growth it is of paramount importance that the precursor is chemically inert towards reactions with itself and also does not undergo decomposition. This also applies to the byproducts formed during the reactions. However, in some cases precursor decomposition may be accepted, provided that the decomposition proceeds in a surface reaction rate limited manner, thereby maintaining the good uniformity and conformality. Thereafter, the precursor must be sufficiently reactive with the functional groups available on the surfaces present. For instance depositions of metallic films are difficult, due to a lacking chemistry. The ALD growth mechanism does not require a constant flux of the precursor pulsed. The only demand is that the pulse length must be sufficient for a complete coverage of the surface. This allows for use of solid precursors even though the sublimation of these often gives a varying flux [75]. However liquid or gaseous precursors should be preferred, if available, as small particles from a solid precursor may be transported into the reaction chamber and cause detrimental defects. Ideally the precursors used should also be non toxic, inexpensive, as well as easy to synthesize and handle.

It is beneficial to use very reactive precursors, as this often implies low activation energies for surface reactions. This is also termed as having a high sticking coefficient which also involves a high utilization factor of the precursor. *Figure 2-2* shows two different Langmuir-models for how

adsorption can take place on the surface. These models are further used to describe the two different reactions that can take place, depending on the precursors used and on the sample surface during an ALD process.

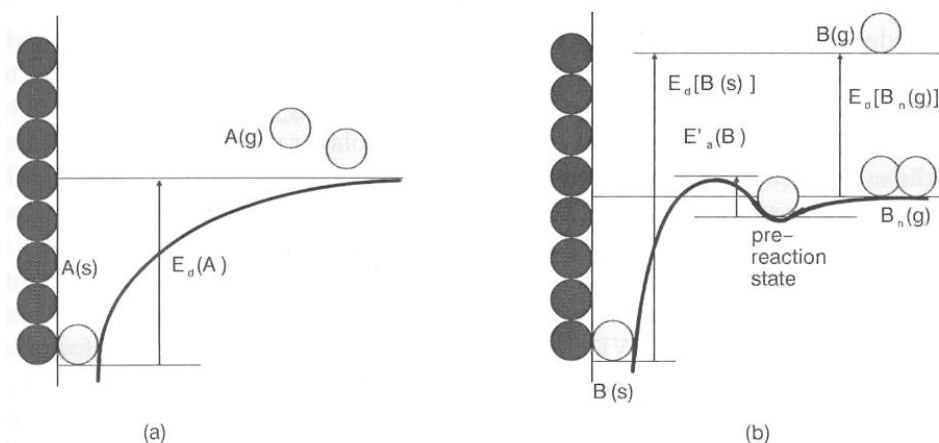


Figure 2-2. Langmuir model of surface energies [69]. In (a) chemisorption of atom A on a B(s) surface take place without a precursor state or an activation energy. In (b) chemisorption of reactant molecule $B_n(g)$ on a A(s) surface via a precursor state $B'(s)$.

Additive reaction

In its early stages, ALD was used with elementary precursors that reacted additive on the surface [70]. Additive ALD growth is based on the use of elements A and B of the compound AB as the precursors. This process demands that both elements must have a suitable vapor pressure for the necessary vapor transport at the growth temperature. Examples of successful additive ALD processes are the growth of several II-VI compounds, such as ZnS, ZnSe, ZnTe, CdS, CdSe and CdTe [69].

In simple words, the basic requirement for monolayer formation is selective desorption, i.e. the desorption rate of atoms A from an A(s) surface should be higher than that of atoms A from B(s) surface. Depending on whether the binding positions are directly available on the surface, the

reaction can take place without any activation energy as shown in *Figure 2-2 a)*. However if a reconstruction of the surface or the precursor molecule is needed, the reaction have an activation energy as shown in *Figure 2-2 b)*.

Exchange reaction using compound precursors

The use of compounds as precursors extends the use of ALD process to materials where the vapor pressures of the elemental components are too low to give rise to the additive mode of the ALD process. The compound precursors reacts with the surface by an exchange reaction, also called ligand exchange reaction [70, 71]. The reaction between TMA and water, which is shown in *Figure 2-1* on page 32, where the methyl groups are exchanged with hydroxyl groups is an example of such an exchange reaction. With use of compound precursors, the self limiting growth mechanism is caused by the remaining ligands on the precursor molecule, which sterically hinders other precursor molecules from binding to the surface, such as the methyl groups in *Figure 2-1 c)* on page 32. These ligands need to be reactive towards the second precursor and, as mentioned earlier, the byproducts from this reaction should not react with the surface or with anything in the gas phase, as this could lead to incorporation of impurities in the film. Exchange reactions follow the reaction pathway described in *Figure 2-2 b)* on page 35, and the byproducts can be important factors regarding the quality and the growth conditions of the deposited film. A deposition process of calcium carbonate (CaCO_3), using $\text{Ca}(\text{thd})_2$ and O_3 as precursors, was improved by pulsing carbon dioxide (CO_2), which is a byproduct from the reaction, into the reaction chamber [76]. On the other hand, deposition of CaO was not feasible due to reactions with the CO_2 byproducts.

Decomposing reaction

Another method that can be used for the ALD-process is in fact decomposing reactions. Here the precursors are first absorbed onto the substrate, in a partial or complete monolayer, before it is exposed to an energy pulse, i.e. laser beam or plasma pulse. The energy pulse decomposes the absorbed precursors and the desired material is deposited in a controlled manner.

The film thickness obtained in one ALD-cycle may be a full monolayer, corresponding to the density of atoms in the corresponding crystal plane of a bulk crystal, or it may be a partial monolayer due to preferred surface reconstructions or steric-hindrance effects related to the precursors used. In ALD the former is true for most processes [77]. Steric-hindrance happens when the physical size of the precursor is so large that it prevents further reactions with the substrate by physically blocking reactive sites from other molecules [69]. The effect of steric-hindrance because of increasing ligand size is illustrated in *Figure 2-3* below.

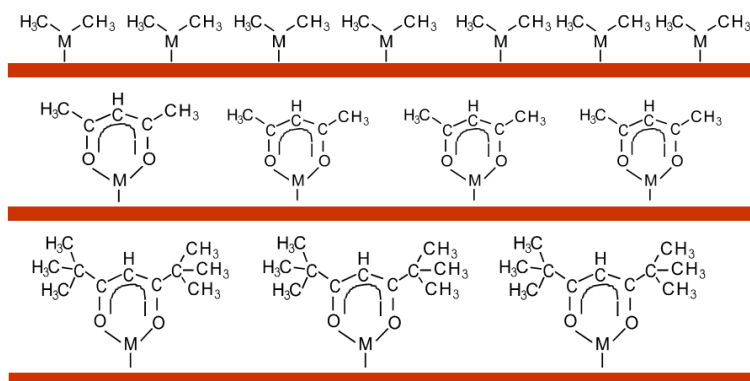


Figure 2-3. An illustration of steric-hindrance as consequence of increasing ligand size on the precursor molecule. *M* represents a metal atom [14].

2.1.1.4.2 ALD temperature window

The most important parameter available to control the saturation mechanism of an ALD process is the deposition temperature. To keep the precursors in the gas phase a specific minimum temperature is needed, some temperature is also necessary to desorb any physisorbed byproducts or excess precursor molecules. Assuming that sufficient pulse times are being used, the effects of different deposition temperatures on the growth rate can be studied, see *Figure 2-4*.

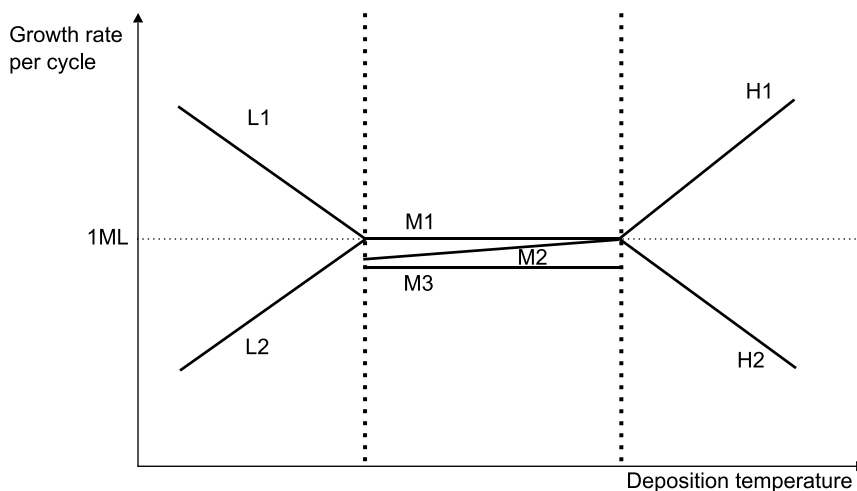


Figure 2-4. Temperature windows of ALD deposition. The letters denotes the different growth conditions, which is described in the text below.

It's important to note that the saturation mechanism is unlike for the different precursors utilized, and that the total growth rate is a consequence of the whole process. The temperature can be mainly divided into three regions, low, medium and high temperature.

For the first region *low temperature (L)*: A decrease in growth rate as the temperature is raised may indicate that the temperature at deposition is too low and that the precursor is condensed in monolayers on the surface (L1). An increase in growth rate per cycle as the temperature is raised may denote that the process is limited by an activation energy, meaning that the

precursor molecules do not form chemical bonds readily with the surface (L2). By increasing the pulse time of the precursor, a saturated growth can be obtained in this region as well, at the expense of an increased deposition time.

Medium temperature (M): A constant growth rate of one monolayer (1 ML) over a certain processing window, means that a complete saturation of the surface is obtained by the precursor molecules. This also indicates that steric-hindrance and surface reconstructions are of negligible importance (M1). A slow increase in growth rate per cycle as the temperature is raised denotes the case when improved surface diffusion of the precursors makes them pack more closely together (M2). A constant growth rate of less than one monolayer per cycle in a given temperature window denote that steric-hindrance or surface reconstructions may take place (M3).

High temperature (H): An increase in growth rate per cycle as the temperature is raised indicates that the precursor is decomposing, leading to an uncontrolled deposition (H1). A decrease in the growth rate per cycle as the temperature is raised denote that adsorbed precursor molecules are evaporating from the surface, or that surface ligands that is essential for the reaction with the next precursor is dissociating.

2.1.1.4.3 Pulse- and purge window

In the same manner as for the temperature window for the ALD process, there also exist pulse- and purge windows. *Figure 2-5* below shows how the growth rate can be affected by the pulse time of a given precursor.

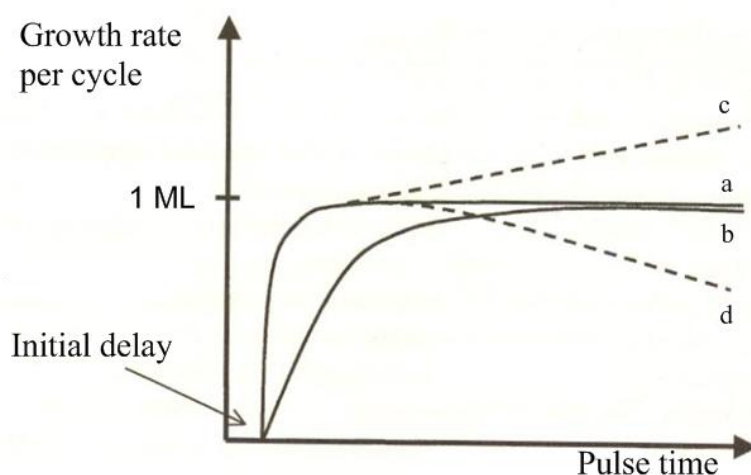


Figure 2-5. Pulse window for the ALD process. The letters denotes the different growth conditions, which is described in the text below [70].

If a reactive precursor is used, the kinetics for the surface reactions is fast, giving rise to a rapid saturation of one monolayer (1 ML) of precursors molecules on the surface *Figure 2-5* (a). If a less reactive precursor is used the reaction kinetics is slower, meaning a longer pulse time is needed to reach the saturation of one monolayer at the surface *Figure 2-5* (b). As the pulse time is increased in both cases (a) and (b) the growth rate may increase due to decomposing of the precursor after chemisorption, *Figure 2-5* (c), or a decrease in growth rate due to etching reactions or diffusion of the precursor into the substrate after the chemisorption, *Figure 2-5* (d) [70]. As *Figure 2-5* indicates, too small pulse times results in incomplete saturation of the substrate, which results in gradients in the deposited film. The steepness of such gradients can give a indication on the reactivity of precursors where a steep gradient indicates highly reactive precursors [69].

Regarding the purge time, an increase in growth rate as it is reduced, with also increased thickness gradients, may indicate a too short purging time. The increase in growth rate for too short purging times may be due to a gas phase reactions as the different precursor may meet in the gas phase, or

insufficient desorption of physisorbed precursors. On the other hand if the purge time is too long, a decrease in thickness may result due to desorption of the precursor or the film material.

It is therefore important to keep the pulse and purge times sufficient to respectively saturate the surface and remove any excess precursors, while avoiding the undesirable effects described above. However, the length of the pulse- and purge times is often more dependent on the reactor used rather than the type of precursor [70].

Since a constant flux of the precursors is not demanded the process is rather robust. This together with the fact that the process is also often unaffected by small changes in the temperature gives good reproducibility, and makes the process straightforward to scale-up.

2.1.1.5 The quality of the deposited film material

For the ALD-process the type of substrate material is not a critical factor for obtaining the characteristic ALD-growth. After deposition of the first monolayer the further growth conditions is ideally only affected by the chemical reactions. Formation of the first monolayer may however be strongly affected by the substrate [78]. This can result in almost non-linear growth in the beginning of a deposition, owing to nucleation problems at the surface. This is often observed for growth on hydrogen terminated surfaces, obtained by etching silicon in hydrofluoric acid [79]. The result is that a complete coverage of the substrate may not be obtained before a certain number of deposition cycles are reached, maybe resulting in as much as 10 nm of film material. This phenomena needs to be considered when depositing very thin films.

A good overview over nucleation in the ALD-process, and the effects substrates has on the deposited film can be found in a review article from 2005 [71] and simulations in the following references [80-82].

Good adhesion between the substrate and first deposited monolayer is critical for the potential use of the deposited film in different applications. A weak adhesion between the substrate and the deposited film may result in delamination of the film. Differences in the thermal expansion coefficient between the substrate and the film can build enough strain to delaminate the film from the substrate. This is especially important when dealing with thick films deposited at a high temperature, as the tension that builds up in the film under cooling is larger for thicker films [74].

The choice of substrate material is, however, important for the texture of the deposited film. The substrate can influence the orientations of the first crystals that form on the surface, thereby effectively directing the orientation of the deposited film. If the material that is being deposited has the possibility of many meta-stable phases, the substrate can guide which one of these phases that will be formed [83]. The factors mentioned above concerns crystalline substrates; however it's important to note that the deposited film can be amorphous when deposited on a crystalline substrate and vice versa on amorphous substrates.

However, crystalline substrates with different orientations can affect the growth rate, as the first crystals can align with the substrate resulting in different growth directions with their respective growth rates [69, 74].

Contaminations in the deposited film are often a result of incomplete reactions giving incorporation of ligands. By increasing the temperature the probability of incomplete reactions decreases, however, if the temperature is raised too high the precursor may start to decompose, giving rise to new impurities [70]. The pulse time can also be increased to

obtain complete reactions, and thereby decreasing the amount of impurities incorporated in the film, however, this will increase the process time and consumption of precursor [69, 70].

The good control of thickness and stoichiometry makes the ALD process well suited for deposition of multilayer structures and complex oxides, and crystallinity is enhanced by formation of a mixture of different atoms at an atomic level [69, 70, 74].

2.1.1.6 Advantages and limitations of the ALD method

The largest limitation of the ALD technique is usually the low growth rate. This can, however, be compensated by scaling-up so that deposition can be done on a large numbers of substrates, or a large substrate-area at the same time. Also the ever shrinking film thicknesses utilized in integrated circuits overcomes this major limitation. A more widespread problem has been the lack of good and cost-effective processes for deposition of some important materials such as Si, SiO₂, Si₃Ni₄ and metals [70]. However, this is an area of increased research [71]. Selective surface growth is beneficial for patterning of films, but is generally difficult to obtain for ALD growth due to the use of highly reactive precursors. There have, however, been some successful attempts in this area. Surface-selective ALD growth was obtained by using PMMA poly(methyl methacrylate), which acted as a passivating layer for ALD growth for some materials [84].

The advantages and limitations of the ALD technique are summarized below in *Table 2-1*.

Table 2-1. Advantages and limitations of the ALD process.

| Advantages | Limitations |
|--|--|
| - Accurate and simple thickness control | - Low growth rate |
| - Precise and easy stoichiometry control | - Depend on that favorable chemical reactions exist |
| - Can utilize highly reactive precursors | - Difficult to obtain a surface selective growth |
| - High quality materials are obtained at low processing temperatures | - Lack good and cost-effective processes for deposition of some important materials as Si, SiO ₂ , Si ₃ Ni ₄ and metals |
| - No problems with inconstant vaporization rates of solid precursors | |
| - Excellent conformality | |
| - Good reproducibility | |
| - Straightforward scale-up | |
| - Good purity | |
| - Depositions can be done over a large temperature window | |
| - Can utilize many different materials for substrates | |

2.1.1.7 Finding suitable bismuth precursors

From the prior art given in section 1.2.2.2 it is obvious that a new bismuth precursor has to be found in order to successfully deposit thin films of Bi₂O₃ and BiCoO₃ by ALD. When planning a new ALD process and choosing precursors for it, prior art should be investigated. Therefore the goal of the following literature survey was to search for possible candidates for a new bismuth precursor, by excluding precursors based on the information found in the literature. When searching for new ALD precursors one should keep in mind the requirements discussed in section 2.1.1.4.1 on page 34.

A short version of the different types of ALD precursors used can more or less be summarized as: In the first ALD experiments in the 70s elements and metal halides were used. In the 80s the selection of precursors widened to metal complexes (alkoxides, β -diketonates) and simple organometallics (alkyl compounds). Before new metal (Cp-compounds, alkylamides) precursors was introduced in the 90s [85].

The types of bismuth precursors that were chosen to investigate in this work were metalorganic and organometallic, as both amines [9] and inorganic precursors as halides [70, 77, 86] seems like a dead-end, due to poor thermal stability and due to contamination and corrosive by products, respectively.

2.1.1.7.1 Metalorganic precursors

The metalorganic precursors discussed below can be divided into two groups, alkoxides and β -diketonate precursors.

Alkoxides

Alkoxides reacts readily with water, and have been used for the growth of several different oxide materials by ALD [70, 77]. Bismuth alkoxides as methoxide, ethoxide and isopropoxide have been investigated in ref. [87]. Bismuth methoxide is insoluble in all common solvents whereas the ethoxide and isopropoxide is slightly soluble, reflecting a polymeric or oligomeric structure. These compounds also indicates poor thermal stability as they gives low yields under sublimation, which is likely to be caused by decomposing [87]. These alkoxides of bismuth are therefore not promising candidates as ALD precursors. However, $\text{Bi}(\text{t-OBu})_3$ is soluble in common solvents and is volatile [88]. The crystal structure of $\text{Bi}(\text{t-OBu})_3$ have not been established, even though several attempts have been made

[89, 90]. The molecule have, however, been characterized in the gas phase by electron diffraction and it is reported to be monomeric [91]. $\text{Bi}(\text{t-OBu})_3$ seems, based on the available literature, as a promising candidate for a bismuth precursor for ALD. The alkoxide precursor $\text{Bi}(\text{mmp})_3$ will not be investigated, as it is reported deposited with ALD in the Bi-Ti-O system [44, 45], and it is therefore likely to assume that it also has been tried for deposition of Bi_2O_3 .

β -diketonate complexes

Metal β -diketonate complexes have been used extensively in oxide MOCVD [92] and ALD [70]. Compared to the alkoxides the β -diketonate precursors are generally not reactive towards water, due to having a stronger metal oxygen bond than the alkoxides. Instead O_3 has to be used as oxidizing precursor, which has the drawback that it is more likely that some impurities as carbonates can be incorporated in the film. $\text{Bi}(\text{thd})_3$ have been utilized in MOVCD for deposition of Bi_2O_3 films [93]. The other β -diketonate precursors such as tfac and hfac can lead to fluorine contamination in the deposited films [94], and $\text{Bi}(\text{acac})_3$ is not reported used in the literature. From the β -diketonate complexes $\text{Bi}(\text{thd})_3$ seems like an good candidate for precursor in ALD depositions.

2.1.1.7.2 Organometallic precursors

Organometallic precursors have been widely utilized for ALD as they are very reactive, the TMA and H_2O process described earlier is an example [77]. However, regarding the BiMe_3 precursor, there are some conflicting reports in the literature. In ref. [95] it is reported to only react slowly with O_2 and H_2O , and in ref. [96] it is reported to be explosive. If it indeed is explosive it could be suitable as a bismuth precursor for ALD. However, if

it is less reactive towards O₂ and H₂O, the similar compounds with longer organic chains, as BiEt₃, will most likely also be less reactive. Based on the conflicting statements in the literature, as well as the compound is not available commercially, and a potential synthesis involves a product that may or may not be explosive, it was decided not to investigate this type of compounds any further.

Cyclopentadienyl compounds [97] and cyclopentadienyl derivatives [98] have been used for ALD. Therefore these types of compounds are interesting to investigate as potential bismuth precursors. However, BiCp₃ undergoes polymerization already around 15°C [99], and are extremely light sensitive. These types of compounds do not seem suitable as bismuth precursors in this work.

BiPh₃, as mentioned earlier, grows if deposited in the Bi-Ti-O [8, 11] and Bi-Si-O [11] system, it would therefore be interesting to test if it also grows in the Bi-Co-O system. In addition it would also be interesting to try to obtain a better understanding for why this precursor can be used for deposition of complex oxides and not bismuth oxides.

The bismuth precursor used for deposition of the (1-x)BiCoO₃-xBiFeO₃ solid solution system by MOCVD [17, 31], BiMe₂(DMP), seems like an interesting candidate for a suitable bismuth precursor for ALD. It was first reported synthesized in 2006 by T. Furukawa et al. in Ref. [96, 100]. It is reported to be a liquid with a high vapor pressure and a reasonable thermal stability, as it decomposes at 230 °C. It is relatively stable towards moisture and air which is not ideally for an ALD precursors, however, it makes it is easy to handle. Also no evidence was found for any incorporated nitrogen in the deposited films by MOCVD [96].

2.1.1.7.3 Summary and choice of bismuth precursors

Based on the literature survey in this section the chosen precursors for investigation are: BiPh_3 , $\text{Bi}(\text{thd})_3$ and $\text{Bi}(\text{t-OBu})_3$. The precursors will be investigated in said order, which is based on availability as BiPh_3 is available commercially and $\text{Bi}(\text{thd})_3$ have been synthesized in our group before. The chosen precursors are also chosen as they are from different types of precursors, aryl-, β -diketonate- and alkoxide-complex. Synthesizing and investigating $\text{BiMe}_2(\text{DMP})$ as an ALD precursor would also be interesting, if time allows it.

2.1.2 Synthesis of metalorganic precursors for ALD

Here the reactions and techniques for synthesizing the metalorganic precursors used in this work, $\text{Co}(\text{thd})_2$, $\text{Bi}(\text{t-OBu})_3$ and $\text{Bi}(\text{thd})_3$, will be given. The synthesis of the mentioned bismuth precursors needs inert conditions, which was done utilizing a schlenk line and a glove box.

2.1.2.1 Synthesis under inert atmosphere

For the synthesis of air/moister sensitive compounds, a Schlenk line and a glove box can be used, see *Figure 2-6* and *Figure 2-7* respectively. The Schlenk line, which is named after its creator Wilhelm Johann Schlenk, consists of two connected glass tubes where one is connected to an inert gas flow and the other to vacuum. This allows for switching between vacuum and inert gas conditions, which again allows for the following to be carried out on the line without exposure to air: reactions, filtration, removal of solvents, mixing of reagents, degassing of liquids and distillation.

The glove box is a sealed box with an inert atmosphere in which reactions, that are air sensitive, can be carried out. In the glove box one can bring most of the equipment needed to carry out a synthesis, however, as

vacuum has to be pumped on everything that goes in, liquids are more cumbersome to bring inside. Also due to cross contamination solvents cannot be evaporated inside the glove box, neither is it suitable to work with volatile compounds, for the same reason.

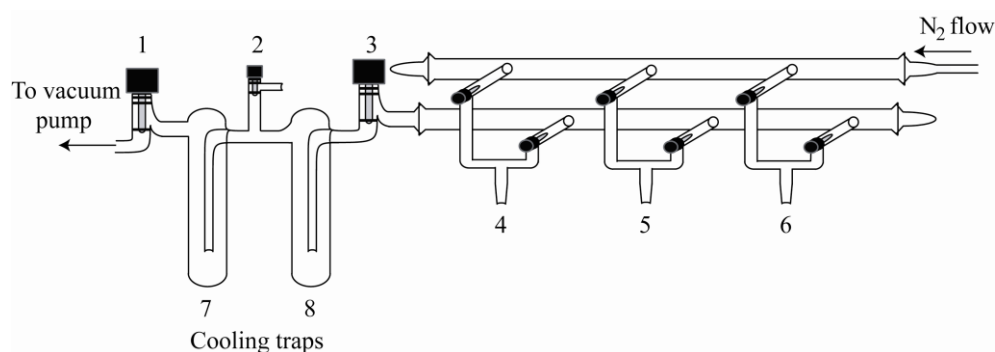


Figure 2-6. A schematic illustration of a Schlenk line. The valves 1, 2 and 3 control the vacuum on the line. Tube 4,5 and 6 is where compounds can be connected to the line, allowing for switching between inert gas and vacuum conditions. 7 and 8 are cooling traps, where trap 7 is lowered in liquid nitrogen when volatile compounds are connected to the line.



Figure 2-7. A picture of a glove box. The two airlocks can be seen on the right side.

2.1.2.1.1 Techniques for synthesis in inert atmosphere

Working with a Schlenk line requires some techniques, these are explained below. The main point can be summarized as to always use the overpressure of an inert gas on the line to keep air away from the system. For the following procedures a Schlenk flask is used, see *Figure 2-8*.

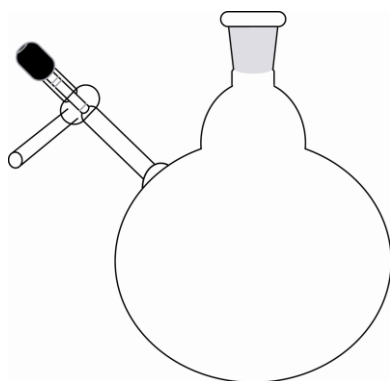


Figure 2-8. An illustration of a Schlenk flask. The side entrance allows the flask to be attached and removed from a Schlenk line without exposing its content to air, by feeding inert gas through it.

Before attaching the inert gas supply onto the side entrance of a Schlenk flask, the air inside the entrance tube has to be removed. This can be done in two different ways. If the Schlenk flask is attached to a Schlenk line, let the inert gas flow go through the flask and out the side tube before attaching the inert gas supply to it, *Figure 2-9 A*). If the flask is not attached to a Schlenk line, a septum and a needle is used, *Figure 2-9 B*).

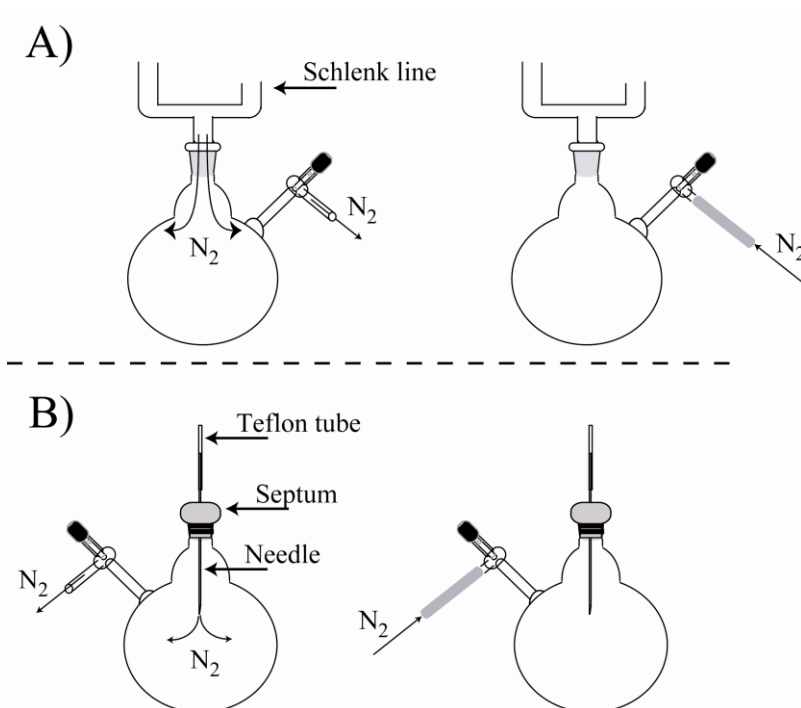


Figure 2-9. Procedures for attaching the nitrogen supply to the side entrance of a Schlenk flask. A Schlenk line can be used as shown in **A**), or a septum and a needle as shown in **B**). The flask can now be mounted/detached from a Schlenk line without exposing its contents to air.

In the description of the following procedures the nitrogen supply has already been mounted on the side entrance on the Schlenk flask.

For removing a Schlenk flask from the Schlenk line, with minimal exposure to air, the following steps are carried out, see *Figure 2-10*.

- A) Open the inert gas supply on the side of the flask.
- B) Remove the flask from the line. The overpressure of inert gas keeps the air away. Proceed to step C) as fast as possible.

- C) Seal the flask with a cap or a septum, and close the valves on the line and on side of the flask.

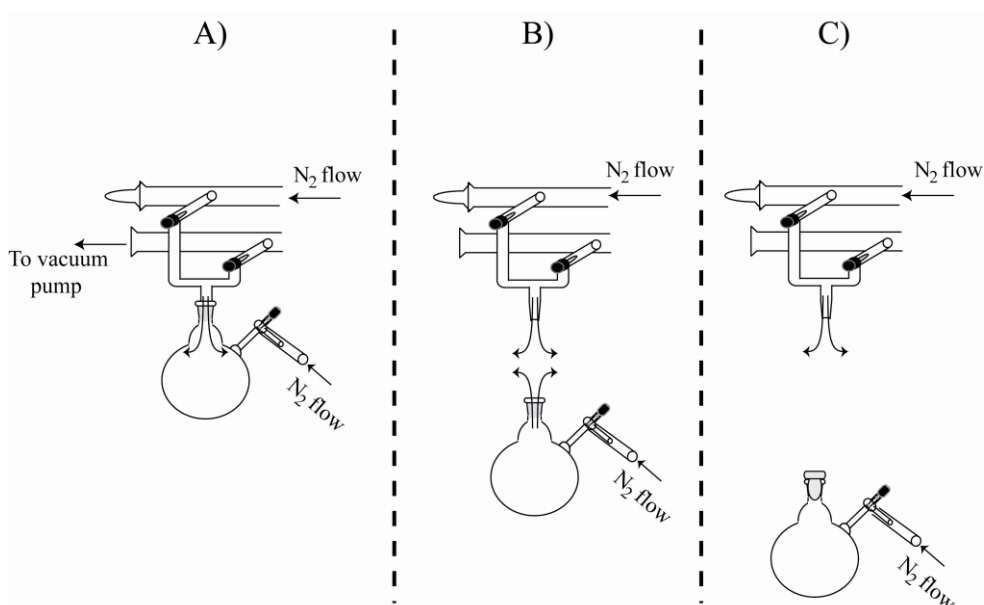


Figure 2-10. Illustration of procedure for detaching a Schlenk flask from the Schlenk line, with minimal exposure to air. When attaching the Schlenk flask, the procedure is done in reverse. The small arrows indicates nitrogen flow.

For attaching a flask to the Schlenk line the reverse order is used.

For transferring liquids from one Schlenk flask to another, the following steps are done, see *Figure 2-11*.

A)

1. Pump vacuum on the flask the liquid is going to be transferred to.
2. Then fill it with inert gas.

Step 1 and 2 are repeated three times for “washing” the flask properly.

B)

On the flask with the liquid, open up the side valve so inert gas flows in.

Stick a teflon tube through the septum, however do not let the teflon tube get in contact with the liquid.

C)

Stick the teflon tube through the septum on the line, thus connecting the two flasks. Push the teflon tube into the liquid, and open up the side valve on the flask which the liquid is being transferred to. The overpressure of nitrogen will now push the liquid through.

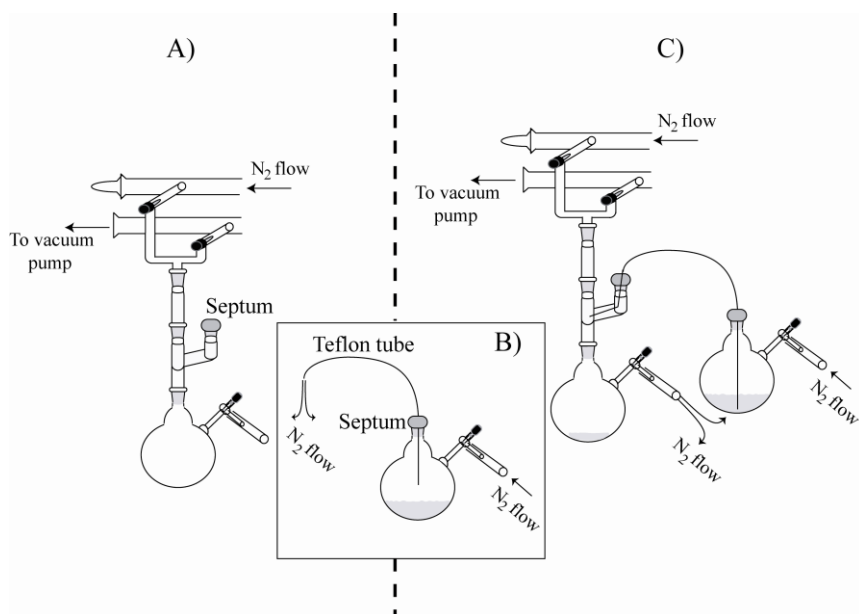


Figure 2-11. Illustration of procedure for transferring liquids from one Schlenk flask to another. The small arrows indicate nitrogen flow.

When filtering a liquid, a needle is used on the flask show in B) in *Figure 2-11*. How the needle is mounted is shown below in *Figure 2-12*.

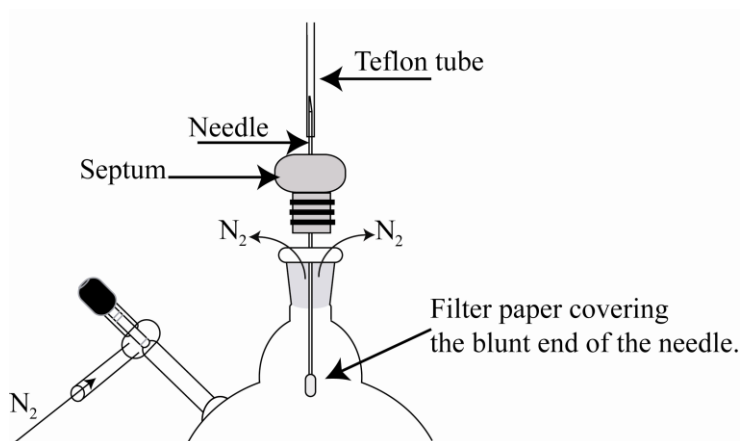
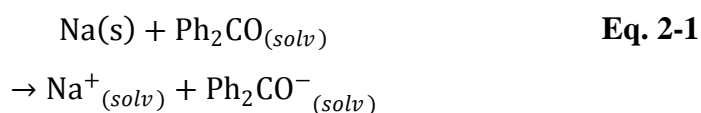


Figure 2-12. How a needle is mounted, through a septum on a Schlenk flask, for filtering liquids.

2.1.2.1.2 Drying of solvents

Solvents may be dried using conventional distillation apparatus. However, in order to avoid dangerous or undesirable reactions, it is important to make the right choice of drying agent. For the hydrocarbons used in this work, hexane and tetrahydrofuran (THF), sodium together with benzophenone was used as a drying agent. Sodium was chosen as it is widely used to dry hydrocarbons and ethers [101], and it also reacts with benzophenone to give a dark blue ketyl radical, see *Eq. 2-1*, which is protonated by water to give colorless products. Thus the sodium-benzophenone system is particularly convenient because it is self-indicating, as to if there are water left in the solution.



When the liquid is dark blue the solvent is dry and is distilled off. The sodium residues are destroyed by slow and careful addition of ethanol until

hydrogen evolution ceases. When this method was applied for drying of hexane a small amount of (50-100 ml/L) of diglyme (diethylene glycol dimethyl ether, b.p. 162 °C) was added in order to dissolve the ketyl. The high boiling point of diglyme allows for easy separation during distillation.

This method was not used for drying of methanol, as alcohols reacts with sodium to forms sodium alkoxides. Methanol was dried by distillation with added CaH_2 .

2.1.2.1.3 Transportation of solvents to glove box

When transporting chemicals into the glove box they have to go through an airlock, where vacuum is first pumped before the lock is filled with inert gas. This means that the container, in which the chemicals are, needs to withstand vacuum conditions. Therefore, before a liquid can be transported into a glove box it has to be degassed. The degassing is done by connecting the flask, containing the liquid, onto the Schlenk line. The liquid is then freeze solid by lowering the flask into liquid nitrogen, and then vacuum is pumped on the flask. The liquid is allowed to melt under a static vacuum, resulting in that only the vapor pressure of the liquid is left inside the Schlenk line and the flask. The flask is then closed and removed from the Schlenk line. The flask containing the degassed liquid can then be transported into the glove box. This procedure also removes any air that could be solved in the liquid, which would ruin the air sensitive compounds.

2.1.2.1.4 Purification of products

Synthesizing precursors often yields some unwanted phases, together with a mixture of salts, solvents or other by-products. The wanted product has to be separated from these, before it can be used as a precursor. This is performed in a sublimation oven, see *Figure 2-13*.

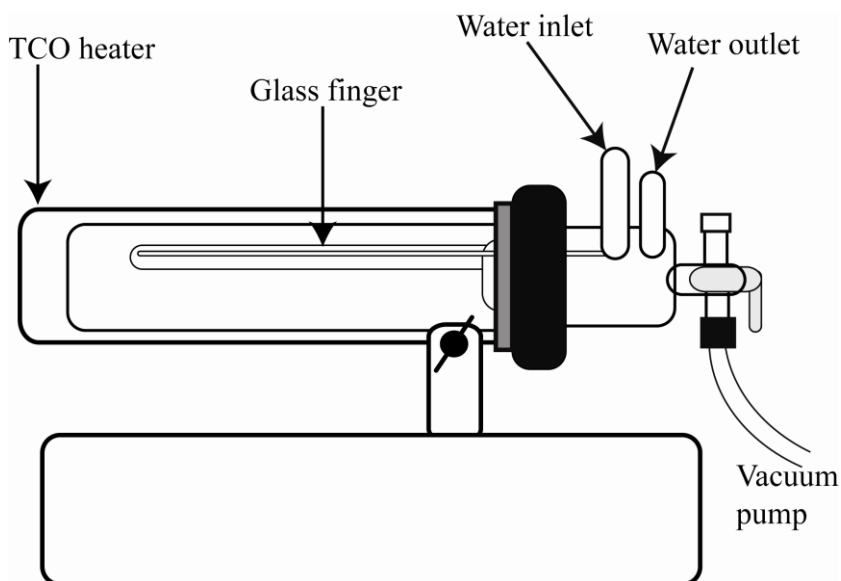


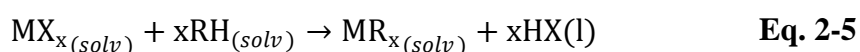
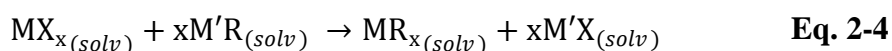
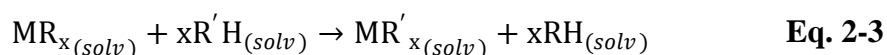
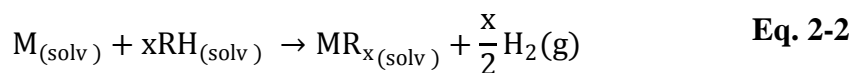
Figure 2-13. A schematic picture of a sublimation oven. The temperature on the glass finger is controlled by water from a temperature controlled bath. The TCO (transparent conducting oxide) heats the oven.

During sublimation, vacuum is maintained by constant pumping. The sublimation is performed by heating the oven up to a certain temperature, where the wanted compound starts to sublime, leaving less volatile by-products behind. The glass finger is kept at a lower temperature allowing the sublimated compound to condensate on the finger, however, the temperature on the finger is high enough that any volatile by-products will not condensate.

2.1.2.2 Reactions for manufacturing metalorganic compounds

Metalorganic compounds can be synthesized by reacting a metal with an organic group, reacting two metalorganic compounds with each other or reacting a metalorganic compound with an inorganic compound [102]. However, only highly electropositive metals like alkali and some of the alkali earth reacts directly with organic groups and these are even limited to

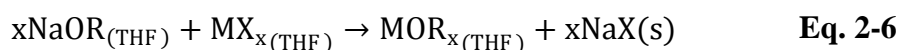
relative reactive organic compounds, such as alcohols [88]. As a consequence synthesizing metalorganic compounds often involves many steps. In this work four different reactions are used for the synthesis of metalorganic compounds, given in *Eq. 2-2* to *Eq. 2-5*.



In *Eq. 2-2* a metal (M) reacts directly with an organic group (RH). The reactions in *Eq. 2-3* and *Eq. 2-4* are called ligand substitution. In *Eq. 2-3* a metalorganic compound (MR) substitutes its ligands with an organic compound (R'H). In *Eq. 2-4* a metal halide (MX) substitutes its ligands with the ligands of a metalorganic compound (M'R). In *Eq. 2-5* a metal halide (MX), where chlorides are the most common, reacts directly with an organic group (RH).

2.1.2.2.1 Synthesis of metalalkoxides

As mainly only alkali earth metals reacts directly with alcohols, the synthesis of other metalalkoxides can be done by reacting a metal halide with sodium alkoxide. The resulting ligand exchange reaction is shown in *Eq. 2-6*. The starting compounds are complexed with THF, and the reactions are carried out under inert conditions.

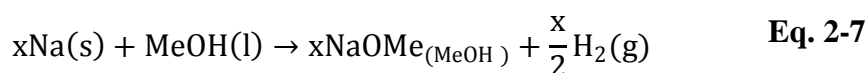


The solvent is then removed, and the resulting product is dried and sublimated.

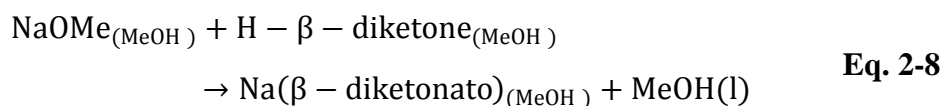
2.1.2.2.2 Synthesis of β -diketonato complexes

There are many methods for synthesizing β -diketonato complexes [92, 103-106]. In this work two different methods are used, hereafter called method 1 and method 2.

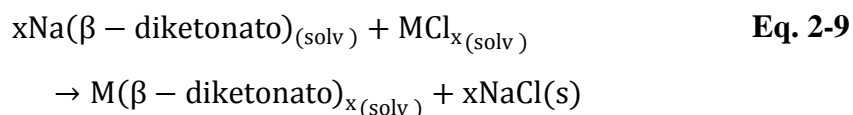
Method 1, described by Baum et al. in ref. [105], is a ligand substitution between a sodium β -diketonato complex and a metal chloride. The first step is to make sodium methoxide (NaOMe) in a surplus of methanol, see *Eq. 2-7*.



The sodium methoxide from *Eq. 2-7* can then be reacted with the β -diketone to yield sodium β -diketonato complex, see *Eq. 2-8*.

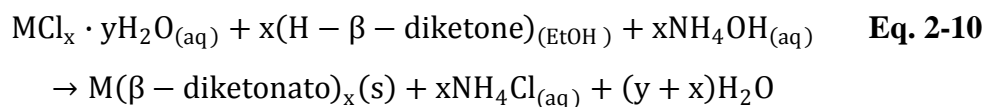


The solvent (MeOH) is removed under vacuum. The obtained sodium β -diketonato complex and the metal chloride are dissolved in a solvent, mixing these two solutions yield the metal β -diketonato complex, see *Eq. 2-9*.



The solvent is removed, the product is dried and the wanted metal β -diketonato complex can be separated by sublimation.

Method 2, which are described by Hammond et al. [104], is a direct reaction between the metal chloride and the β -diketone in aqueous ethanol, where concentrated ammonia is added to push the reaction towards completion, see *Eq. 2-10*.



The product is filtered, dried and the wanted metal β -diketonato complex is separated by sublimation.

2.2 Characterization techniques

This section is divided in four parts, the first describes methods based on X-ray diffraction, the second spectroscopy, the third microscopy, and the fourth characterization of growth mechanisms and thermal properties of precursors.

2.2.1 X-ray diffraction (XRD)

First X-ray diffraction will be discussed generally, before a more detailed description will be given on the different methods used in this work.

X-rays have a wavelength that is comparable to the distance between crystallographic planes in a crystal, which makes X-rays very suitable to characterize crystalline materials by diffraction. XRD can give information on the crystallographic structure, composition, texture and the size of the crystallites in the studied material. XRD can be used to characterize single-crystals, powders and thin films. For analysis of thin films X-rays can also be used to measure the thickness of deposited films, even if they are amorphous. In addition, information about surface roughness and density of the films can be obtained.

Diffraction occurs as the incident X-rays are scattered elastically from the crystal planes in a crystal. For diffraction to take place, Bragg's law (*Eq. 2-11*) has to be fulfilled [107].

$$2d_{hkl}\sin\theta = n\lambda \qquad \text{Eq. 2-11}$$

where λ is the wavelength of the X-rays, n is a whole number, d is the distance between the crystallographic planes in the crystal and θ is the angle between the incident beam and the crystal plane. By keeping λ constant, different values of d can be determined by varying the θ angle for the incident X-rays. *Figure 2-14* below shows the principle for X-ray diffraction.

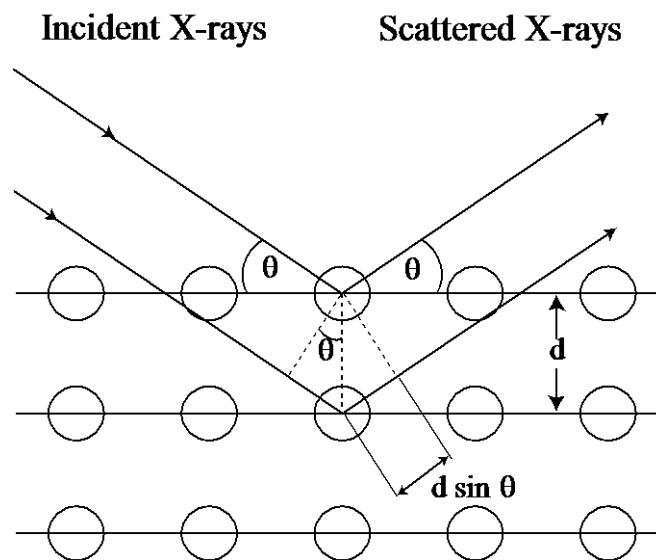


Figure 2-14. Schematic representation of the atoms in a crystal, and how the crystallographic planes give rise to diffraction. The phase difference between the scattered X-rays determines whether constructive or destructive interference occurs.

As a reminder the scattering vector \mathbf{Q} , which will be used in the following explanations, is defined as the scattered beam minus the incident beam [108], see *Figure 2-15*.

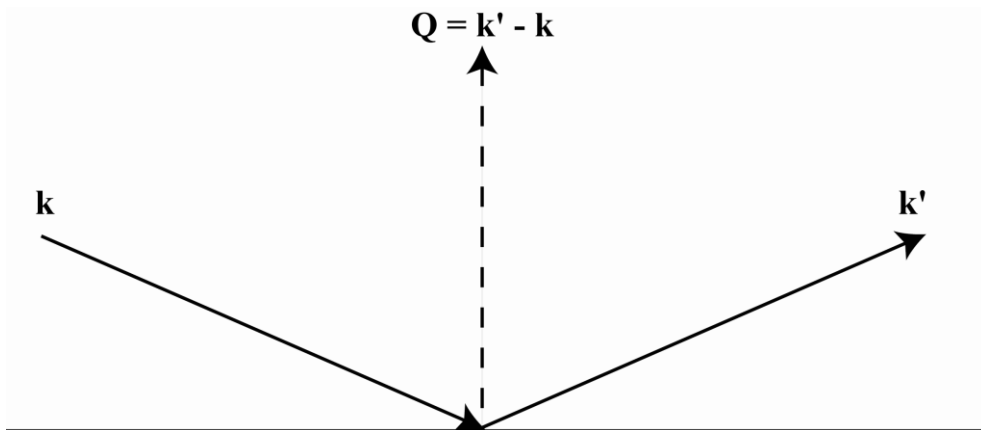


Figure 2-15. Definition of the scattering vector \mathbf{Q} such that the incident beam $\mathbf{k} + \mathbf{Q}$ equals the scattered beam \mathbf{k}' . In elastic scattering the magnitude satisfy $k' = k$.

2.2.1.1 Diffraction from thin films

The intensities of diffractograms from thin films are generally different from the ones from their respective bulk materials. The reason for this difference is that the majority of crystallites in thin films may be oriented in some preferred direction with respect to the substrate surface. This is called preferred orientation or texture. The reason for these variations in intensities is that some crystallographic planes reflects the beam more often than in a randomly oriented sample. With respect to the shape of the reflections in bulk diffractograms, the observed reflections from thin films may also be broader and have a slightly different position due to strain between the film and the substrate, or due to small crystallites sizes [109]. The broadening of the reflections can provide information about the approximate crystallites sizes by using the Scherrer equation, see *Eq. 2-12*.

$$t = \frac{K\lambda}{B \cos \theta_B} \quad \text{Eq. 2-12}$$

where t is the diameter of the crystallites, K is a shape factor that normally is 0.9 and λ is the wavelength of the incident X-rays. θ_B is the Bragg-angle, the angle of the initial reflection that is being studied, and B is the full-width at half-maximum (FWHM) value in radians of the peak being studied with respect to a standard, see *Eq. 2-13*.

$$B = \sqrt{B_M^2 - B_S^2} \quad \text{Eq. 2-13}$$

where B_M and B_S is the FWHM value in radians of the peak being studied and the standard material, respectively. By using the value 0.9 for the shape factor, the crystallites are assumed to be spherical [109]. It should be noted that the calculated crystallites sizes obtained by this equation is only a very rough approximation.

2.2.1.2 Diffraction techniques

This chapter explains the different diffraction techniques used in this work.

2.2.1.2.1 θ - 2θ Reflection geometry

In this setup a monochromatic parallel beam illuminates the sample at an angle θ and the diffracted beam is registered by a detector at the same angle, see *Figure 2-16*. As a consequence, this technique gives the intensities of the diffracted planes as a function of the 2θ angle. In the reciprocal space the scattering vector \mathbf{Q} is always perpendicular to the sample surface, and it only changes its length during the measurement. Thus this setup can only give information about the crystallographic planes that are aligned parallel with the surface [109], and the preferred orientations of the film are the same as the observed peaks. By measuring the broadening of these peaks, an

approximation about the sizes of the crystallites in the direction normal to the substrate can be obtained by the Scherrer equation.

Preferred orientation is not a problem when analyzing powder samples in this setup, as the powder is randomly oriented on the sample holder. In this work θ - 2θ reflection geometry was used to analyze thin films and powder samples.

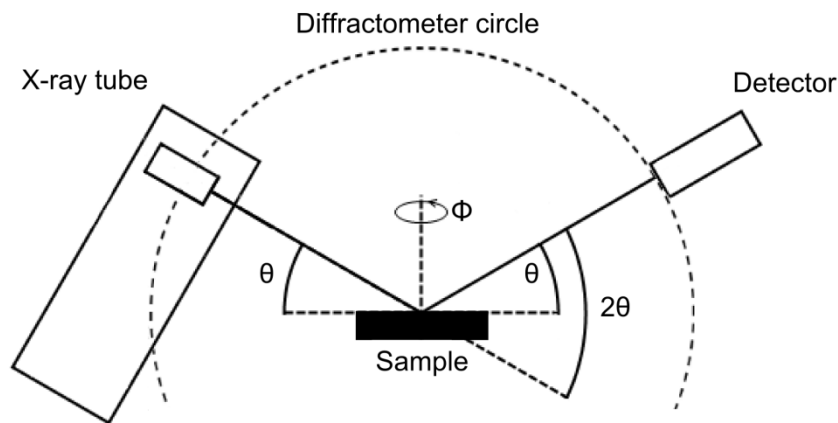


Figure 2-16. Illustration of θ - 2θ reflection geometry. The sample can be rotated around its plane (Φ axis).

2.2.1.2.2 Grazing incident X-ray diffraction, GIXRD

In GIXRD the incident beam is kept at a constant low angle, α , with regard to the sample surface during the measurement [109]. The measurement is performed by moving the detector along the diffraction circle. This is the decisive distinction compared to the symmetric configuration where the entrance angle θ is also varied during the measurement. However, the scattering angle 2θ again denotes the angle between the outgoing beam and the elongation of the incoming beam. By plotting the measured intensity versus 2θ , Bragg reflections are found at comparable positions as with the θ - 2θ measured pattern. During the measurement the \mathbf{Q} vector starts almost

parallel with the sample surface normal, it increases in length and moves towards the incident beam, as the detector is moved in the same direction. Therefore in the GIXRD configuration reflections with distinct Bragg angles θ_{hkl} are caused by lattice planes that are neither parallel with the substrate surface nor with each other. As a low incident beam angle is used, this technique gives little to none reflections from the substrate and a large area of the film is analyzed. In this work GIXRD was used to give supplementary information, regarding analysis of thin films, to the θ - 2θ reflection measurements.

2.2.1.2.3 θ - 2θ Transmission geometry

In this setup the intensity is recorded as a function of the 2θ angle. The sample is crushed into a fine powder which is then placed inside a capillary tube, with a typical diameter of 0.5 mm. The use of a capillary tube allows for air sensitive samples to be measured, as the sample can be prepared inside a glove box. During the measurement the tube is rotated, and is placed such as the X-rays goes through the sample before reaching the detector. By rotating the sample the effect of preferred orientation of the crystallites are eliminated. In this work this technique is used for characterization of powder samples of air sensitive compounds.

2.2.1.2.4 X-ray reflectivity, XRR

For characterization of thin films the XRR method is a useful tool. In XRR parallel X-rays are sent towards the sample surface at a very low incident angle, usually between 0 to 5° [109]. The use of low angle incident X-rays can give information on the thickness and the density of the films as well as the surface and interface roughness. From 0° up to a critical angle θ_c the incident beam will be totally reflected. At incident angles larger than the

critical angle some of the X-ray beam will enter the film material, see *Figure 2-17*.

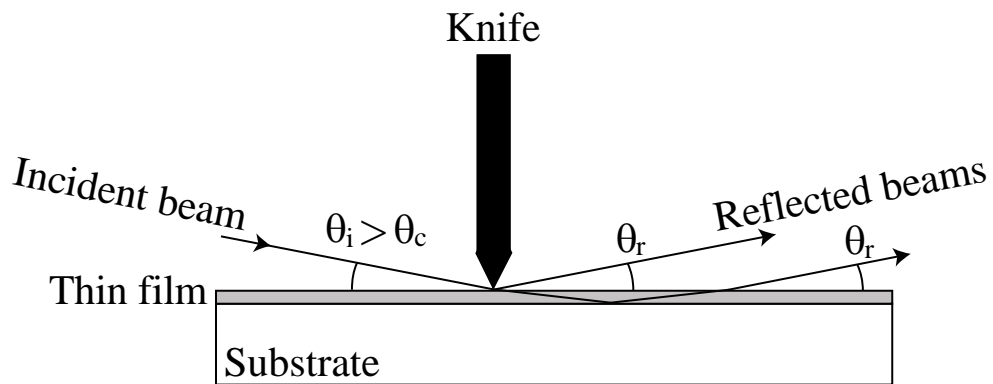


Figure 2-17. Schematic representation of the beam line in XRR. The θ_i angle is larger than the critical angle θ_c , allowing the beam to enter the film material. The incident beam is reflected both from the surface and from the interface between the film and substrate.

As the beam enters the film material, it will first be refracted and bent and then reflected at the interface between the film and substrate, due to variations in density at the interface. If the sample consists of a multilayered film, the beam will be reflected by all the different layers, and the result will become much more complicated than described here. The reflected beams from the different layers will interfere with each other, giving rise to constructive and destructive interference as the θ angle is varied. This results in a diffractogram with an oscillating curve. For thicker films the number of oscillations will increase, see *Figure 2-18*. The intensity will decrease for increasing θ angles, as the X-ray beam penetrates deeper into the material as well as a smaller surface area is irradiated by the incident beam [109].

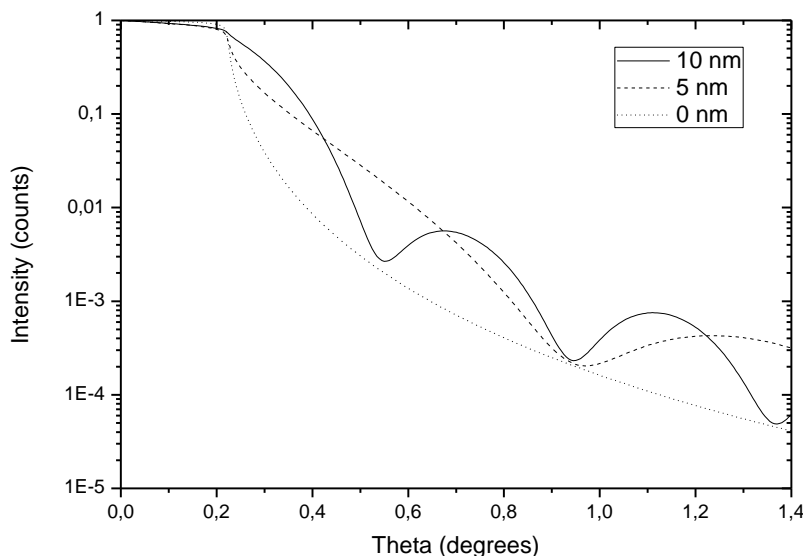


Figure 2-18. Simulation of a XRR diffractogram from cobalt oxide films on a silicon substrate, where the films have different thickness.

The thickness, density and roughness parameters are obtained by fitting the measured diffractogram from experiments with a theoretical model. The thickness is determined from the number of oscillations, the density can be determined from the critical angle and the roughness can be determined from the amplitude of the oscillations. The XRR method is most suitable for films with thickness between 5 to 100 nm, although the upper limit is dependent on the roughness of the deposited film. If the film is very rough, the amplitude will decrease so much that it can be difficult to detect the deposited film [109].

2.2.1.3 Program used for analysis of XRD data

For processing and presenting the obtained X-ray diffraction data the program EVA was used. The program is made by Bruker AXS, and is part of a program package called DIFFRAC^{plus} Evaluation.

2.2.2 Spectroscopy

In this section a description of the characterization method, based on spectroscopy, used for analyzing the deposited thin films will be given.

2.2.2.1 Fourier transform infrared (FT-IR) spectroscopy:

Radiation in the infrared region (IR radiation) of the electromagnetic spectrum is of relative low energy. As a consequence IR radiation cannot excite electrons, however, it can excite the phonons of chemical bonds. A chemical bond can have one or more vibrational modes with a given self-resonant frequency, which is determined by the mass of the atoms at its ends and the strength of the bond. Thus, the frequency of these vibrations can be used to identify a particular bond type. For a vibrational mode to be IR active it must be associated with changes in the permanent dipole. A bond will absorb IR radiation which has the same frequency as the self-resonant frequency of the bond. A FT-IR measurement gives information about such absorptions from the studied material [110].

In FT-IR spectroscopy the sample is scanned with all wavelengths at the same time. The incident IR beam goes first through a beam splitter, before the two beams are reflected from a stationary and movable mirror respectively. Depending on the position of the movable mirror, interference occurs as the two separate beams are merged again at the beam splitter, before the merged beam goes through the sample, see *Figure 2-19*.

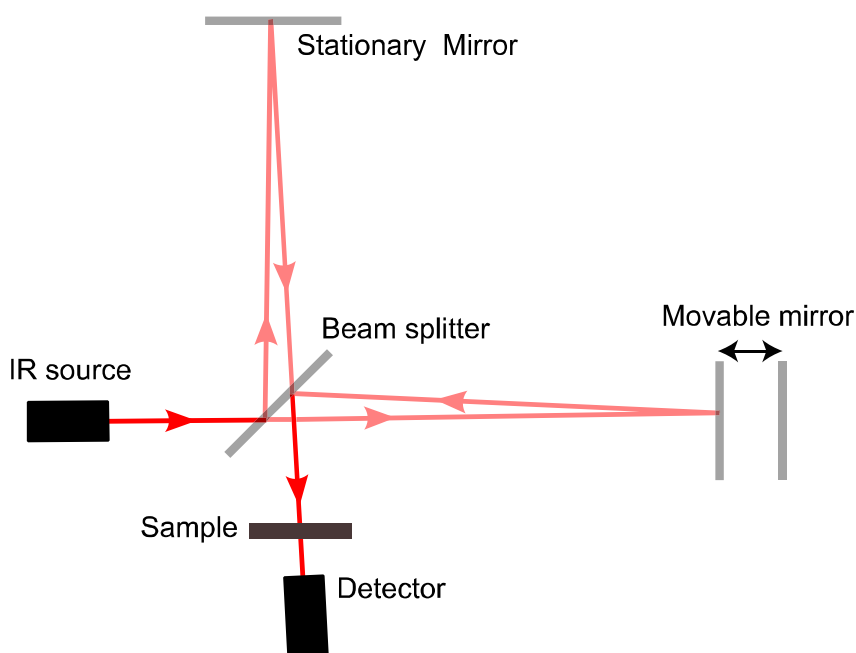


Figure 2-19. A schematic illustration of the beam path during a FT-IR measurement. The position of the movable mirror determines the interference conditions when the two separated beams are merged.

The signal obtained from the detector is an interferogram, which contains intensity information about all frequencies present in the infrared beam. The interferogram must then be analyzed with a computer using Fourier transforms to obtain the FT-IR spectra, which are usually presented as plots of intensity versus wavenumber, given in cm^{-1} . Wavenumber is the reciprocal of the wavelength. The intensity can also be plotted as the percentage of light transmittance or absorbance at each wavenumber.

2.2.2.2 X-ray fluorescence spectrometry (XRF)

XRF is a quantitative method for chemical analysis. The method is based on that when atoms are irradiated with X-rays, electrons may be transferred to a higher energy level in the respective atoms, hence exciting the atoms. As the excited atoms undergo de-excitation by relaxation, where an electron in a

higher energy level jumps down to the vacant position, characteristic X-rays are emitted. This type of radiation is called characteristic fluorescent X-ray, and gives an emission spectrum that is element specific. These characteristic emission lines are used in XRF analysis to identify the elements present in a sample and their specific amounts. This is done by comparing the intensities of the sample with specific standards and compare for absorption from the sample itself. For the analysis of thin films this method is cumbersome, and an alternative method using general standards is utilized. This can be done through the program Uniquant [111]. Uniquant utilizes known universal standards to calibrate the sensitivity of the XRF-equipment. By comparing the standards and the film samples the program can calculate elements present and the composition of the films [111].

2.2.3 Microscopy

In this section the microscopy technique used for analyzing the deposited thin films will be given.

2.2.3.1 Atomic force microscopy (AFM)

When it comes to surface analysis of a sample, AFM is an excellent tool where some of the properties that can be measured is topography, as well as chemical-, electrical-, and magnetic properties. The method can be used on almost all materials which has a relatively hard surface as metals, semiconductors, ceramics, composite materials, glass, thin films, polymers and biological samples [112].

The main component in an atomic force microscope (AFM) is a micro scale cantilever with a sharp tip (probe) mounted on one of its ends, which is used to scan the specimen surface, see *Figure 2-20*. The dimensions of the

cantilever is usually in the order of 100 – 200 μm long, 20 – 40 μm in width, and 0.5 – 1 μm thick. The cantilever is typically made of silicon or silicon nitride (Si_3N_4), with a tip radius of curvature in the order of nanometers. The Si tips gives a sharper image, due to a smaller tip size, however, they become more easily worn than the Si_3N_4 tips. As the cantilever is brought into close proximity of the sample surface, forces between the tip and the surface will deflect the cantilever. This deflection is measured by using a laser which is reflected form the top surface of the cantilever into a position sensitive photodiode. The difference in light intensity is calculated into a voltage which is then used to adjust the distance between the cantilever-tip and the sample surface so the force between them is kept constant [113].

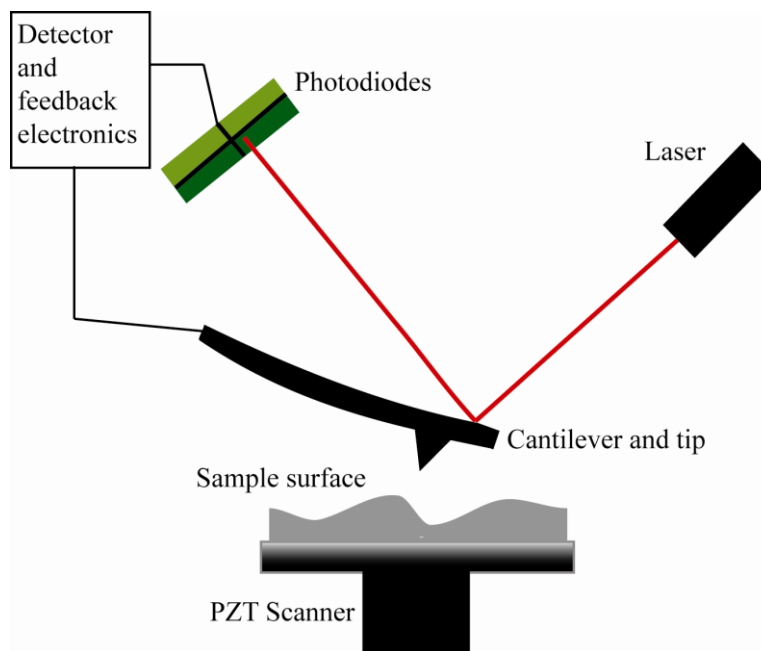


Figure 2-20. A schematic picture of an operating AFM-instrument.

The topography of the sample is determined by recording the deflection of the cantilever as it moves over the sample surface. The movement along the

x-, y- and z-axis is done by a piezo scanner made of piezoelectric ceramics like e.g. lead zirconate titanate (PZT).

The AFM can be run in two different modes, contact- or tapping mode. In contact mode the tip is in contact with the sample during the measurement. The cantilever deflection, and thus the force, is kept constant by readjusting the sample in vertical direction following the topographic features on the surface and recoding the adjusted height [113]. If contact mode is done in air, the surface tension of adsorbed layers of water vapor can pull the tip towards the sample surface. This can damage the sample and deform the image.

The effects of surface tension can be avoided using tapping mode which also images the topography under more gentle conditions for the tip and the sample. In tapping mode the cantilever with the tip is driven near its resonance frequency by means of a piezo oscillator. Thus, only intermittent contact between tip and sample occurs. As the tip is in contact with the surface, the oscillating amplitude is reduced compared to the resonance frequency, which is used as feedback in order to adjust the height of the sample and to produce the topographic information.

The resolution of an AFM-instrument is limited by two factors: the size of the tip utilized and the mode of AFM operation. A small tip diameter will give better resolution, and also tapping mode provides better resolution than contact mode. An advantage of the AFM measurements is that it does not require vacuum conditions.

2.2.4 Characterization of precursors

In this section a description of the methods used for characterization of the thermal properties and growth mechanics of the different precursors will be given.

2.2.4.1 Thermogravimetric analysis (TGA)

In thermogravimetric analysis the mass of the sample is measured as a function of temperature. As the sample is gradually heated any increase or decrease in mass of the sample can be monitored. Weight reduction can be due to sublimation, decomposition or desorption. An increase in weight can be due to oxidation or absorption.

In this work TGA is used for determination of the sublimation temperature of different precursors. However, the TGA measurements performed in this work was done under atmospheric pressures of N₂-flow, as a result the determined sublimation temperature will be higher than for the vacuum conditions utilized in the ALD-process.

2.2.4.2 Thermal decomposition of precursors

A simple method to measure the decomposition temperature of a precursor is to place it into a long tube in an oven with a controlled temperature gradient, see *Figure 2-21*. In order to simulate the conditions under the ALD-process the tube, in which the precursor is placed, is sealed under vacuum. As the precursor starts to sublime, diffusion will bring the compound through the tube until it reaches an area where the temperature is high enough for it to decompose. After some time, one can easily observe where the precursor has decomposed through optical effects. By measuring the distance from the end of the tube to the area where the precursor has

decomposed, and comparing to the heat profile of the oven, it is possible to determine the decomposing temperature of the precursor.

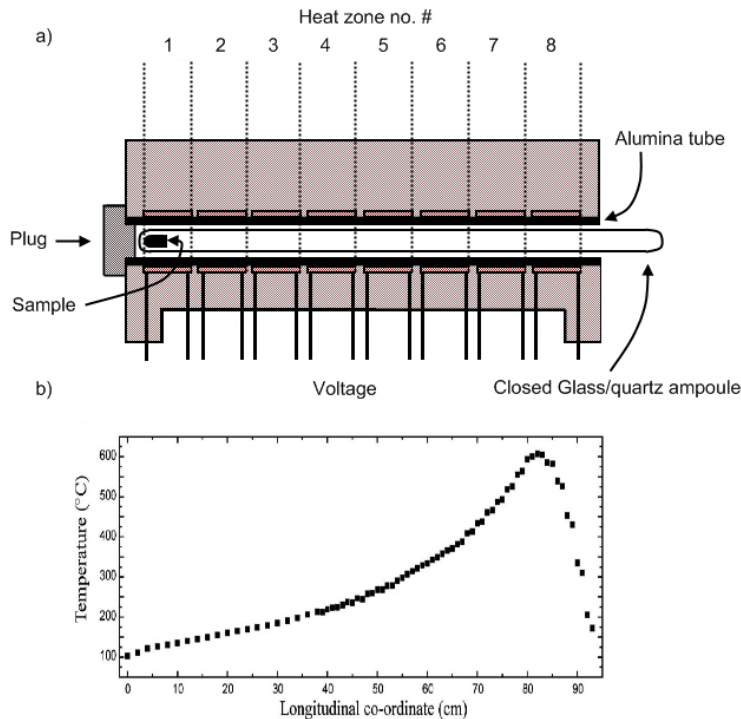


Figure 2-21 (a): Schematics of a thermal gradient furnace used for measuring the decomposition temperature of a precursor. Separate power supply to each heating zone is indicated. **(b)** Typically temperature profile. This figure is based on figure 1 (a) and (b) in reference [114].

2.2.4.3 Quartz crystal microbalance (QCM)

QCM is a useful method for monitoring the growth of thin films under vacuum. A study regarding deposition on QCM was done in 1959 by Sauerbrey [115], and today QCM analysis is regarded as a standard procedure in many commercial thin film deposition methods to obtain better control of the deposition [116].

The principle of QCM analysis is based on changes in the self-resonant frequency, f_0 , of a quartz crystal as a function of the systems mass. The quartz crystal is piezoelectric and an applied external electric field set it

in oscillation at its self-resonant frequency. The strength of this technique is its extreme sensitivity for very small changes in mass of the system. QCM analysis can register changes in mass of much less than a monolayer. The crystals change in frequency as a function of the change in the mass can be expressed as:

$$\Delta f = -\frac{2f_0^2 \Delta M}{A\sqrt{\mu\rho}} = -C\Delta m \quad \text{Eq. 2-14}$$

Where f_0 is given above, ΔM is the total change in mass, A is the surface area, μ is the shear modulus of the quartz crystal, ρ is the density of quartz, Δm is the added mass per unit area and C is a crystal dependent constant [117]. For QCM-measurements it is assumed that the surface area of the quartz crystal is constant. As seen from *Eq. 2-14* an increase in mass will lead to a decrease in frequency.

There are several factors than can alter the self-resonant frequency of a quartz crystal. In the ALD technique, however, temperature is the only other factor besides change in mass that is taken into consideration [118]. An increase in temperature will increase the self-resonant frequency of the quartz crystal. To minimize the effects of temperature, the system should be kept at a constant temperature for some time in order to reach thermal equilibrium. For very exothermal reactions, the measurement can be affected by the local increase in temperature as a result of the reactions. It is possible, however, to calculate what impact the exothermic reaction may have on the QCM results.

In the ALD-process, QCM is can be used to determine the optimal pulse- and purge times for the precursors. This is done by recording the changes in frequency as a function of time. A QCM measurement showing the change in frequency during a TMA and H₂O process is given in *Figure 2-22*.

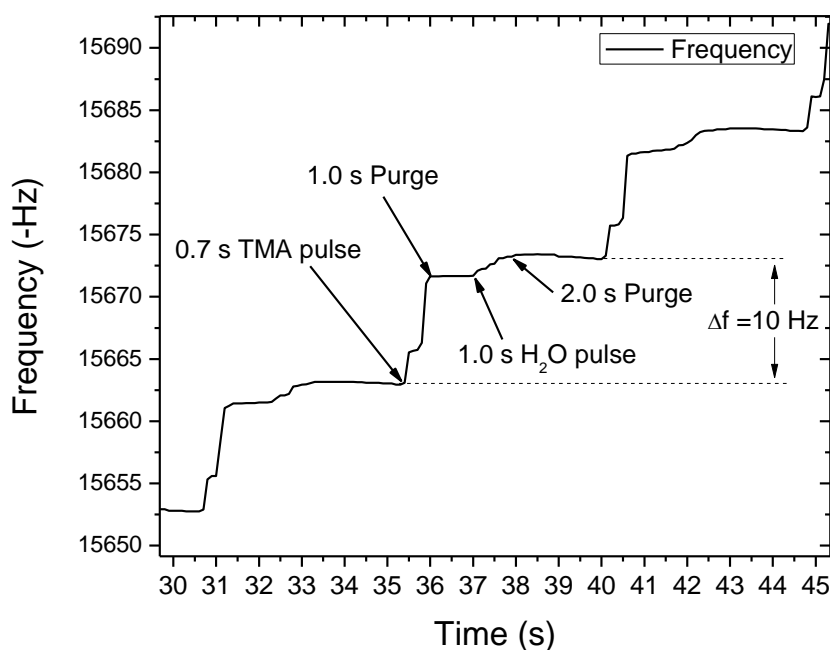


Figure 2-22. A QCM measurements showing the change in frequency through all the steps of one cycle of TMA with H₂O at 200 °C.

As the first precursor is pulsed in and adsorbs on the surface of the quartz crystal the mass increases. When the second precursor is pulsed in a new change in mass can be observed as the precursors reacts with each other. To make sure that the decided pulse and purge times are sufficient to maintain the self-limiting growth mechanism, pulse and purge times are kept longer than necessary. When complete saturation of the surface is obtained, plateaus can be observed in the frequency. Information on growth rate can be obtained by comparing the change in frequency of the sample of interest with a standard that has a given growth rate. The standard used in this work was the TMA and H₂O process. In this work QCM was used for investigation of the growth conditions for different precursors.

3 Experimental work

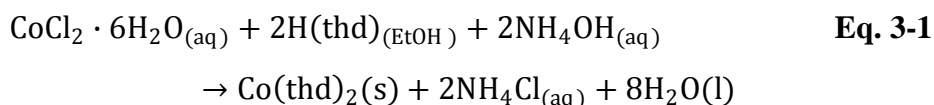
This chapter provides a detailed description of the chemicals and reactions used for synthesis of the different precursors. Thereafter the ALD equipment used for deposition of thin films by said precursors is described. Finally a description of the substrates, precursors and the characterization equipments used to study the precursors and the deposited films will be given.

3.1 Precursor synthesis

This section gives a detailed description of the different precursor synthesis methods used in this work.

3.1.1 Synthesis of Co(thd)₂

The synthesis of Co(thd)₂ is based on method no. 2, described in section 2.1.2.2.2 on page 58. As Co(thd)₂ is stable towards water and air the synthesis is much less demanding than synthesis of the bismuth precursor, as inert synthesis procedures are not required. For synthesis of Co(thd)₂ the following reaction was used:



Cobalt chloride was dissolved in aqueous ethanol, 50%, and H(thd) was added slowly with stirring. As aqueous ammonia was added drop-wise while stirring, a pink precipitate deposited. Distilled water was added and the solution was allowed to stir for 6 hours. The precipitate was filtered

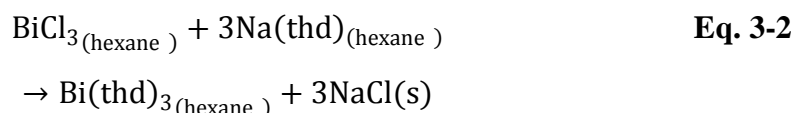
using a glass-funnel, washed with distilled water, dried in vacuum at 60 °C for 1 day, before it was purified by sublimation using 90 and 60 °C on the oven and finger, respectively.

3.1.2 Synthesis of Co(thd)₃

Co(thd)₃ was synthesized at the Department of Chemistry at the University of Oslo, by Mohammed A. K. Ahmed, according to the procedure described in ref. [106].

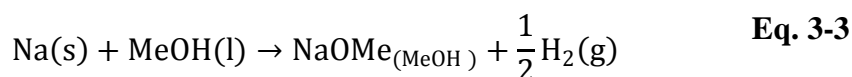
3.1.3 Synthesis of Bi(thd)₃

The synthesis of Bi(thd)₃ was based on method no. 1, described in section 2.1.2.2.2 on page 58. All reactions described below were carried out under inert atmosphere inside a glovebox. The following reaction was used for the synthesis of Bi(thd)₃ in this work:

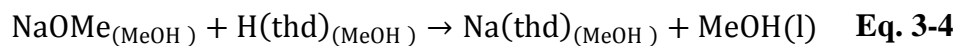


This reaction is claimed to yield anhydrous mononuclear Bi(thd)₃ as described in the patent by Baum et al. in Ref. [105].

The first step is to obtain Na(thd), which was done by the following reactions shown in *Eq. 3-3* and *Eq. 3-4*. Sodium metal was first reacted with dry methanol.



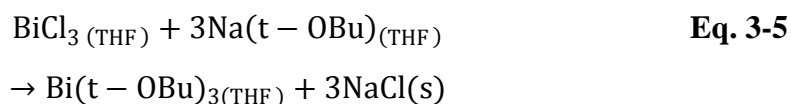
Then appropriate amounts of H(thd) was added to the sodium methoxide solution.



The solvent (MeOH) was removed under vacuum, leaving a white powder of Na(thd) which was dissolved in dry hexane. BiCl₃ was dissolved in dry hexane before the Na(thd) solution was added, see *Eq. 3-2*, and the resulting white solution was left to stir for 5 hours. The solvent was removed under vacuum, first at room temperature for 1 hour, then for overnight at 50 – 55 °C. The resulting white compound was then dried at 60 °C, before the product was sublimed. Unreacted Na(thd) was first removed by sublimation at 75 °C, the product was then sublimed at 120 °C for 4 hours, and finally at 137 °C, with 65 °C at the finger, for 1 day. The product was transferred to the glove box, where it was weighted and stored.

3.1.4 Synthesis of Bi(t-OBu)₃

The synthesis of Bi(t-OBu)₃ was based on the method described in section 2.1.2.2.1 on page 57, and was carried out as described in Ref. [88]. All reactions and steps described below were done under inert atmosphere using a glove box and a Schlenk line. For the synthesis of the Bi(t-OBu)₃ compound the chemical reaction given in *Eq. 3-5* was used.



BiCl₃ was complexed in dry THF under cooling by liquid nitrogen, as this complexation reaction is very exothermic. Na(t-OBu) was then dissolved in

dry THF, and mixed with the BiCl_3 solution under stirring. The resulting milk white solution was heated gently under reflux over the night, while covered in alumina foil to protect the product from light. NaCl was separated from the solution by centrifuging for 20 minutes. The solvent (THF) was removed under vacuum. The remaining yellow-compound was sublimed, first for half an hour with $40\text{ }^\circ\text{C}$ on both the finger and oven, to remove any volatile impurities, then for 2 days with the oven and the finger at 60 and $30\text{ }^\circ\text{C}$, respectively. The product was transferred to the glove box where it was weighted and stored.

3.2 The ALD reactor

The ALD reactor used in this work was a commercial F-120 Sat reactor from ASM Microchemistry Ltd. The reactor is a hot wall reactor, which means that films are deposited on all the surfaces inside the reaction chamber. The reactor consists of a large silica glass tube, with heating coils around it, in which the schematically viewed parts in *Figure 3-1* are placed. The reactor has eight temperature zones and eight supply pipes, one of these supply pipes are used for exhaust and one for thermocouples. The remaining six supply pipes are connected three by three to two assembly pipes, which again leads to the reaction chamber. To avoid film growth inside the pipes, only precursors that do not react with each other are placed inside supply pipes that are connected to the same assembly pipe.

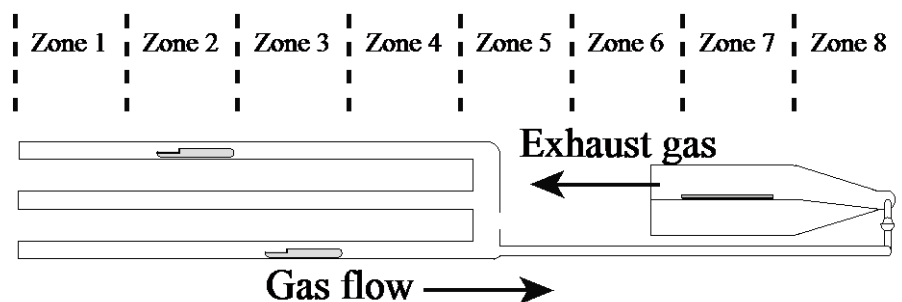


Figure 3-1. A schematically overview of the supply pipes, the reaction chamber and the eight temperature zones in the ALD reactor. The temperature increases from zone 1 to 5, zone 5 to 8 are adjusted to give the same temperature. Two precursors placed in different zones are also indicated.

The pulsing of the precursors is controlled by an inert gas flow barrier, schematically viewed, in *Figure 3-2*.

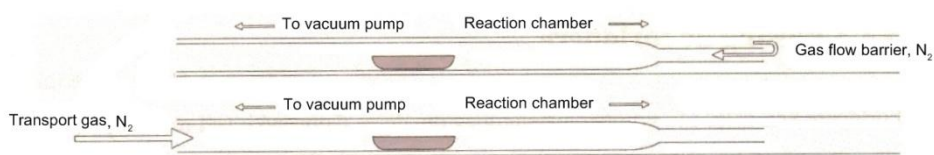


Figure 3-2. Schematic view of the pulsing system using an inert gas flow barrier. The situation shown at the top is when the gas flow barrier keeps the precursor away from the reaction chamber. At the bottom of the picture, the precursor is transported into the reaction chamber [14].

When the precursors are not pulsed a nitrogen flow of $300 \text{ cm}^3/\text{min}$ in the direction towards the vacuum pump, keeps the precursors away from the reaction chamber. When pulsed, the nitrogen flow is directed in the opposite direction which transports the precursor vapor into the reaction chamber.

3.2.1 The reaction chamber

The reaction chamber is composed of a glass tube with an inner diameter of 5.5 cm. It becomes narrower at the end where the precursors are pulsed in, where it ends in two separate tubes that can be connected to the two separate assembly pipes, described earlier. During deposition the substrates are placed upon an aluminum plate, which are cut to fit the profile of the reaction chamber, see *Figure 3-3*.

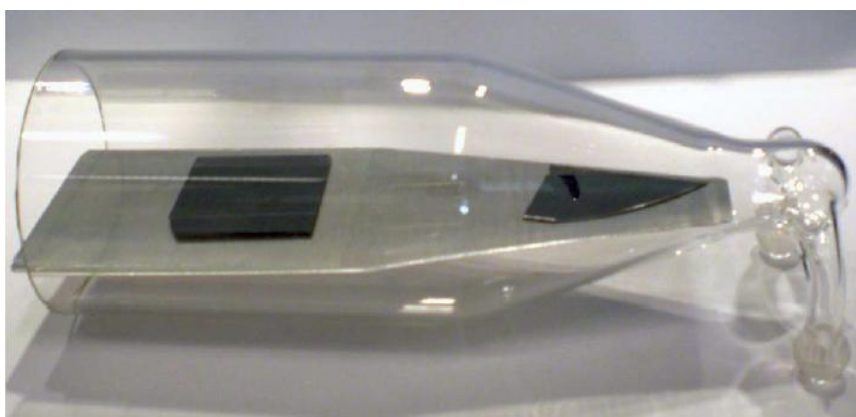


Figure 3-3. A picture of the reaction chamber with two silicon substrates [119].

3.2.2 Transport gas

An inert gas of nitrogen, $N_2(g)$, was used as transport gas and for purging the reaction chamber. A crucial aspect of the transport gas is purity as it is the main source of impurities in an ALD process. As a minimum for transport gases, 99.999% purity should be used [70]. The transport gas used in this work was produced in a Schmidlin UHP3001 N_2 purifier with a claimed purity of 99.999% with regard to $N_2(g) + Ar(g)$ content. The gas was further purified by passing it through P_2O_5 in order to remove remains of water and an oxygen trap type Mykrolis MINI XL.

3.2.3 Growth parameters for deposition of thin films

For the different precursors used in this work, the sublimation temperatures together with the pulse and purge schemes for depositions done with ALD are given below in *Table 3-1*.

Table 3-1. The sublimation temperatures together with the pulse and purge schemes used for the different precursors, for deposition with ALD.

| Precursor pair | Co(thd) ₂ + O ₃ | Co(thd) ₂ + H ₂ O | Co(thd) ₃ + O ₃ | BiPh ₃ + H ₂ O | Bi(thd) ₃ + H ₂ O |
|------------------------------|---------------------------------------|---|---------------------------------------|--------------------------------------|---|
| Sublimation temperature (°C) | 115 | 115 | 95 | 90 | 137 |
| Metal pulse (s) | 2.5 | 3.0 | 3.0 | 2.0 | 5.0 |
| Purge (s) | 1.0 | 1.0 | 1.5 | 0.5 | 2.0 |
| Non-metal pulse (s) | 3.0 | 5.0 | 6.0 | 1.5 | 1.5 |
| Purge (s) | 1.5 | 1.5 | 2.0 | 1.0 | 1.5 |

The listed parameters for Bi(thd)₃ + H₂O are the ones used in the second round of investigation. In the first round of investigation a pulse and purge scheme of 2.0s Bi(thd)₃, 0.5s purge, 1.5s H₂O, 1.0s purge was used.

3.3 Substrates

The depositions in this work were mainly done on Si(111) and silica glass substrates. A large soda lime glass plate, with the dimensions 5.1 x 7.6 cm and 1 mm thickness, was used as a supporting substrate on which both the Si(111) and small glass substrates were placed. The large soda lime glass

plate acts as an indicator whether any film has been deposited or not, as it is easy to observe “shadow effects” after a deposition as the area under the substrates are usually not covered by the deposited film. The dimensions on the Si(111) and small glass substrates used were 3.5 x 3.5 cm with 0.7 mm thickness, and 18 x 18 mm with 0.1 mm thickness, respectively.

The large glass plate and the smaller glass substrates were cleaned with ethanol and then blown clean with pressurized air. The Si(111) substrates are sufficiently clean as delivered, and were therefore only blown with pressurized air to remove any possible dust particles.

3.4 Precursors

The precursors used in this work are listed in *Table 3-2*, together with purity and supplier.

Table 3-2. *The different precursors used in this work, together with purity and supplier.*

| Precursor | Purity | Supplier |
|------------------------------------|---------------------------|--|
| Co(thd) ₂ | sublimed | In house |
| Co(thd) ₃ | sublimed | In house |
| Bi(thd) ₃ | sublimed | In house |
| Bi(Ph) ₃ | 99% | ABCR GmbH |
| Bi ^t O(Bu) ₃ | sublimed | In house |
| Water (distilled) | - | Distilled at UiO |
| Oxygen | 99.999% | AGA |
| Ozone | 99.999% (O ₂) | OT-020 ozonegenerator from Ozone technology O2, gives 15 volume % O ₃ |
| Nitrogen | 99.999% | Schmidlin UHPN3001 N ₂ purifier, inert gas (N ₂ +Ar) |

3.5 Characterization equipment

This section describes the different instruments used for characterization of the synthesized samples in this work.

3.5.1 X-ray based methods

In this work three different instruments were used to characterize samples using X-rays, these are described in the sections below.

3.5.1.1 X-ray diffraction on capillary powder samples

X-ray analysis of capillary powder samples was performed using a Siemens D5000 diffractometer in transmission mode in θ - 2θ configuration. A Johansson-type monochromator with a germanium crystal provides $\text{CuK}\alpha$ radiation and the detector used was a position sensitive detector (PSD).

3.5.1.2 X-ray diffraction on thin films

X-ray analysis of deposited thin films was performed with a Siemens D5000 diffractometer using a Bragg-Brentano reflection setup in θ - 2θ configuration. A Göbel mirror was used as a monochromator, which gives a parallel beam of $\text{CuK}\alpha$ radiation. The Göbel mirror consists of parabolically bent multilayers and gives a higher intensity than a Johansson-type monochromator, which is desirable when working with thin films. However, the intensity comes at an expense of beam purity and the radiation consists of both $\text{K}\alpha_1$ and $\text{K}\alpha_2$, and fragments of $\text{Cu K}\beta$ and $\text{W}\text{L}\alpha$. The detector used was a scintillation counter equipped with a secondary $\text{Si}(111)$ monochromator. During GIXRD measurements an incident beam angle of 0.5° was used.

3.5.1.3 XRF

In this work XRF was used for determination of the elemental composition of the deposited films. The instrument was a Philips PW2400 X-ray fluorescence spectrometer, which can detect concentrations from ppm to 100 %. The results were analyzed by using the program Uniquant [111].

3.5.2 FT-IR

FT-IR was used in this work to investigate the deposited thin films for possible carbonate contaminations. The instrument used was a VERTEX 80 FT-IR spectrometer from Bruker.

3.5.3 AFM

AFM was used to investigate the topography, and roughness of the deposited films. The instrument used was a NanoScope Dimension 3100 from Digital Instruments. The measurements were performed in tapping mode and both Si and Si₃N₄ tips were used. The Si tips often give a sharper image, due to a smaller tip size, however, they become more easily worn than the Si₃N₄ tips.

3.5.4 Equipment used for characterization of precursors

The sublimation and decomposing temperature together with the ALD growth parameters was investigated for the precursors used in this work. The instruments by which this was done are described in this section.

3.5.4.1 TGA

TGA was used to investigate the sublimation temperature of different precursors. The instrument used was a TGA 7 Thermogravimetric Analyzer from PerkinElmer. The data was analyzed by using the program Pyris. TGA analysis relies on a high degree of precision in three parameters: weight, temperature, and temperature change. The equipment used in this work is able to detect a change in mass of 1 μg .

3.5.4.2 Thermal decomposition of precursors

For determination of the decomposing temperature of the precursors a thermal gradient furnace was used, as described in section 2.2.4.2 on page 73.

3.5.4.3 QCM analysis

In this work QCM was used for in-situ analysis of the growth mechanisms of the different precursors. The obtained data was logged with a Maxtek.inc TM400 data logger and the program Labview. The quartz crystals used were AT-cut, 6 MHz quartz crystals with gold electrodes.

3.6 Heat treatment of the deposited thin films

Some of the deposited thin films were heat treated in oxygen atmosphere in order to investigate the crystal structure in more detail. For this procedure a standard tube furnace was used which was connected to temperature controller from Eurotherm. 4.0 O₂ gas from AGA was led through a pre-combustion furnace in order to remove any organic impurities, whereupon any possible CO₂ products were removed by filtering the gas through CaO before the entering the tube furnace.

4 Results

This chapter is divided in three sections, where the first section presents results obtained during this work on the different precursors in the order $\text{Co}(\text{thd})_2$, $\text{Co}(\text{thd})_3$, BiPh_3 , $\text{Bi}(\text{t-OBu})_3$ and $\text{Bi}(\text{thd})_3$. The second section give results regarding deposition and investigation of thin films in the Co-O and Bi-O systems. The final section present results from depositions and investigations of thin films in the Bi-Co-O system. This chapter contains some discussions to enlighten on the path chosen during this work. Where it is appropriate, some parts will be concluded in order to keep the following discussion in chapter 5 more clear and tidy.

4.1 Synthesis and investigation of precursors

In this section, the synthesis and investigation of the different precursor used in this work will be presented. Work carried out on the precursors will be presented in the following order: First the cobalt precursors, $\text{Co}(\text{thd})_2$ and $\text{Co}(\text{thd})_3$, then the bismuth precursors, BiPh_3 , $\text{Bi}(\text{t-OBu})_3$ and $\text{Bi}(\text{thd})_3$.

4.1.1 $\text{Co}(\text{thd})_2$

Here the results obtained from the work on the $\text{Co}(\text{thd})_2$ precursor are given.

4.1.1.1 Synthesis of $\text{Co}(\text{thd})_2$

Two batches of $\text{Co}(\text{thd})_2$ was synthesized in this work according to the procedure described in section 3.1.1. The chemicals used for the synthesis of $\text{Co}(\text{thd})_2$ and their respective amounts are given in *Table 4-1*.

Table 4-1. The chemicals and their respective amounts used for the synthesis of $\text{Co}(\text{thd})_2$.

| Batch | 1 | 2 |
|--|--------------|--------------|
| Chemicals | Amounts | |
| $\text{CoCl}_2 \cdot 6 \text{H}_2\text{O}$ | 7.20 g | 7.20 g |
| H(thd) | 11.05 g | 11.09 g |
| NH_4OH (2.5M) | 25 ml | 25 ml |
| Theoretical yield | 12.76 g | 12.76 g |
| Yield | 5.24 g (41%) | 4.9 g (38 %) |

$\text{Co}(\text{thd})_2$ is reported to adopt a tetragonal crystal structure with the space group $I4_1/a$ [14, 120]. A recorded powder pattern, by XRD, from the synthesized $\text{Co}(\text{thd})_2$ together with a silicon standard is given in *Figure 4-1*.

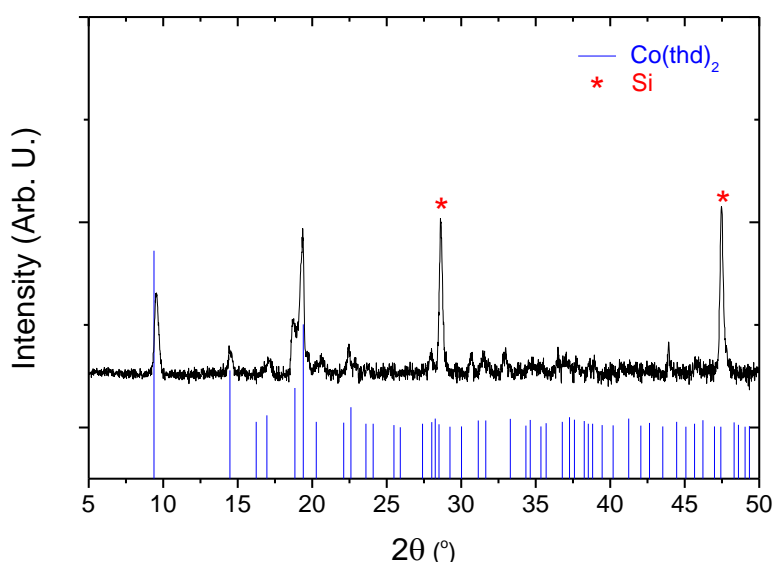


Figure 4-1. Powder x-ray diffractogram of synthesized $\text{Co}(\text{thd})_2$ together with a silicon standard (*), background is subtracted. The blue $\text{Co}(\text{thd})_2$ diffractogram is simulated based on Ref. [14, 120].

As can be seen from the diffractogram presented in *Figure 4-1* the observed peaks from the synthesized powder corresponds fairly well with the simulated powder diffraction file (PDF) based on Ref. [14, 120].

During storage and use the cobalt precursor may become hydrated and as a consequence it changes color from dark purple to pink [104]. This reduces its performance in the ALD process, and in order to remove the hydrated water the precursor has to be resublimated.

4.1.2 Co(thd)₃

Co(thd)₂ is well investigated in the literature [12, 13, 32] as an ALD precursor whereas the similar precursor Co(thd)₃ is not. It was therefore decided to include a study of this novel precursor for possible use in an ALD process. If an ALD process was obtained, it would be interesting to compare the two growth systems from the two similar precursor Co(thd)₂ and Co(thd)₃. Furthermore, this novel cobalt precursor could turn out to be an important parameter when trying to obtain thin films of the multiferroic phase BiCoO₃ as well. This assumption was based on that the cobalt ion is in the 3+ oxidation state in the Co(thd)₃ precursor, which is the same oxidation state as for cobalt in the phase BiCoO₃.

However, before starting depositions with a new precursor it is useful to determine its sublimation and decomposition temperature, as these two parameters in principle determines the lower and upper limit for the precursors ALD window, respectively.

4.1.2.1 Sublimation temperature

From the literature it is know that Co(thd)₃ sublimes at ca. 90 °C under 0.5 mbar pressure [106] for purification purposes. A TG analysis was carried out in order to check the sublimation temperature of Co(thd)₃ against the reported values in Ref. [106], see *Figure 4-2*.

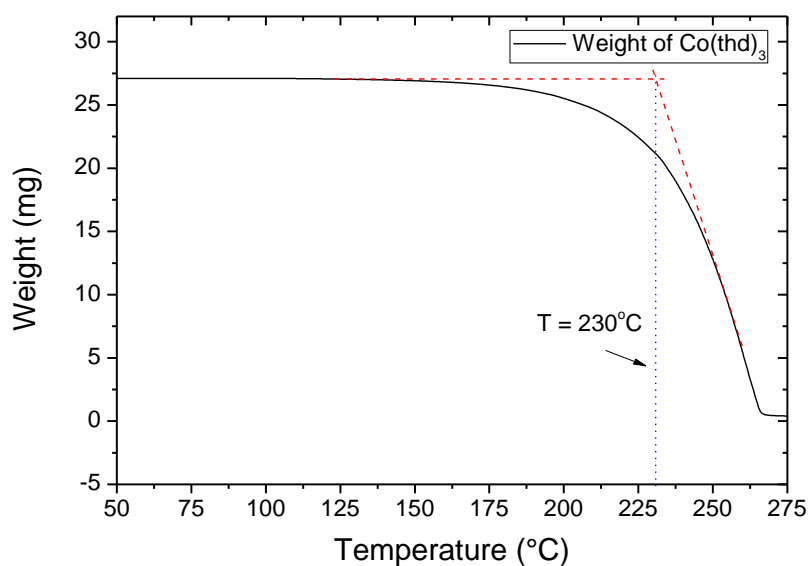


Figure 4-2. Thermogram for $\text{Co}(\text{thd})_3$, heating rate 5 $^{\circ}\text{C}/\text{min}$ under ambient pressure of nitrogen atmosphere. The temperature for sublimation onset is determined to be 230 $^{\circ}\text{C}$.

The thermogram in *Figure 4-2* shows that under ambient pressure of nitrogen, the onset temperature for sublimation is at 230 $^{\circ}\text{C}$, and the maximum rate of evaporation was found from the second derivative to be around 250 $^{\circ}\text{C}$. In Ref. [106] it is reported that, with a heating rate of 5 $^{\circ}\text{C}/\text{min}$, $\text{Co}(\text{thd})_3$ samples with weight in the range 15-30 mg had a sublimation onset at ca. 150-160 $^{\circ}\text{C}$ and that the sublimation was completed at ca. 260-280 $^{\circ}\text{C}$. The onset temperature determined in this work is much higher than the reported value. However, it has been confirmed by the author of Ref. [106] that the definition of the onset temperature used was where the TG curve started to drop. In addition, *Figure 4-2* shows that $\text{Co}(\text{thd})_3$ can be subject to almost total sublimation, where only 0.8% of the initial mass remains at 275 $^{\circ}\text{C}$. The small remaining mass may be due to the system not being in a complete steady state when the sample weight was measured initially. Nevertheless, this observation is also in good agreement

with Ref. [106], where a total sublimation of $\text{Co}(\text{thd})_3$ is reported. From the TGA results together with the know sublimation temperature from [106], the sublimation temperature to be used for depositions was chosen to be $95\text{ }^\circ\text{C}$. A higher temperature than $90\text{ }^\circ\text{C}$ was chosen since the ALD reactor used in this work operates under a slightly higher pressure than 0.5 mbar .

4.1.2.2 Decomposition of $\text{Co}(\text{thd})_3$ in an closed ampoule

A glass ampoule for thermal decomposition was placed 12 cm into the oven from the cold side. The temperature at the sample position was measured to be $120\text{ }^\circ\text{C}$. A higher temperature than $90\text{ }^\circ\text{C}$ was used to ensure good sublimation, as it was unlikely that the precursor would decompose already at this temperature. The ampoule was left in the furnace for 36 hours and the result of this experiment is shown schematically in *Figure 4-3*.

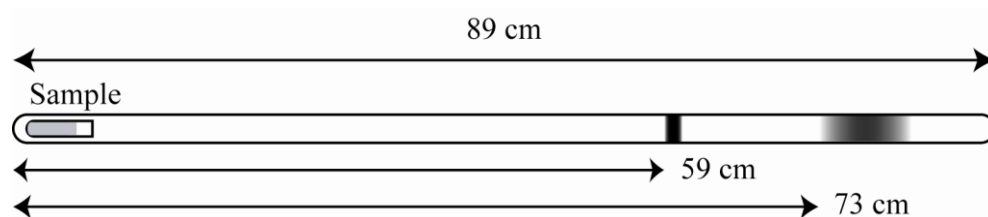


Figure 4-3. Schematic drawing of the glass ampoule after 36 hours of heat treatment in thermal gradient furnace. Measured temperatures: at the sample $120\text{ }^\circ\text{C}$, at 59 cm $436\text{ }^\circ\text{C}$ and at 73 cm $630\text{ }^\circ\text{C}$.

The temperature at the first and second decomposition, at 59 cm and 73 cm , was measured to be 436 and $630\text{ }^\circ\text{C}$, respectively. The measurement indicates that $\text{Co}(\text{thd})_3$ is thermally stable up to around $430\text{ }^\circ\text{C}$, which is a relatively high temperature for the ALD process, and a much higher temperature than used for the depositions in this work. For comparison the decomposition temperature of $\text{Co}(\text{thd})_2$ has been measured by the same method to be $310\text{ }^\circ\text{C}$ [14]. The observed decomposition at $630\text{ }^\circ\text{C}$ is likely to

be due to the subsequent decomposition of the organic products from the decomposition of the precursor.

4.1.3 BiPh₃

BiPh₃ has been, as mentioned earlier in the prior art (section 1.2.2.2), used for deposition of bismuth containing films with the ALD method. Since it is reported in Ref. [8] that metallic bismuth was found in the films deposited at 260 °C, it was decided to first check the sublimation and decomposing temperature of BiPh₃ before starting any depositions.

4.1.3.1 TGA of BiPh₃

The sublimation temperature of BiPh₃ was investigated by TGA and the obtained thermogram is given in *Figure 4-4*. As mentioned earlier, indications that BiPh₃ decomposes at 260 °C can be assumed based on the results obtained in Ref. [8]. In addition, based on the sublimation temperatures used for BiPh₃ in the ALD process in Ref. [8] and [11], it can be assumed that BiPh₃ has a sublimation onset below 200 °C. In the following TG analysis of BiPh₃ it was therefore decided not to raise the temperature higher than 200 °C, to avoid any decomposition. As a consequence of this decision, the result has to be presented as shown in *Figure 4-4* to better show the decrease in mass during the whole measurement.

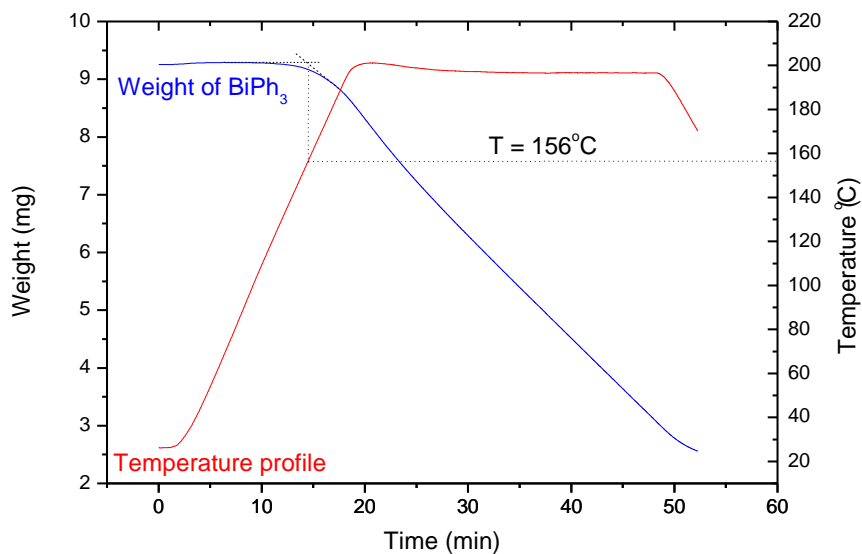


Figure 4-4. Thermogram for BiPh_3 , heating rate $10\text{ }^\circ\text{C}/\text{min}$ under ambient pressure of nitrogen atmosphere. The temperature for sublimation onset is determined to be $156\text{ }^\circ\text{C}$.

The remaining mass at the end of the measurement is a consequence of a too short dwell time at $200\text{ }^\circ\text{C}$. By analyzing the obtained data, the onset of sublimation was determined to be $156\text{ }^\circ\text{C}$, and the maximum rate of evaporation was found, from the second derivative, to be $193\text{ }^\circ\text{C}$. In Ref. [8] and [11] a sublimation temperature of 125 and $115\text{ }^\circ\text{C}$ was used for BiPh_3 , respectively. Based on the observations in the $\text{Co}(\text{thd})_3$ system it was assumed that an even lower sublimation temperature could be used, hence it was decided to use a sublimation temperature of $90\text{ }^\circ\text{C}$ for BiPh_3 .

4.1.3.2 Decomposition of BiPh_3 in an closed ampoule

The sample was placed at 36 mm into the gradient furnace, where the temperature was measured to be $100\text{ }^\circ\text{C}$, which is higher than the

sublimation temperature for BiPh_3 . The sample was left in the oven for 29 hours. The decomposition was observed as a grey-brown shadow on the walls of the ampoule, 40 cm into the oven, where the temperature was measured to be 240 °C.

4.1.4 $\text{Bi}(\text{t-OBu})_3$

In this section the results regarding the work on the $\text{Bi}(\text{t-OBu})_3$ precursors are given.

4.1.4.1 Synthesis of $\text{Bi}(\text{t-OBu})_3$

The synthesis of $\text{Bi}(\text{t-OBu})_3$ was performed as described in section 3.1.4. In this work four attempts for the synthesis of $\text{Bi}(\text{t-OBu})_3$ has been carried out. The three first attempts were unsuccessful due to leakage on the Schlenk line, which destroyed the desired product. The chemicals and their respective amounts used in the fourth and successful synthesis are given below in *Table 4-2*.

Table 4-2. *The chemicals used and their respective amounts for the synthesis of $\text{Bi}(\text{t-OBu})_3$.*

| Chemicals | Amounts |
|----------------------------------|----------------|
| BiCl_3 | 18.43 g |
| $\text{Na}(\text{O}^t\text{Bu})$ | 16.82 g |
| Theoretical yield | 24.99 g |
| Yield | 3.40 g (13.6%) |

4.1.4.2 Decomposition of $\text{Bi}(\text{t-OBu})_3$ in an closed ampoule

The sample placed at 36 mm in the gradient furnace where the temperature of the source was 100 °C and left in the oven for 4 days. When investigating the ampoule afterwards it became clear that $\text{Bi}(\text{t-OBu})_3$ decomposed already

at the sample temperature. To investigate the decomposing temperature more thoroughly, an in-situ QCM measurement was performed at 65 °C which showed that the precursor decomposed heavily already at this temperature [1].

4.1.4.3 Concluding remarks

The decomposition temperature of $\text{Bi}(\text{t-OBu})_3$ is too low for it to be used for depositions in the Bi-Co-O system together with $\text{Co}(\text{thd})_2$ or $\text{Co}(\text{thd})_3$, as these precursors need a deposition temperature of at least 114 and 162 °C, respectively. It was therefore chosen not to investigate this precursor further in this work.

However, the crystal structure of the $\text{Bi}(\text{t-OBu})_3$ precursor synthesized in this work was solved in Ref. [1]. The crystal structure is reported to be trigonal with the space group $P3c$, and the molecules in $\text{Bi}(\text{t-OBu})_3$ are packed monomerically. This is the first time the crystal structure of $\text{Bi}(\text{t-OBu})_3$ is solved, in addition it is also the first reported solved structure of an alkoxide that only contains bismuth.

4.1.5 $\text{Bi}(\text{thd})_3$

Here the results regarding the synthesis and investigation of $\text{Bi}(\text{thd})_3$ are given.

4.1.5.1 Synthesis of $\text{Bi}(\text{thd})_3$

In this work a total of five syntheses of $\text{Bi}(\text{thd})_3$ has been carried out. All the syntheses have been performed as described in section 3.1.3, except for the last synthesis hereafter called *E*. In *E* BiI_3 was used instead of BiCl_3 , and a commercially bought powder of NaOMe (Fluka, purum; > 97.0%) was used

instead of homemade NaOMe. A lack of BiCl_3 powder was the reason for the exchange done in *E*. An overview of the reactants and the obtained yield for the different syntheses are given below in *Table 4-3*. The labels given for different syntheses are traceable in the Appendix (9.1).

Table 4-3 shows that there are large differences in the yield from the syntheses performed in this work. However, there were some changes in the parameters and the execution for the different syntheses, which may have influenced both the obtained product and the yield. These factors are listed below in *Table 4-4* and discussed more in detail in the following text.

Table 4-3. Reactants and products given with their respective amounts from the $\text{Bi}(\text{thd})_3$ syntheses. Samples A-D use BiCl_3 whereas sample E use BiI_3 .

| Sample name | Na(thd) (g) | $\text{BiCl}_3 / \text{BiI}_3$ (g) | Yield (g) | Theoretical Yield (g) | % theoretical yield |
|--------------------|--------------------|--|------------------|------------------------------|----------------------------|
| A | 16.66 | 8.28 | 5.30 | 19.92 | 27 |
| B | 16.25 | 8.28 | 9.36 | 19.92 | 47 |
| C | 16.62 | 8.278 | 4.12 | 19.92 | 21 |
| D | 17.04 | 8.32 | 16.80 | 20.02 | 84 |
| E | 18.56 | 17.69 | 5.29 | 22.76 | 23 |

Table 4-4. Different factors that may have influenced the syntheses of $\text{Bi}(\text{thd})_3$.

| Sample name | A | B | C | D | E |
|--------------------|-----------------|-----------------|-----------------|-----------------|----------------|
| Contamination | | | | | |
| of methanol | Yes | No | No | Yes | Yes |
| Exposed to air | No | Yes | No | No | No |
| Sublimed two times | No | No | Yes | Yes | Yes |
| Dry solvents | No | No | No | Yes | Yes |
| One-phase | Unknown | No | No | No | No |
| Reactants used | BiCl_3 | BiCl_3 | BiCl_3 | BiCl_3 | BiI_3 |

In the first synthesis, *A*, $\text{H}(\text{thd})$ was, by an error, reacted with NaOMe after the methanol solvent was removed under vacuum. When $\text{H}(\text{thd})$ reacts with NaOMe and forms $\text{Na}(\text{thd})$, methanol is formed as a by-product. This may lead to contamination of methanol in the final product, and it was assumed that this contamination could have had an effect on the final product. Therefore this was attempted to be reproduced, however, it turned out that the possible contamination of methanol did not have any significance on the properties of the synthesized precursor.

The second synthesis *B* was exposed to air during the synthesis due to leakage on the Schlenk line. This turned out to not have any significant impact on the yield, the final product or the properties of the synthesized precursor. Some loss of product occurred most likely during this synthesis, due to lack of stirring while the solvents were removed under vacuum which resulted in eruptions of sudden boiling.

Some samples, *C*, *D* and *E* were sublimed two times in order to increase the yield of the syntheses. This was done by removing the sublimed product

from the finger inside the glove box, whereupon the remaining product was sublimed again. The samples from the first and second sublimation was stored separately, and in all cases the compounds from the first sublimation was more sticky with a faint yellow color, in contrast to the dry white powder obtained from the second sublimation. In addition, for the first sublimations some of the crystals crystallized on the finger as long needle shaped crystals, in contrast to the second sublimations where more square-like crystals were obtained.

Dry solvents were used in *D* and *E* in order to try to obtain a phase without crystal water. Compared to the other syntheses where BiCl_3 was used as a reactant, *D* showed an extremely high yield, which may indicate that the use of dry solvents are beneficial. However, as other parameters also were changed in that synthesis, it is uncertain that the increased yield can be subscribed to the use of dry solvents alone.

For the synthesis where BiI_3 was used, it should be noted that BiI_3 appeared to have a very poor solubility in hexane, which was the solvent used. In addition, the product obtained from both the first and second sublimation was a mixture of a white and red powder. It was observed that the red powder seemed to have a higher sublimation temperature than the white powder, and in order to separate the white powder a new sublimation was done. The products from both the first and second sublimation was mixed and placed in the sublimation oven. The temperature in the oven and the finger was kept at 128 and 40 °C, respectively. After three days most the white powder had been recrystallized on the finger, while a fluffy faint red colored powder remained in the flask.

In addition, the θ - 2θ transmission XRD measurements performed on the synthesized precursors indicated that they all consisted of more than one phase.

4.1.5.2 Purification of $\text{Bi}(\text{thd})_3$

During deposition with the synthesized $\text{Bi}(\text{thd})_3$ precursors, it was found that recrystallization occurred in two different temperature-zones in the ALD reactor, see *Figure 4-5*. This indicated the presence of at least two different phases which had different sublimation temperatures.

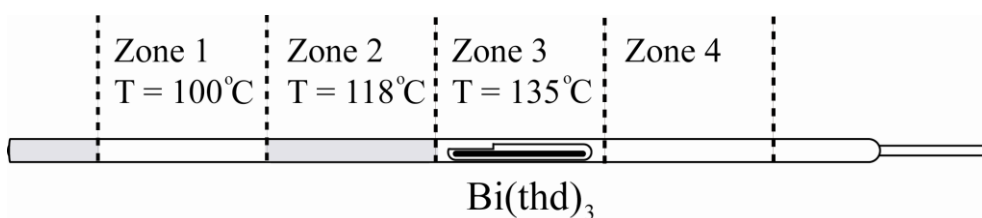


Figure 4-5. The observed recrystallization inside the precursor tube, during ALD deposition, at two different temperature zones for the $\text{Bi}(\text{thd})_3$ precursor.

A TG measurement was performed in order to check if separate sublimation of the different phases could be observed. The obtained thermogram is given in *Figure 4-6*.

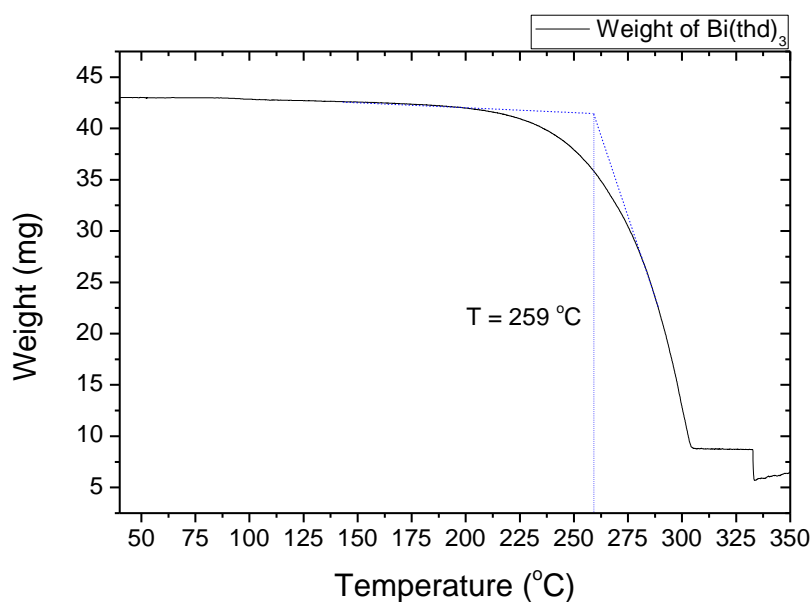


Figure 4-6. Thermogram for $\text{Bi}(\text{thd})_3$, heating rate $10^{\circ}\text{C}/\text{min}$ under ambient pressure of nitrogen atmosphere. The temperature for sublimation onset is determined to be 259°C .

As the TG curve in *Figure 4-6* shows, only one step sublimation can be observed. A possible reason for this may be that a too high heating rate was used in the measurement. The onset temperature for sublimation was determined to be 259°C , and the rate of maximum rate of sublimation was determined, from the second derivative, to be at 291°C . It should be noted that the remaining mass at 310°C is probably due to some decomposition of the precursor. Yellow bismuth oxide could be observed in the quartz container used as sample holder at the end of the measurement. Additionally, the sudden drop in weight with a following increase observed above 325°C is most likely due to malfunction of the TG equipment.

In an attempt to separate and study these two fractions in more detail, the sublimation oven was used. By reference to *Figure 4-5* it was decided to heat the sublimation oven up to 100°C , while keeping the finger at 40°C .

By doing so it was assumed that the fraction that recrystallized below 100 °C would be deposited on the finger.

The amounts of *D* purified are given in *Table 4-5*, together with the obtained amounts of powder from the finger and the flask. The compound was left inside the sublimation oven for 5 days.

Table 4-5. *The amounts of Bi(thd)₃ purified, together with the obtained amounts from the finger and the flask.*

| Pre purification | | Post purification | | |
|------------------|---------|-------------------|------------|------|
| Sample | Amounts | From finger | From flask | Loss |
| Unit | (g) | (g) | (g) | % |
| D | 3.69 | 0.66 | 2.31 | 19.5 |

Capillary powder samples were made of the compounds obtained from both the finger and the flask and was studied with XRD. A comparison of the diffractograms obtained from the two separated fractions is given in *Figure 4-7*.

As *Figure 4-7* shows, the two obtained diffractograms are almost identical. The broad peak in the area 3-6° for the blue line is due to background noise, which most likely hides the peak observed around 4.5° on the red line. The only noticeable difference can be seen in the area around 8.5-9.2°, which is magnified in the insert in *Figure 4-7*. Here, the compound from the flask shows two small peaks which is absent in compound from the finger.

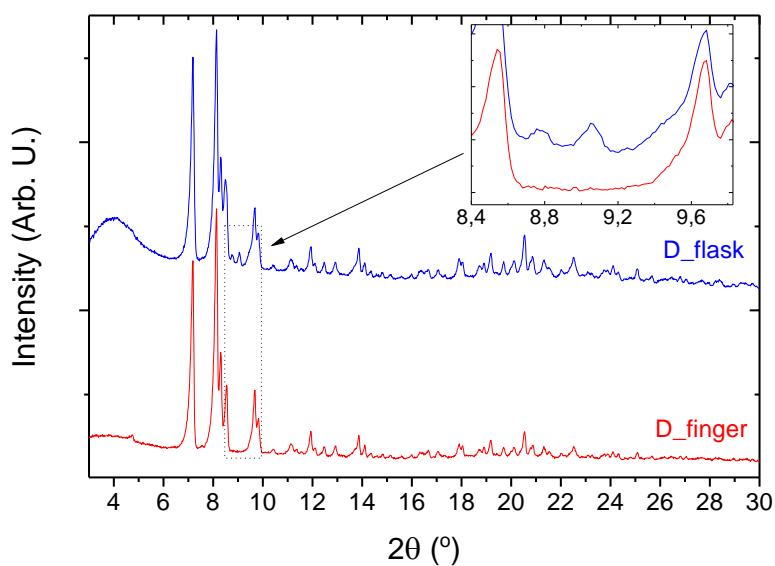


Figure 4-7. The measured diffractograms, by XRD on capillary powder samples, from the purification of D. The insert shows a magnified view of the marked box on in the figure.

In both cases the compound obtained from the finger was observed to have a faint yellow colour in contrast to the white powder remaining in the flask. In addition during capillary XRD measurements, it was observed that the compound from the finger melted to a faint yellow oil, while the compound from the flask remained a dry white powder.

4.1.5.3 Structural investigation of Bi(thd)₃

The recorded diffractograms, obtained by capillary powder XRD, of the synthesized Bi(thd)₃ compounds were compared with reported phases of Bi(thd)₃ in the literature. There are reported three phases of Bi(thd)₃, these are given below in *Table 4-6*.

Table 4-6. An overview over the three reported phases of Bi(thd)₃.

| Labeled Ref. | Fukin [103] | Armela01 [121] | Armela02 [121] |
|---------------------|--|---|--|
| Year | 1993 | 1998 | 1998 |
| Compound | [Bi(thd) ₃] ₂ · 0.5Hthd | Bi(thd) ₃ · H ₂ O | Bi(thd) ₃ · 3H ₂ O |
| Crystal system | monoclinic | monoclinic | orthorhombic |
| Space group | C2/c | P2 ₁ /n | Pbcn |
| a (Å) | 43.396 | 12.426 | 20.953 |
| b (Å) | 20.455 | 19.565 | 19.619 |
| c (Å) | 18.499 | 15.820 | 19.475 |
| α, β, γ (°) | 90/104.27/90 | 90/94.31/90 | 90/90/90 |
| V (Å ³) | 15914 | 3835 | 8006 |
| Z | 8 | 4 | 8 |
| λ (Å) | 0.71073 | 0.71073 | 0.71073 |

The synthesized compounds, given in *Table 4-7*, was found to correspond well with the reported phase labelled Armela01, see *Figure 4-8*. The diffractogram of Armela01, was simulated based on the values given in Ref. [121].

Table 4-7. The synthesized $\text{Bi}(\text{thd})_3$ compounds in this work, that contains the phase $\text{Bi}(\text{thd})_3 \cdot \text{H}_2\text{O}$ (Armela01).

| Compound | Labeled |
|---|---------|
| The fraction from the second sublimation of D | D2 |
| B | B |
| The fraction from the second sublimation of C | C2 |
| The red powder obtained in the synthesis of E | R |

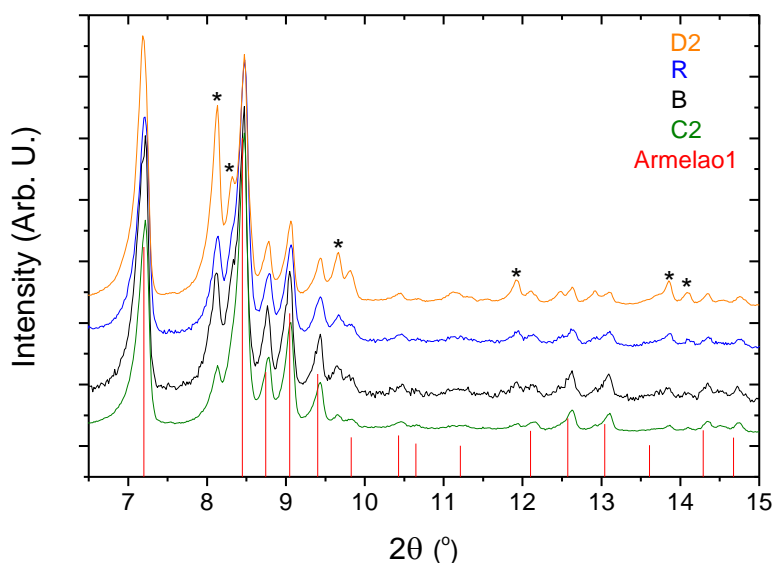


Figure 4-8. Diffractogram, obtained by XRD, of the synthesized compounds in this work together with the reported phase $\text{Bi}(\text{thd})_3 \cdot \text{H}_2\text{O}$ (Armela01). Unknown phase is marked with (*).

The diffractograms in *Figure 4-8* shows that there are some peaks that do not correspond with Armela01, which may suggest the presence of another phase. It should be noted that the other reported phases Armela02 and Fukin, given in *Table 4-6*, did not correspond with any of the compounds synthesized in this work.

The remaining synthesized compounds in this work, given in *Table 4-8*, shows little resemblance to Armela01, see *Figure 4-9*.

Table 4-8. Synthesized $\text{Bi}(\text{thd})_3$ compounds in this work, that contain little or no amounts of Armelao1.

| Compound | Labeled |
|---|---------|
| The fraction from the first sublimation of D | D1 |
| The fraction from the first sublimation of C | C1 |
| The white powder obtained in the synthesis of E | W |

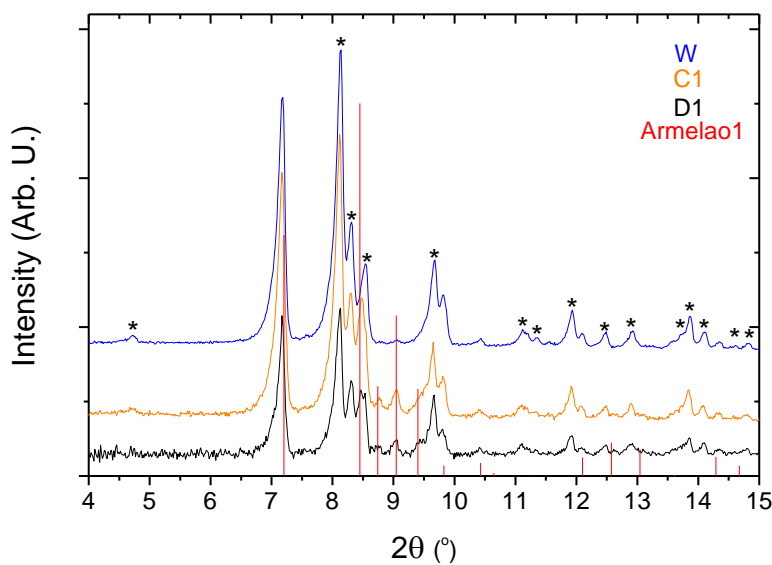


Figure 4-9. X-ray diffractogram of the synthesized compounds in this work that corresponds poorly with the reported phase $\text{Bi}(\text{thd})_3 \cdot \text{H}_2\text{O}$ (Armelao1). Unknown phase marked with (*).

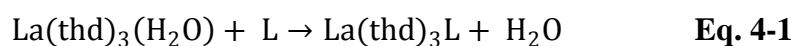
As can be seen from *Figure 4-9*, some of the peaks in the recorded diffractograms correspond with the phase reported in Armelao1. This may be due to small amounts of the Armelao1-phase in the investigated samples, or due to one or more possible unknown phases of $\text{Bi}(\text{thd})_3$ that may have some peaks overlapping with the Armelao1-phase.

The presented diffractograms in both *Figure 4-8* and *Figure 4-9* indicates that the synthesized $\text{Bi}(\text{thd})_3$ compounds in this work consisted of more than one phase, and that the phase that could be identified contained crystal water. None of the synthesized samples contained any of the other reported

phases of Bi(thd)₃, it is therefore likely that there exist one or more additional unknown phases of Bi(thd)₃.

4.1.5.4 Removal of crystal water from Bi(thd)₃

In an attempt to remove the crystal water from the synthesized Bi(thd)₃, tetraglyme (tetraethylene glycol dimethyl ether) was used. It is reported that reacting equal amounts of tetraglyme with β-diketonates such as La(thd)₃(H₂O), Eu(thd)₃(H₂O) and Tb(thd)₃(H₂O), which are similar in size to Bi(thd)₃, in hexane has resulted in monomeric complexes of La(thd)₃L, Eu(thd)₃L and Tb(thd)₃L (L = tetraglyme), see *Eq. 4-1* [122].



In Ref. [122] an oily product was obtained, which crystallized into crystals after a short time. It is further reported that products were stable towards air/moisture. In addition, it was observed that the melting points of the investigated β-diketonates decreased with about 60 °C on complexation with tetraglyme, compared to their respective hydrates.

In this work two different syntheses were carried out based on the work reported in Ref. [122], one where tetraglyme was in excess and one where stoichiometric amounts of tetraglyme and Bi(thd)₃ was reacted, see *Table 4-9*. When determining the proper amounts of Bi(thd)₃ it was assumed that it contained one amount of crystal water per formula unit. The solvent was dried prior to use and all the manipulations were carried out in inert atmosphere by using a glove box and a Schelnk line. The tetraglyme used was manufactured by Fluka and had a given purity > 98%.

Table 4-9. Amounts used in the two reactions of tetraglyme with $\text{Bi}(\text{thd})_3$.

| Synthesis nr. | Compound | Weight (g) | mmol |
|---------------|--|------------|-------|
| 1 | $\text{Bi}(\text{thd})_3 \cdot \text{H}_2\text{O}$ | 0.5945 | 0.763 |
| | Tetraglyme | 1.0213 | 4.595 |
| 2 | $\text{Bi}(\text{thd})_3 \cdot \text{H}_2\text{O}$ | 0.6730 | 0.869 |
| | Tetraglyme | 0.1933 | 0.869 |

Both synthesis 1 and 2 yielded a yellow oily product. It was not possible to obtain crystals or a solid product at room temperature, however, the oil seemed to crystallize into a white powder when cooled in ice water. Because it is difficult to characterize a liquid by XRD, this investigation was not pursued any further. The failure to recrystallize the oil, may indicate that the melting point of $\text{Bi}(\text{thd})_3$ drops from around 137 °C down to around 0 °C when complexed with tetraglyme. However, more investigation is needed before any conclusions can be made. Due to lack of time, the obtained products were not investigated further.

4.2 Thin films in the Co-O and Bi-O systems

This chapter presents the work on deposition and investigation of the thin films in the Co-O and Bi-O system. For deposition in the Co-O system, four growth systems was investigated and the results will be given in the order: $\text{Co}(\text{thd})_2 + \text{O}_3$, $\text{Co}(\text{thd})_3 + \text{O}_3$, $\text{Co}(\text{thd})_3 + \text{H}_2\text{O}$, and $\text{Co}(\text{thd})_2 + \text{H}_2\text{O}$. For depositions in the Bi-O system, two growth systems was investigated and the results will be given in the order: $\text{BiPh}_3 + \text{H}_2\text{O}$ and $\text{Bi}(\text{thd})_3 + \text{H}_2\text{O}$.

4.2.1 Thin films based on $\text{Co}(\text{thd})_2$ and O_3

The $\text{Co}(\text{thd})_2/\text{O}_3$ system was investigated as basis for comparison with the novel $\text{Co}(\text{thd})_3/\text{O}_3$ combination. The $\text{Co}(\text{thd})_2/\text{O}_3$ system is well investigated

in the literature [12-14], and the results obtained from the work on this system would therefore also serve as a reference to the prior art.

The growth rate per cycle of Co_3O_4 from $\text{Co}(\text{thd})_2$ and O_3 has varied slightly throughout the duration of this work. This is probably due to changes done on the equipment, such as a new ozone generator and possible leaks on the reactor. An overview over the recorded growth rate per cycle of Co_3O_4 from $\text{Co}(\text{thd})_2$ and O_3 during this work is given in *Table 4-10*.

The observed growth rates given in *Table 4-10* are somewhat lower than what reported in Ref. [13] (average growth rate of 20 ± 1 pm/cycle in the temperature range 114 – 307 °C).

Table 4-10. Overview of the growth rate per cycle of Co_3O_4 from $\text{Co}(\text{thd})_2$ and O_3 during this work.

| Sample | Cycles | Temperature | Thickness | Growth rate/cycle | Date |
|---------|--------|-------------|-----------|-------------------|----------|
| | Number | °C | nm | pm/cycle | dd.mm.yy |
| KBG1007 | 1000 | 186 | 15 | 15 | 25.03.08 |
| KBG1037 | 1000 | 186 | 16 | 16 | 30.10.08 |
| KBG1072 | 1000 | 186 | 17.5 | 17.5 | 05.04.09 |
| KBG1080 | 1000 | 167 | 18 | 18 | 20.05.09 |

4.2.1.1 Crystal structure and orientation on Si(111)

Co_3O_4 adopts the normal spinel structure and is described by the space group $Fd3m$. When heated above 900 °C Co_3O_4 converts to CoO , which adopts the NaCl-type structure with space group $Fm-3m$ [14, 123].

A 100 nm thick film (KBG1051) was deposited on Si(111) at 186 °C in order to verify the results reported in the literature [13]. The diffractogram, obtained by θ - 2θ measurements, is shown in *Figure 4-10* indicates that the

film deposited on Si(111) show a tendency towards (100)-oriented growth as a relatively strong (004) reflection can be observed. The orientation is not perfect since some rather weak peaks can be observed from the (113), (115) and (333) reflections. For comparison, Ref. [13] reports a (100)-oriented growth for films deposited on Si(100) in the temperature range 138-186 °C, and (111)-oriented growth in the temperature range 235-283 °C. However, films deposited at both 186 and 235 °C in Ref. [13] seems to be more crystalline than the film deposited at 186 °C in this work, as more and clearer peaks can be observed in the reported θ - 2θ diffractograms.

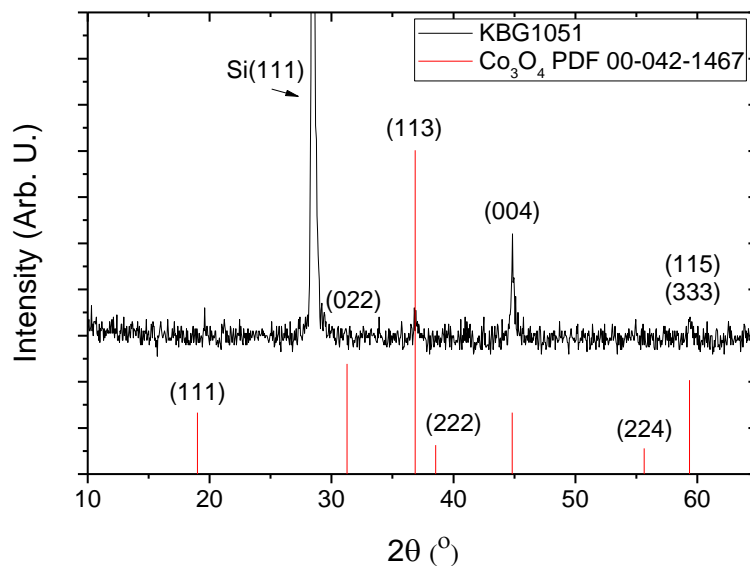


Figure 4-10. Diffractogram, obtained by θ - 2θ measurement, of a 100 nm thick Co_3O_4 film deposited from $\text{Co}(\text{thd})_2$ and O_3 at 186 °C on Si(111).

The height of the crystallites in the deposited film was estimated from the θ - 2θ measurement using the Scherrer equation, see Table 4-11.

Table 4-11. The crystallite height calculated from the θ - 2θ measurement. FWHM value of Si(111) used as standard.

| Sample | Co ₃ O ₄ (004) FWHM ($^{\circ}$) | Si (111) FWHM ($^{\circ}$) | Height of crystallites (nm) |
|---------|--|------------------------------------|-----------------------------------|
| KBG1051 | 0.264 | 0.118 | 47.4 |

4.2.1.2 AFM study of Co₃O₄ deposited on Si(111)

The roughness and topography of a 100 nm thick film deposited from Co(thd)₂ and O₃ on Si(111) at 186 °C (KBG1051) was investigated by AFM.

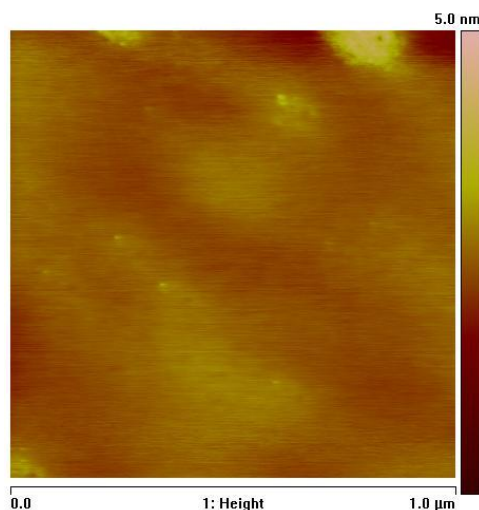


Figure 4-11. Topography of a 100 nm thick film, as measured by AFM, deposited on Si(111) using Co(thd)₂ and O₃ at 186 °C.

Figure 4-11 shows that the film is rather smooth, and the root mean square (RMS) value which was measured to be 0.22 nm confirms this. This value is much lower than reported RMS value of 2.1 nm, for a film deposited from Co(thd)₂ and O₃ at 186 °C on Si(100) [13]. A possible explanation may be that utilizing Si(111) as substrate yields a smoother film than if the film is deposited on a Si(100) substrate. However, both Si(111) and Si(100) have a native oxide layer, which is likely to be amorphous, and any difference in

the crystallinity and/or orientation of the deposited films on the two different substrates should therefore not be expected. A more likely explanation is that the temperature in the reactor has been slightly higher than 186 °C during this deposition. As Co_3O_4 grows with (100)- and (111)-orientation at 186 and 235 °C, respectively, if the deposition temperature was somewhere in between these two temperatures, where a shift of the orientation occurs, the resulting film is expected to be poorly crystalline and hence also have a smooth surface [76].

4.2.1.3 FT-IR study of Co_3O_4 deposited on Si(111)

To check for any carbonate contaminations in the deposited film, a 100 nm thick film deposited at 186 °C on Si(111) (KBG 1051) was investigated by FT-IR.

The FT-IR measurements, given in *Figure 4-12*, show no evidence of carbonate contamination at the temperature used for deposition. The main absorption peak of CoCO_3 is in the 1424-1452 cm^{-1} range [14], and the measured film show no absorption in this area. Absorption peaks at 570 cm^{-1} and 661 cm^{-1} for Co_3O_4 is reported in Ref. [123]. Where the first band at 570 cm^{-1} is associated with the OB_3 vibration in the spinel lattice, where B denotes Co^{3+} in an octahedral hole, and the second band at 661 cm^{-1} is attributed to the ABO_3 vibration, where A denotes the Co^{2+} in a tetrahedral hole. From the obtained FT-IR data the measured film have its main absorption peaks at 560 cm^{-1} and at 660 cm^{-1} . When comparing the wavenumbers of the main absorption peaks for the thin film and the bulk values reported in [123], the absorption peaks for the thin film are shifted down. This shift in wavenumber can be due to the restricted size of the crystallites [14].

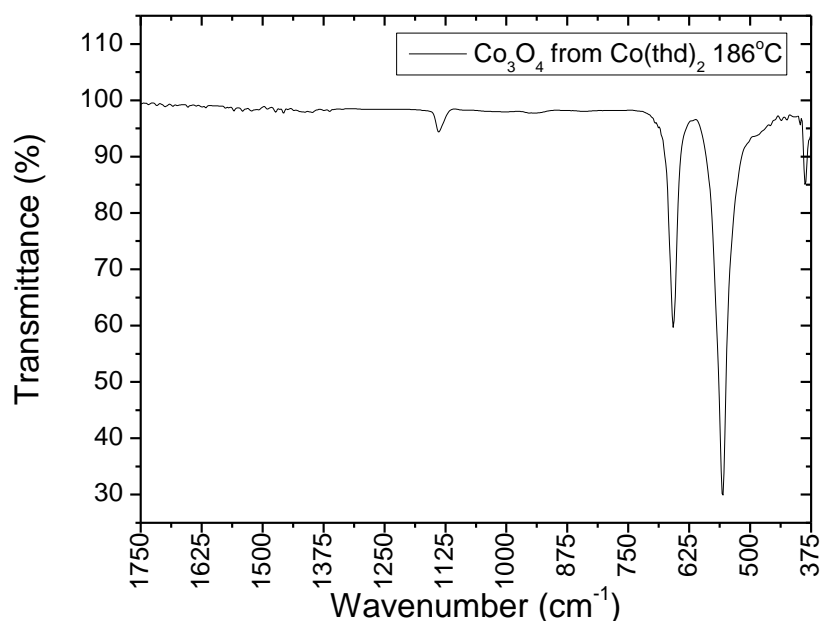


Figure 4-12. FT-IR spectra of Co_3O_4 deposited from $\text{Co}(\text{thd})_2$ and O_3 on $\text{Si}(111)$ at 186°C .

4.2.2 Thin films based on $\text{Co}(\text{thd})_3$ and O_3

Here the results both regarding deposition of thin films and investigation of said films from the novel precursor combination $\text{Co}(\text{thd})_3$ and O_3 are presented.

4.2.2.1 Pulse stability

Based on the information on sublimation temperature and thermal stability obtained in section 4.1.2, the precursor was tested for ALD growth together with O_3 . The pulse and purge parameters were kept at such high values that it was assumed that they were all in their respective ALD windows.

To investigate the pulse stability, the growth rate was measured as a function of the length of both $\text{Co}(\text{thd})_3$ - and O_3 -pulses at 186 °C. The $\text{Co}(\text{thd})_3$ pulses was varied between 1.0-3.0s and O_3 pulses was varied between 0.5-6.0s. When one of the $\text{Co}(\text{thd})_3$ - or O_3 -pulse times was investigated the other parameters where kept constant at 1.5s purge, 6.0s O_3 and 2.0s purge, and 3.0s $\text{Co}(\text{thd})_3$, 1.5s purge and 2.0s purge, respectively.

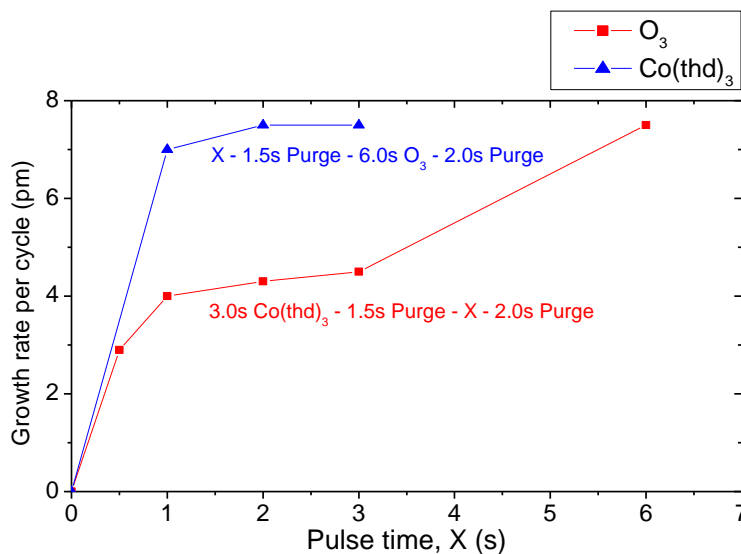


Figure 4-13. Growth rate as a function of $\text{Co}(\text{thd})_3$ pulse times (blue line) and O_3 pulse times (red line) at 186 °C on $\text{Si}(111)$, measured with XRR.

The blue line in *Figure 4-13* shows that for the growth rate as a function of $\text{Co}(\text{thd})_3$ pulse time, self-limiting growth occurs at a pulse length of 2.0s $\text{Co}(\text{thd})_3$. However, it was found necessary to keep the pulse length at 3.0s to obtain complete coverage over the whole substrate. The growth rate as a function of the O_3 pulse length, red line in *Figure 4-13*, seems to proceed in two separate steps. The growth rate increases rapidly up to 1.0s pulse length and remain more or less constant up to 3.0s, before increasing as the pulse length is increased to 6.0s. This behaviour is not observed for the similar

system $\text{Co}(\text{thd})_2/\text{O}_3$. For $\text{Co}(\text{thd})_2/\text{O}_3$ the thickness as a function of the O_3 pulse length increases rapidly up to a pulse length of 0.75s, where subsequently there are only small changes in the growth rate up to the investigated pulse length of 6.0s [14]. The reason for this step-like growth as a function of the O_3 pulse length is unknown, however, it may be due to kinetics or surface reconstructions. The growth rate increases with almost a factor of two when the pulse length is 6.0s compared to 1.0-3.0s. This could indicate that the number of thd-ligands on the adsorbed $-\text{Co}(\text{thd})_x$ complex has an influence on the reaction with O_3 in the gas phase. It may be that when $-\text{Co}(\text{thd})$ comprises the terminating complex, a reduced reactivity towards O_3 results, viz. the reaction from $-\text{Co}(\text{thd})_2$ to $-\text{CoO}_x(\text{thd})$ is rapid, whereas the following reaction from $-\text{CoO}_x(\text{thd})$ to $-\text{CoO}$ is slow. A more in-depth investigation has to be performed before a likely mechanism for this step-like behavior can be proposed.

4.2.2.2 ALD temperature window

The ALD temperature window was determined by measuring the thickness of the deposited films at different temperatures. The obtained results are also shown below in *Figure 4-14*.

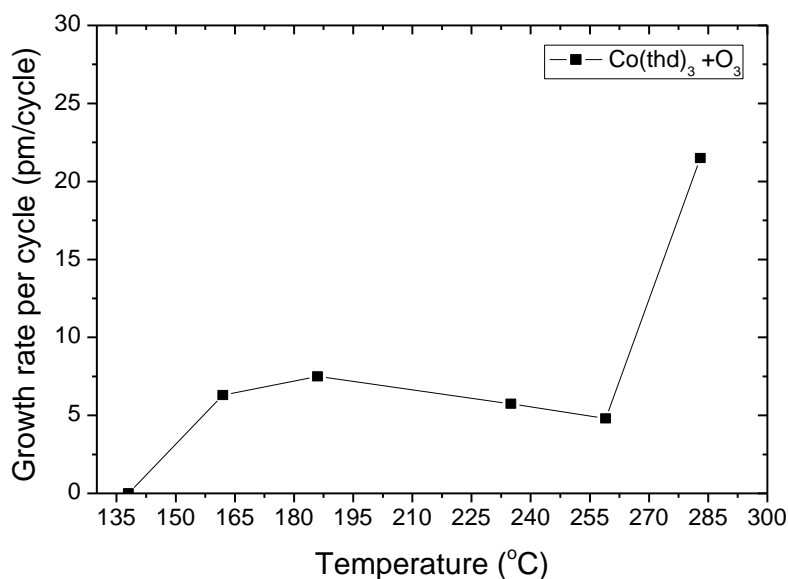


Figure 4-14. Growth rate per cycle for the $\text{Co}(\text{thd})_3/\text{O}_3$ precursor combination as a function of deposition temperature, measured with XRR.

As *Figure 4-14* shows, the temperature window for the $\text{Co}(\text{thd})_3/\text{O}_3$ system is between 162 and 259 °C. There was no observable film growth at 138 °C, and the increased growth rate at 283 °C is likely due to decomposing of the precursor. This could also be observed as large gradients on the films in the direction of the precursor flow. Based on the results shown in *Figure 4-14* the ALD temperature window for the $\text{Co}(\text{thd})_3 + \text{O}_3$ process is interpreted to be in the temperature range 162 – 259 °C, with an average growth rate of 6 pm/cycle.

4.2.2.3 Crystal structure on Si(111)

A 74 nm thick film (KBG1047) was deposited on Si(111) at 186 °C in order to determine the crystal structure of the deposited films from the $\text{Co}(\text{thd})_3/\text{O}_3$ precursor combination. The obtained diffractogram from both XRD and GIXRD measurements is shown in *Figure 4-15*.

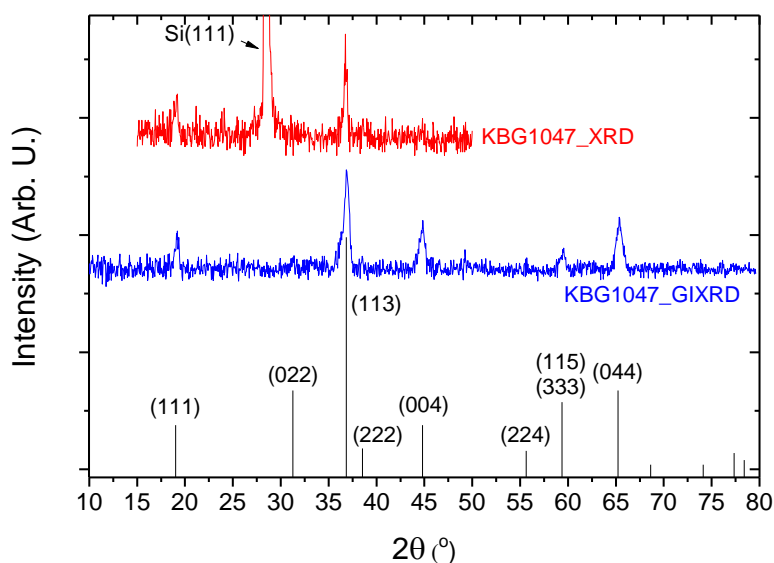


Figure 4-15. Diffractogram, obtained by θ - 2θ (red line) and GIXRD (blue line), of a 74 nm thick Co_3O_4 film deposited on Si(111) at 186 °C. PDF 00-042-1467 is represented by the black line. The background has been subtracted from the GIXRD diffractogram.

As the GIXRD measurement shows, the film is probably polycrystalline and all the observed peaks can be indexed as the Co_3O_4 phase. The diffractogram obtained from θ - 2θ -measurement shows only the (111) and (113) reflections which indicates that the film show a tendency towards (111)-oriented growth.

An estimate of the crystallite height was obtained, from the θ - 2θ -measurement, by the Scherrer equation, see *Table 4-12*.

Table 4-12. The calculated height of crystallites from the θ - 2θ measurement. FWHM value of Si(111) used as standard.

| Sample | Co ₃ O ₄ (113) FWHM | Si (111) FWHM | Height of crystallites |
|---------|--|------------------|---------------------------|
| Unit | ($^{\circ}$) | ($^{\circ}$) | (nm) |
| KBG1047 | 0.41 | 0.125 | 25.4 |

4.2.2.4 FT-IR study of Co₃O₄ from Co(thd)₃ deposited on Si(111)

To investigate for any carbonate contamination in the deposited films FT-IR was used. The obtained FT-IR spectra are presented in *Figure 4-16*.

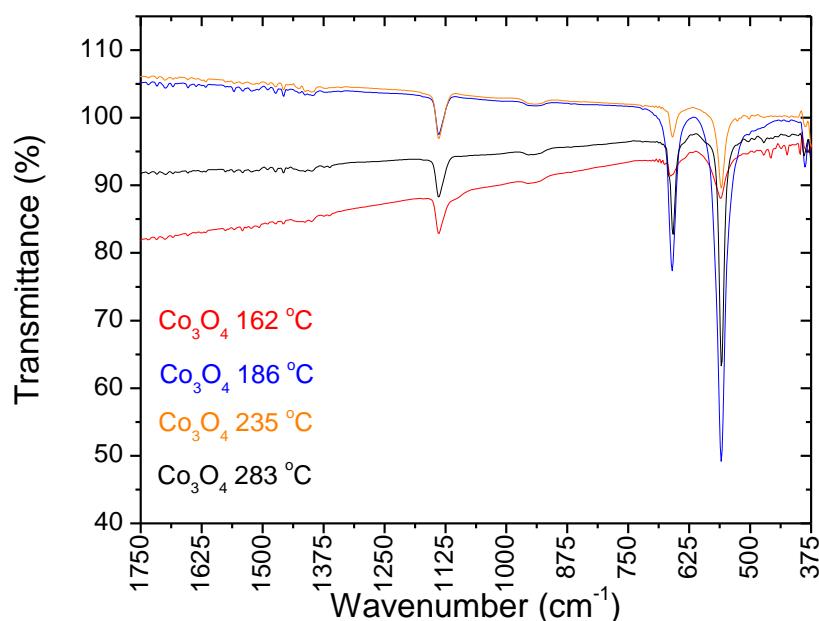


Figure 4-16. FT-IR spectroscopy data of Co₃O₄ films deposited from Co(thd)₃ and O₃ on Si(111), in the temperature range 162-283 °C.

The FT-IR measurements show no evidence of carbonate contamination at any temperature (CoCO₃ absorbs in the 1424-1452 cm⁻¹ range [14]). From the obtained FT-IR data the measured films have their main absorption peaks at 560 cm⁻¹ and at 660 cm⁻¹. When comparing the wavenumbers of

the main absorption peaks for the thin films and the bulk values reported in [123], the absorption peaks for the thin films are shifted down, from 570 cm^{-1} and 661 cm^{-1} to 560 cm^{-1} and 660 cm^{-1} , respectively. As mentioned earlier, this shift in wavenumber can be due to the restricted size of the crystallites. In addition, there seems to be no connection between the deposition temperatures and the obtained FT-IR spectra. It should be noted that the dissimilarity in the measured absorbance, at the two areas 560 cm^{-1} and 660 cm^{-1} are probably caused by different thickness of the measured films (ca. 12 nm for films deposited at 162 and 235 °C and ca. 74 nm for films deposited at 186 and 283 °C).

4.2.2.5 AFM study of Co_3O_4 deposited on Si(111)

The roughness of films deposited in the temperature range 162 - 283 °C, was investigated by AFM. *Figure 4-17* on the next page shows the topography with the corresponding roughness value, given in RMS, for the different temperatures. In *Figure 4-18* the measured roughness is presented graphically as a function of deposition temperature.

The measured roughness values presented in *Figure 4-17* and *Figure 4-18* shows that the RMS value is fairly constant in the measured part of the ALD temperature window, 162 – 235 °C. There is a slight increase in the measured roughness for the film deposited at 235 °C, which would be expected as the films are likely to be more crystalline with increasing deposition temperature. The relatively large increase in roughness observed at the deposition temperature of 283 °C, is likely due to decomposing of the $\text{Co}(\text{thd})_3$ precursor. When the topography of the samples deposited at 162 and 186 °C are compared with the sample deposited at 235 °C there seems

also to be an indication of increasing crystallinity for the sample deposited at 235 °C, as larger crystallites can be noted on the surface.

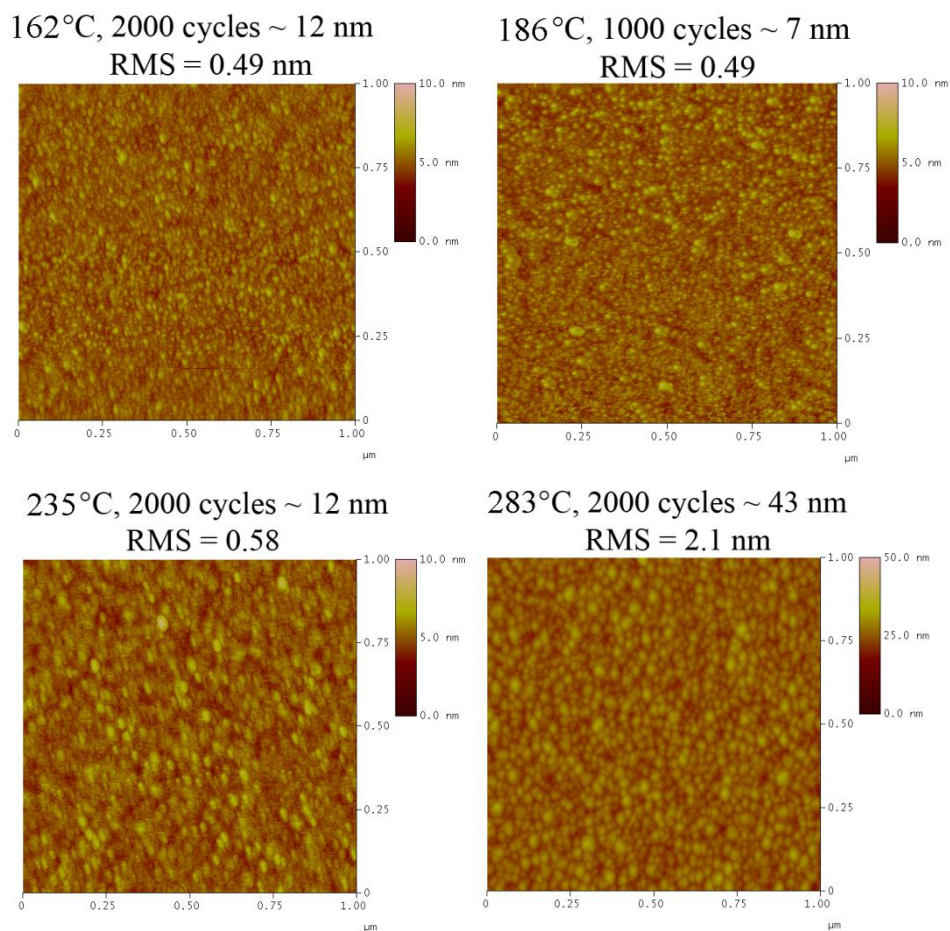


Figure 4-17. Topography, as measured by AFM, and measured roughness in RMS of Co_3O_4 films deposited from $\text{Co}(\text{thd})_3$ and O_3 in the temperature range 162 - 283 °C on Si(111), note the differences in the height profile.

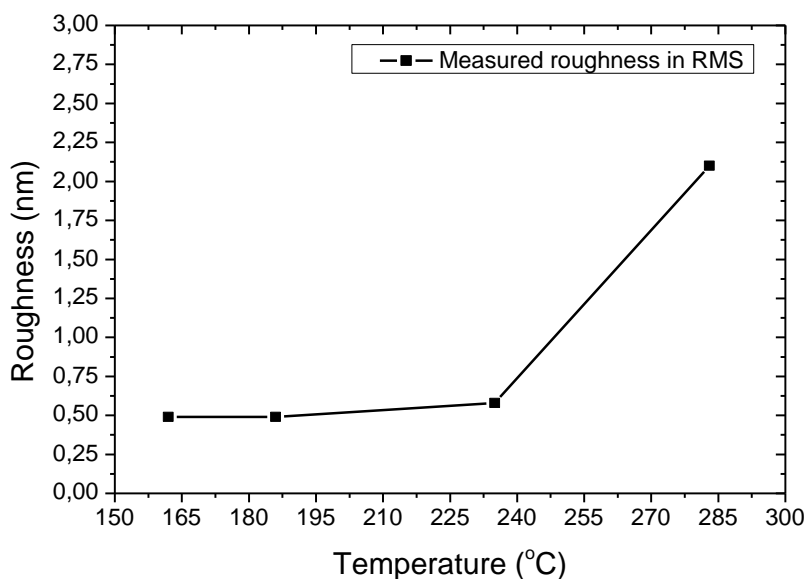


Figure 4-18. Measured roughness, in RMS, of Co_3O_4 films deposited from $\text{Co}(\text{thd})_3$ in the temperature range 162-283 °C on Si(111). Same samples as in Figure 4-17.

It should be noted that the almost constant roughness in the ALD temperature window, as shown in Figure 4-18, was also observed for the similar $\text{Co}(\text{thd})_2/\text{O}_3$ precursor combination in Ref. [14].

4.2.2.6 AFM study of Co_3O_4 deposited on silica glass and Si(111)

To investigate for the effect of substrate on the on the surface topography, two 74 nm thick films deposited on respectively silica glass and Si(111) was measured by AFM, see Figure 4-19a) and b). The film deposited on silica glass has a somewhat lower roughness (RMS = 4.7 nm) than the film deposited on Si(111) (RMS = 5.6 nm). The measured grains are also smaller and more uniformly distributed on the surface for the film deposited on silica glass, see Figure 4-20, which may indicate that the $\text{Co}(\text{thd})_3/\text{O}_3$ growth system has a higher nucleation density on silica glass than Si(111).

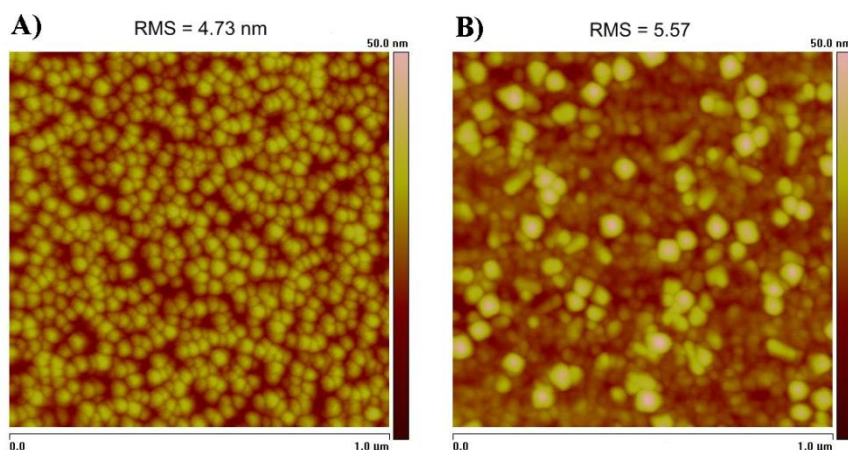


Figure 4-19. Topography of 74 nm thick films, as measured by atomic force microscopy, deposited on silica glass (A) and Si(111) (B) using $\text{Co}(\text{thd})_3$ and O_3 at 186 °C.

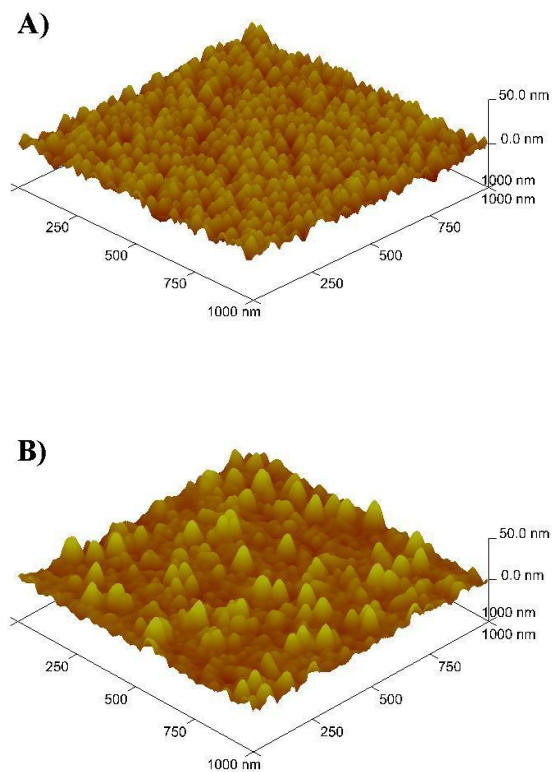


Figure 4-20. Topography of 74 nm thick films, as measured by atomic force microscopy, deposited on silica glass (A) and Si(111) (B) using $\text{Co}(\text{thd})_3$ and O_3 at 186 °C.

4.2.3 Thin films based on $\text{Co}(\text{thd})_3$ and H_2O

The novel ALD precursor was also tested for growth together with H_2O . At the tested temperatures of 186 and 235 °C, no deposited film could be observed. This precursor combination was therefore not investigated any further.

4.2.4 Thin films based on $\text{Co}(\text{thd})_2$ and H_2O

To investigate the similarities of the $\text{Co}(\text{thd})_2$ and $\text{Co}(\text{thd})_3$ system further, $\text{Co}(\text{thd})_2$ was also tested for deposition together with H_2O . The use of a strong oxidizing agent, such as ozone, makes it rather futile to try and utilize the different oxidation states on the metal atoms in the precursors to deposit different phases.

β -diketonates are generally considered to not be reactive towards water, however, preliminary tests showed that film was indeed deposition from the $\text{Co}(\text{thd})_2/\text{H}_2\text{O}$ combination at 235 °C. This indicated that this new precursor combination could be used in the ALD process and it was decided to investigate this system further.

4.2.4.1 Growth rate and temperature window

To investigate the ALD temperature window for the $\text{Co}(\text{thd})_2$ and H_2O process, films were deposited using 5000 cycles in the temperature range 162 – 283 °C whereupon the thickness was measured by XRR. In *Figure 4-21* the measured growth rate is shown as a function of the deposition temperature.

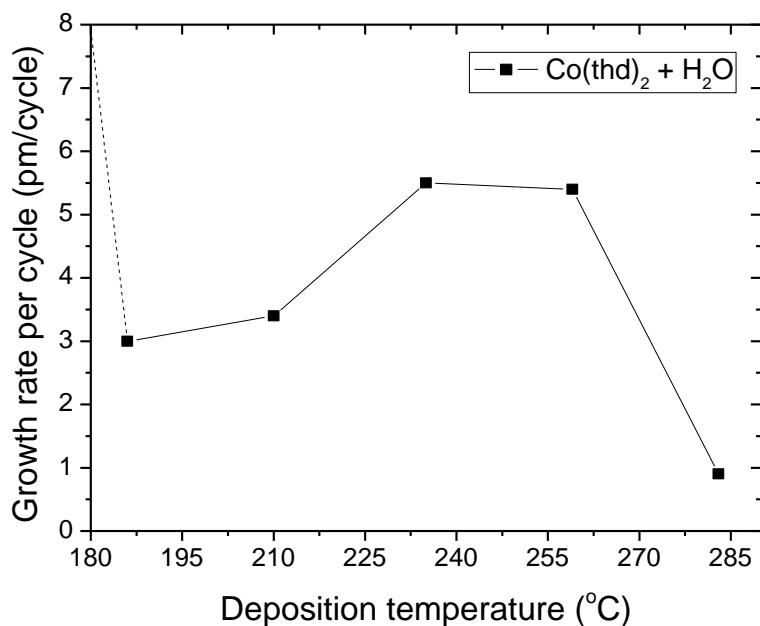


Figure 4-21. The effect of temperature on the growth rate per cycles for the precursor combination Co(thd)_2 and H_2O . Deposited from 5000 cycles at the given temperatures. Stippled line indicates increased growth rate at lower temperatures.

The film deposited at 162 °C showed large gradients and the film was too thick and/or a too high roughness for the thickness to be measured by XRR. The olive green color of the deposited film indicated that the film consisted of CoO , which was confirmed by GIXRD. A natural explanation for this increase in growth rate at lower temperatures would be that the temperature is so too low for potential physisorbed precursor molecules to be removed from the surface, however, this is not the case for the similar process $\text{Co(thd)}_2/\text{O}_3$. Suggesting that the mechanism for the observed increase in growth rate is not likely due to the condensation of the Co(thd)_2 precursor on the surface. There might be some properties with the CoO surface that causes this behavior, and that is why a similar observation is not made for the $\text{Co(thd)}_2/\text{O}_3$ process at the same temperature. Nevertheless, in order to

propose a likely mechanism for this observed increase in growth rate, thorough investigations are necessary. The decrease in growth rate observed at 283 °C is likely due to decomposition of the precursor, because a black deposit was observed formed on the inside of the precursor tube at the hot end. This indicates that the $\text{Co}(\text{thd})_2$ precursor began to decompose before it entered the reaction chamber, which could explain the observed decrease in the growth rate per cycle at 283 °C. Nevertheless, *Figure 4-21* shows a rather uncharacteristic shape for an ALD temperature window. The temperature window seems to have two plateaus at 186 – 210 °C and at 235 – 259 °C, which could suggest that two different phases are deposited with their respective growth rate in each of the observed plateaus. The difference may also be due to surface reconstructions, increased kinetics or different growth orientations. However, the uncharacteristic ALD temperature window indicates that the growth mechanics may be rather complex, and that a more detailed investigation is needed before a suggestion for this step-like growth can be made.

4.2.4.2 Crystal structure

GIXRD analysis was applied on selected samples in order to investigate the uncharacteristic growth rate observed in the proposed ALD temperature window for the $\text{Co}(\text{thd})_2/\text{H}_2\text{O}$ process, the effect of the deposition temperature on the crystallinity and obtained phase. GIXRD was utilized because θ - 2θ measurements revealed no peaks. The selected samples were the same as those investigated in *Figure 4-21*, except for the sample deposited at 235 °C which was exchanged with a thicker sample, deposited using 9055 cycles.

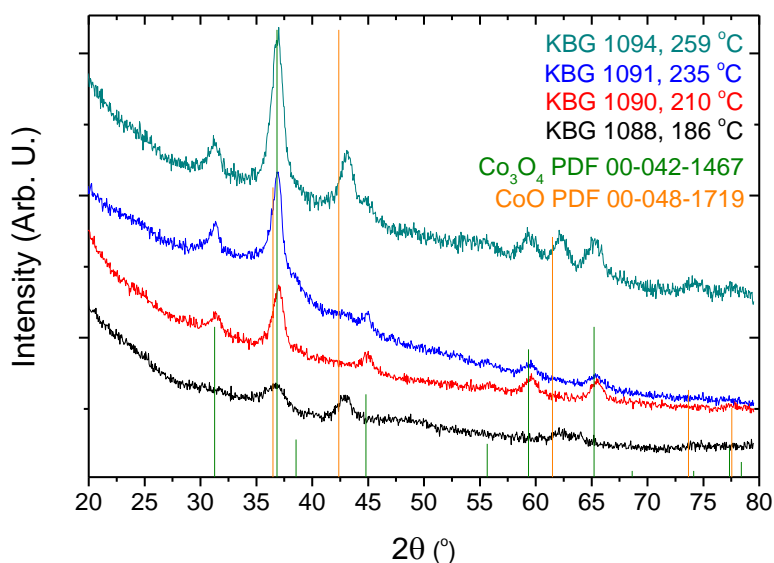


Figure 4-22. Diffractogram, obtained by GIXRD, showing the effect of different depositions temperature on the crystal structure of films deposited from $\text{Co}(\text{thd})_2$ and H_2O .

Figure 4-22 indicates that the CoO phase is deposited at 186 °C. Co_3O_4 is deposited in the temperature range 210 to 235 °C, whereupon a mixture of the CoO and Co_3O_4 phase is deposited at 259 °C. There may also be some traces of CoO for the deposition at 235 °C as a possible weak reflection from CoO can be observed around 42.5°. This is nevertheless an interesting result, as the observed deposition of CoO at 186 °C is the lowest temperature reported for deposition of CoO with ALD. As mentioned in section 1.2.2.1 the only prior report on deposition of CoO with ALD is Ref. [42], where CoO was deposited from $\text{Co}(\text{iPrAMD})_2$ and H_2O at 250 °C.

4.2.5 Thin films based on $\text{BiPh}_3 + \text{H}_2\text{O}/\text{O}_3$

In this work, around 20 depositions were carried out, in order to investigate depositions of BiO_x from BiPh_3 . BiPh_3 was tested together with both H_2O and O_3 with different pulse/purge times at different temperatures, in the temperature range 162 – 186 °C. None of the attempts resulted in a successful deposition of a BiO_x film, which would be expected based on the prior art given in section 1.2.2.2. To investigate the growth of BiPh_3 with H_2O closer, an in-situ QCM measurement was performed at 186 °C where 50 cycles of BiPh_3 was deposited on Co_3O_4 , which was deposited from 50 cycles of $\text{Co}(\text{thd})_2 + \text{O}_3$. The goal was to investigate if BiPh_3 could be used together with cobalt for depositions in the Bi-Co-O system and also try to obtain a better understanding for why BiPh_3 does not yield BiO_x films when deposited alone.

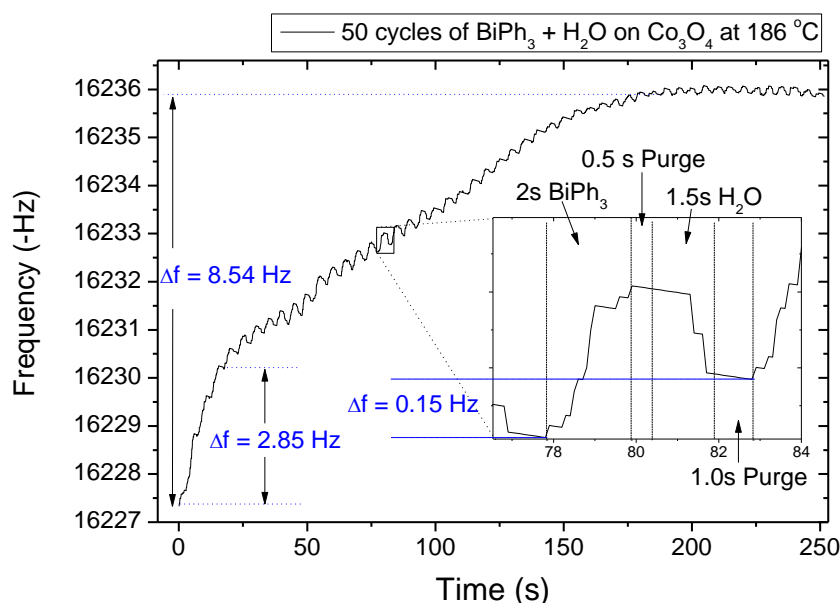


Figure 4-23. 50 cycles of BiPh_3 and H_2O deposited on Co_3O_4 at 186 °C. The graph is an average of three consecutive measurements. A baseline is subtracted from the shown graph. The marked square area on the graph is magnified in the small window.

The QCM measurement, shown in *Figure 4-23*, indicates that during the first three cycles of BiPh_3 there seems to be a relatively large mass increase, whereupon it decreases and almost no growth occurs, as the ΔHz becomes as low as 0.15 Hz, until it flattens out and ceases to grow. For comparison 1 cycle of TMA and H_2O gave a ΔHz of ca. 7.5 Hz. The QCM measurement suggests that BiPh_3 does not react with its own surface, as the growth decreases until it seemingly stops as more and more BiO_x are deposited on the surface. This could also explain why depositions of BiO_x are problematic using BiPh_3 . However, some growth seems to occur when BiPh_3 is deposited on a Co_3O_4 surface, which may indicate that this precursor can be used for deposition in the Bi-Co-O system. The increased reactivity towards the Co_3O_4 surface may be due to a catalytic effect, which is also a suggested mechanism for the observed growth of BiPh_3 when deposited in the Bi-Ti-O system [8]. On the other hand, maybe the Co_3O_4 surface presents favorable reactive sites for the BiPh_3 molecule, which the BiO_x surface lacks.

4.2.6 Thin films based on $\text{Bi}(\text{thd})_3 + \text{H}_2\text{O}$

The results from the second round of investigation of the $\text{Bi}(\text{thd})_3$ precursor are presented in this section. The first round of investigation of $\text{Bi}(\text{thd})_3$ was carried out on the Bi-Co-O system, these results are presented later in section 4.3.2.1 on page 142.

4.2.6.1 Growth conditions

A sublimation temperature of 137 °C was used for the deposition from $\text{Bi}(\text{thd})_3$ as this is the sublimation temperature used in the synthesis. In the

preliminary depositions the pulse and purge times used are given in *Table 4-13*.

Table 4-13. Pulse and purge parameters for the $\text{Bi}(\text{thd})_3 / \text{H}_2\text{O}$ ALD process, deposited at 206 °C.

| Sample | $\text{Bi}(\text{thd})_3$ pulse (s) | $\text{Bi}(\text{thd})_3$ purge (s) | H_2O pulse (s) | H_2O purge (s) | Comments |
|--------|---|---|--------------------------------------|--------------------------------------|--------------------------------------|
| EØ1070 | 2 | 1 | 1.5 | 1 | Film only deposited on the left side |
| EØ1071 | 2.5 | 1 | 1.5 | 1 | Film only deposited on the left side |
| EØ1072 | 5 | 1 | 1.5 | 1 | Film deposited uniformly |

The results from the preliminary depositions in *Table 4-13* shows that a uniformly covered substrate was obtained with the use of 5s $\text{Bi}(\text{thd})_3$ pulse length. Therefore the same parameters as EØ1072 was used for the following depositions from $\text{Bi}(\text{thd})_3$.

4.2.6.2 ALD temperature window

In order to determine the ALD temperature window, depositions were carried out at different temperatures and the thickness of the deposited film was then measured with XRR. The measured thickness as a function of the deposition temperature is presented in *Figure 4-24*.

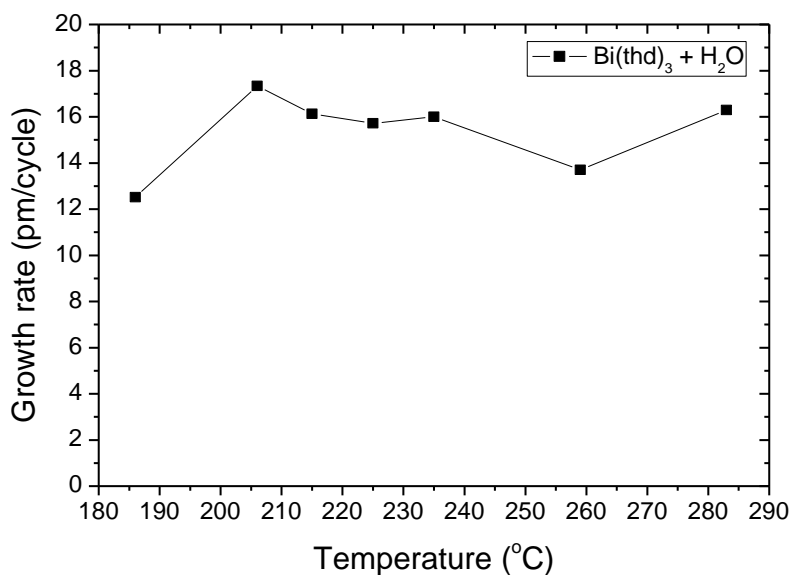


Figure 4-24. Growth rate as a function of the deposition temperature, measured with XRR. All measured films was deposited using 2000 cycles of $\text{Bi}(\text{thd})_3 + \text{H}_2\text{O}$.

Figure 4-24 shows that the growth rate per cycles shows only small variations in the temperature range 206 – 283 °C, except at 259 °C where a relatively large decrease in the growth rate can be observed. However, after the deposition at 259 °C the precursor had melted and decomposed, which indicates that this is not a reproducible result. The observed lower growth rate at 186 °C may indicate that the temperature is too low for possible surface reconstructions or slow kinetics. Decomposition of the precursor to metallic bismuth was observed for depositions carried out at 332 °C. Based on the results presented in Figure 4-24, an ALD window for the $\text{Bi}(\text{thd})_3$ and H_2O process was determined to be in the temperature range 206 - 283 °C with an average growth rate of 16 pm/cycle.

4.2.6.3 In-situ QCM analysis of the growth mechanism

As investigation of the synthesized $\text{Bi}(\text{thd})_3$ precursor revealed that it contained a phase with crystal water, it was suggested that the precursor might react with its own crystal water during deposition. In order to investigate the growth mechanism of $\text{Bi}(\text{thd})_3$ in more detail, an in-situ QCM measurement was carried out at 235 °C. In the measurement, Al_2O_3 was first deposited using 30 cycles of TMA and H_2O whereupon, after a 120s long purge, a 20s long $\text{Bi}(\text{thd})_3$ pulse was applied, followed by 10s purge, 4s H_2O pulse and a 120s purge. The result is given in *Figure 4-25*.

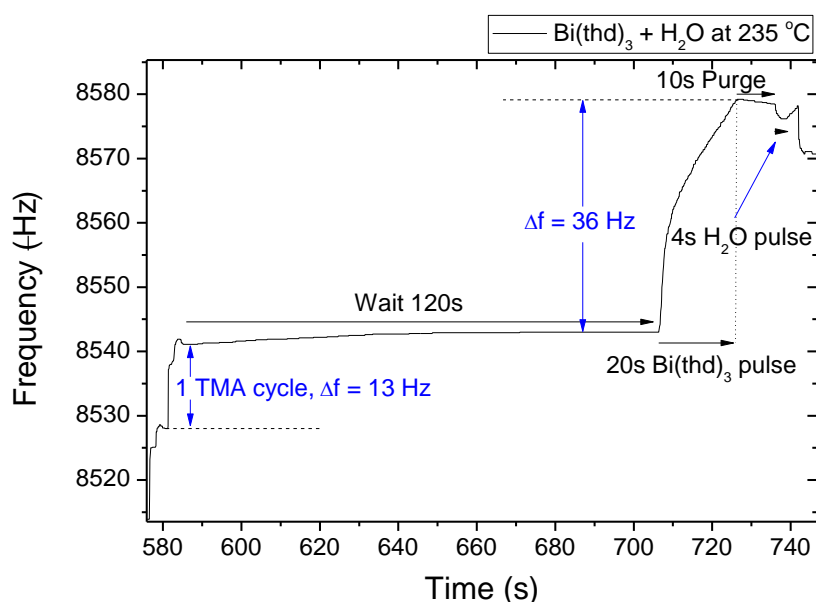


Figure 4-25. In-situ QCM measurement of $\text{Bi}(\text{thd})_3$ with H_2O , carried out at 235 °C.

Figure 4-25 shows that growth occurs as long as $\text{Bi}(\text{thd})_3$ are pulsed into the reaction chamber. This indicates that the precursor is reacting with its own crystal water and/or decomposing. As the obtained films are uniform in thickness and consists of Bi_2O_3 , the former is more likely. The M-O bond is the weakest bond in the precursor molecule [124], a decomposition reaction

is therefore likely to yield metallic bismuth as is observed for depositions at 332 °C. The reaction between the precursor and the crystal water seems to be surface controlled which could explain why uniform films are obtained. However, no deposited film is observed in the precursor supply tube which indicates that the growth is dependent on an external supply of water, or a given time is needed at high enough temperatures for the reaction with its own crystal water. Meaning when the precursor is pulsed, no reaction takes place during the short time window were the precursor molecules are transported to the reaction chamber. This could also be an explanation for why the thickest film was observed deposited on the substrate side closest to the exhaust, when only Bi(thd)₃ was pulsed. Nevertheless, this is not an ideal ALD growth where the thickness is only dependent on the number of cycles, as it is also dependent on the pulse length of Bi(thd)₃. However, as mentioned in section 2.1.1.4.1 this kind of process is allowed in depositions by ALD as long as the decomposition/reaction are surface controlled which results in uniform thickness.

4.2.6.4 θ -2 θ investigation of thin films of α -Bi₂O₃

The effect of the deposition temperature on the crystallinity of the deposited films was investigated by θ -2 θ measurements on three samples deposited using 2000 cycles at 206, 235 and 283 °C. The obtained diffractograms are given in *Figure 4-26*.

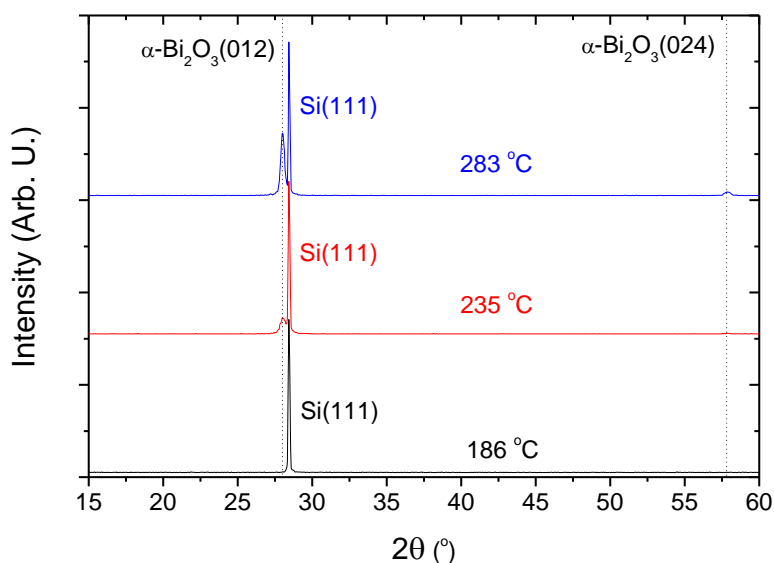


Figure 4-26. Diffractograms of $\alpha\text{-Bi}_2\text{O}_3$ films deposited at various temperatures. $\alpha\text{-Bi}_2\text{O}_3$ peaks from PDF 00-041-1449.

In *Figure 4-26* the observed peaks corresponds to the (012) and (024) reflexes of the monoclinic $\alpha\text{-Bi}_2\text{O}_3$ phase, with the space group $P2_1/c$. By reference to the phase diagram in *Figure 1-3* in section 1.2.1 on page 6 $\alpha\text{-Bi}_2\text{O}_3$ is the stable phase up to 730 °C. Based on the obtained θ - 2θ results in *Figure 4-26* films deposited above 206 °C are crystalline, and the deposited films grows with a (012) orientation. As the deposition temperature is increased, the measured intensity from the $\alpha\text{-Bi}_2\text{O}_3$ (012) and (024) reflections increase as compared to the Si(111) reflection from the substrate. This indicates an increase in the crystallinity with increasing deposition temperature.

The height of the crystallites in the crystalline films were estimated by using the Scherrer equation, the results are given in *Table 4-14*.

Table 4-14. The crystallite heights calculated from the θ - 2θ measurement. FWHM value of Si(111) used as standard.

| Temperature (°C) | α -Bi ₂ O ₃ (012) FWHM (°) | Si(111) FWHM (°) | Height of crystallites (nm) |
|---------------------|--|---------------------|--------------------------------|
| 235 | 0.426 | 0.133 | 22.2 |
| 283 | 0.309 | 0.114 | 31.3 |

The calculated crystallite heights, given in *Table 4-14*, also indicate that the degree of crystallinity improves with increasing deposition temperature. In addition, the crystallite height calculated at 283 °C is in the same range as the thickness of the deposited film, suggesting a columnar growth of the crystallites through the entire film.

4.2.6.5 FT-IR study on Bi₂O₃

FT-IR spectroscopy was applied to investigate for any possible carbonate contamination in the deposited Bi₂O₃ films. The obtained FT-IR spectrums are given in *Figure 4-27*.

The absorption peaks observed below 600 cm⁻¹, in *Figure 4-27*, is mainly due to the displacement of oxygen in the Bi-O bond [125]. In addition the FT-IR spectrums in *Figure 4-27* shows a broad band in area round 940 cm⁻¹, a strong absorption around 1140 cm⁻¹, a broad band around 1400 cm⁻¹, small absorptions in the area 1350-1850 cm⁻¹, a broad band around 2330 cm⁻¹, and a broad band with two peaks around 3000 cm⁻¹. The broad absorption peak at 1400 cm⁻¹ corresponds well with the strongest absorption peak of (BiO)₂CO₃ reported in Ref. [126]. There seems also to be no connection between the deposition temperature and the obtained FT-IR spectrums.

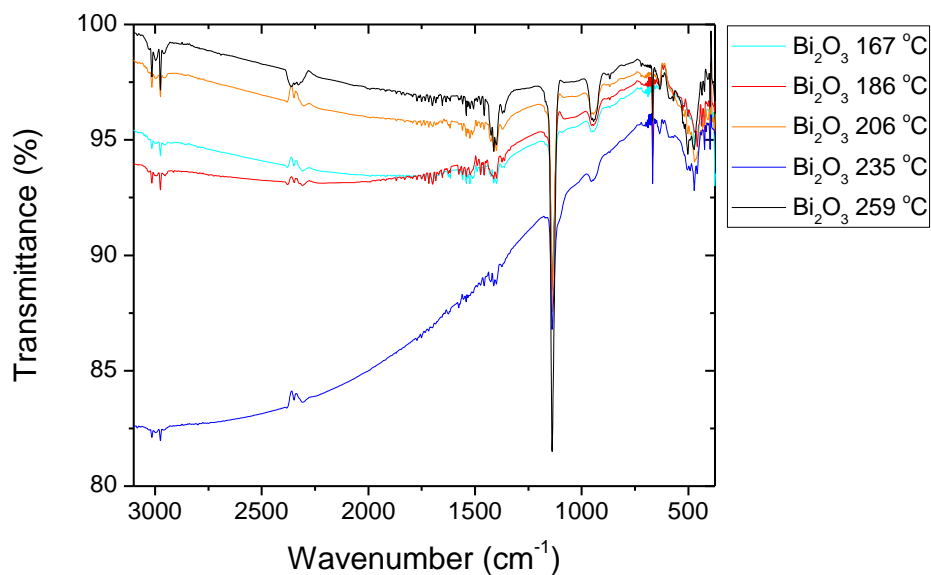


Figure 4-27. FT-IR spectrums of Bi₂O₃ films deposited from Bi(thd)₃ and H₂O at different temperatures.

4.3 Thin films in the Bi-Co-O system

In this section, the results obtained from the deposition in the Bi-Co-O system are presented. First results regarding the deposition of BiPh₃ with H₂O together with the different cobalt precursor combinations are given. Then the results obtained from the depositions of Bi(thd)₃ with H₂O together with Co(thd)₂ and O₃ are presented.

4.3.1 Thin films based on BiPh₃

As the results from the QCM analysis presented in section 4.2.5 on page 128 indicated that BiPh₃ could be used for deposition in the Bi-Co-O system, BiPh₃ was tested together with Co(thd)₂/O₃.

4.3.1.1 Thin films based on $\text{BiPh}_3 / \text{H}_2\text{O}$ and $\text{Co(thd)}_2 / \text{O}_3$

To investigate if BiPh_3 could be used together with Co(thd)_2 and O_3 two series of films with varying composition was made at 162 and 186 °C, and analyzed by XRF, *Figure 4-28*. The XRF data presented in *Figure 4-28* show similar trends for both temperatures investigated, where the highest bismuth content in the deposited films are reached at 50/50 pulse ratio between bismuth and cobalt. However, for the investigated temperatures it is evident that this precursor combination does not yield high enough bismuth content in the deposited films to be applicable for the deposition of the desired BiCoO_3 phase.

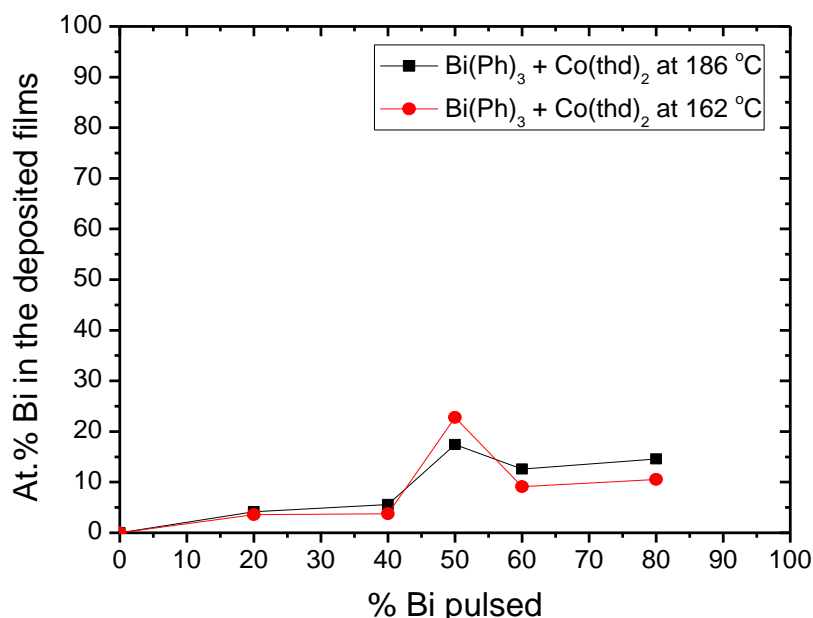


Figure 4-28. The atomic percentage of bismuth in the as deposited films at 162 °C (red line and circles) and 186 °C (black line and boxes) as a function of the percentage of pulsed bismuth precursor.

In an attempt to increase the bismuth content in the films deposited from BiPh_3 , preliminary deposition was done with BiPh_3 and the two novel precursor combinations found in this work, $\text{Co(thd)}_3/\text{O}_3$ and $\text{Co(thd)}_2/\text{H}_2\text{O}$.

The obtained growth rate for these two systems given in section 4.2.2.2 on page 116 and section 4.2.4.1 on page 124, respectively, shows that both these systems have a much lower growth rate than the $\text{Co(thd)}_2/\text{O}_3$ precursor combination. Therefore, it was suggested that by the use of these precursor combinations the bismuth content could be increased in the deposited films, by effectively decreasing the amount of cobalt deposited each cycle.

4.3.1.1.1 Thin films based on $\text{BiPh}_3/\text{H}_2\text{O}$ and $\text{Co(thd)}_3/\text{O}_3$

A preliminary deposition was made with the $\text{Co(thd)}_3 + \text{O}_3$ precursor combination together with $\text{BiPh}_3 + \text{H}_2\text{O}$ at 186°C to test the concept of increased bismuth content by using a cobalt precursor that with lower growth rate than the $\text{Co(thd)}_3/\text{O}_3$ combination. The obtained XRF data is presented in *Table 4-15*.

Table 4-15. The obtained data from the XRF measurement from films deposited at 186°C from $\text{BiPh}_3 + \text{H}_2\text{O}$ and $\text{Co(thd)}_3 + \text{O}_3$.

| Sample | Temperature ($^\circ\text{C}$) | Pulse ratio Bi% / Co% | Wt.% | | At.% | |
|---------|-------------------------------------|--------------------------|-------------------------|-------------------------|------|-------|
| | | | Bi_2O_3 | Co_3O_4 | Bi | Co |
| KBG1115 | 186 | 50 / 50 | 13.65 | 86.35 | 5.15 | 94.85 |

The obtained XRF data showed rather a decrease in Bi-composition by exchanging the $\text{Co(thd)}_2/\text{O}_3$ precursor combination with the $\text{Co(thd)}_3/\text{O}_3$ combination.

It should be noted, however, that the film thickness of the KBG1115 sample was measured to be 14.0 nm by XRR, which would be an expected thickness if the film had only been deposited from 2000 cycles of $\text{Co(thd)}_3 + \text{O}_3$. This indicates that the additional pulses of BiPh_3 resulted in an even lower growth rate for the system. Thus, from the preliminary deposition it

can be assumed that the combination of the $\text{BiPh}_3 + \text{H}_2\text{O}$ system with a cobalt precursor with a lower growth rate than the $\text{Co}(\text{thd})_2 + \text{O}_3$ system, such as $\text{Co}(\text{thd})_3 + \text{O}_3$, is not a solution for obtaining higher bismuth content in the deposited films.

4.3.1.1.2 Thin films based on $\text{BiPh}_3 / \text{H}_2\text{O}$ and $\text{Co}(\text{thd})_2 / \text{H}_2\text{O}$

Even though the $\text{Co}(\text{thd})_3 + \text{O}_3$ precursor combination did not result in a higher bismuth content when deposited together with $\text{BiPh}_3 + \text{H}_2\text{O}$, it was decided to do a preliminary test with $\text{Co}(\text{thd})_2 + \text{H}_2\text{O}$ as well. The $\text{Co}(\text{thd})_2 + \text{H}_2\text{O}$ precursor combination was tested together with $\text{BiPh}_3 + \text{H}_2\text{O}$ at 186 °C using a total of 8000 cycles. The obtained XRF data is given in *Table 4-16*.

Table 4-16. The obtained data from the XRF measurement from films deposited at 186 °C from $\text{BiPh}_3 + \text{H}_2\text{O}$ and $\text{Co}(\text{thd})_3 + \text{O}_3$.

| Sample | Temperature (°C) | Pulse ratio Bi / Co | Wt.% | | At.% | |
|---------|---------------------|------------------------|-------------------------|-------------------------|------|-------|
| | | | Bi_2O_3 | Co_3O_4 | Bi | Co |
| KBG1117 | 186 | 50% / 50% | 1.89 | 98.11 | 0.66 | 99.34 |

As can be seen from the XRF data the use of precursor combination $\text{Co}(\text{thd})_2 / \text{H}_2\text{O}$ together with $\text{BiPh}_3 / \text{H}_2\text{O}$ resulted in a significantly decrease in the bismuth content in the deposited film. However, the film had large gradients, where the film was yellow/orange in the middle and blue/green on the sides of large silica-glass substrate. The film was too thick to be measured by XRR, and the calculated thickness from the XRF data was 175 nm.

The enormous increase in thickness can only have two explanations. Either the alternating cycles of $\text{BiPh}_3 + \text{H}_2\text{O}$ increases the growth rate of the $\text{Co}(\text{thd})_2 + \text{H}_2\text{O}$ system or the reactor was malfunctioning during this

deposition leading to CVD growth of the cobalt precursor. The former is most likely, as there were no problems with the reactor before and after the deposition. The film was investigated with XRD and GIXRD and the crystalline phase was identified as CoO (Appendix 9.2). The result is additionally surprising since three single-crystal substrates, MgO(100), SrTiO₃(100) and Al₂O₃(1102), was introduced into the deposition chamber together with the Si(111) substrate in the KBG1117 experiments. All these additional substrates showed only reflections from Bi₂O₃ and none from cobalt oxide when investigated by GIXRD (Appendix 9.2). Although this is surprising, a critical and thorough investigation has to be carried out before any conclusions can be made.

4.3.1.2 FT-IR analysis of films based on BiPh₃/H₂O + Co(thd)₂/O₃

FT-IR was used to investigate for carbonate contaminations of the mixed oxide films deposited using a 1:1 pulsing ratio of BiPh₃/H₂O and Co(thd)₂/O₃ at 162 and 186 °C. In addition it was interesting to analyze for presence of incorporated phenyl groups in order to shed light on the difficulties of depositing BiO_x from BiPh₃. One scenario was that the adsorbed BiPh₃ precursor would be unreactive towards the water pulse. The surface would then be phenyl terminated when Co(thd)₂ was pulsed into the reaction chamber. A reaction could then be imagined between these precursors which again made the surface reactive towards further depositions from BiPh₃. If so, would such a mechanism incorporate the phenyls or release them into the gas phase?

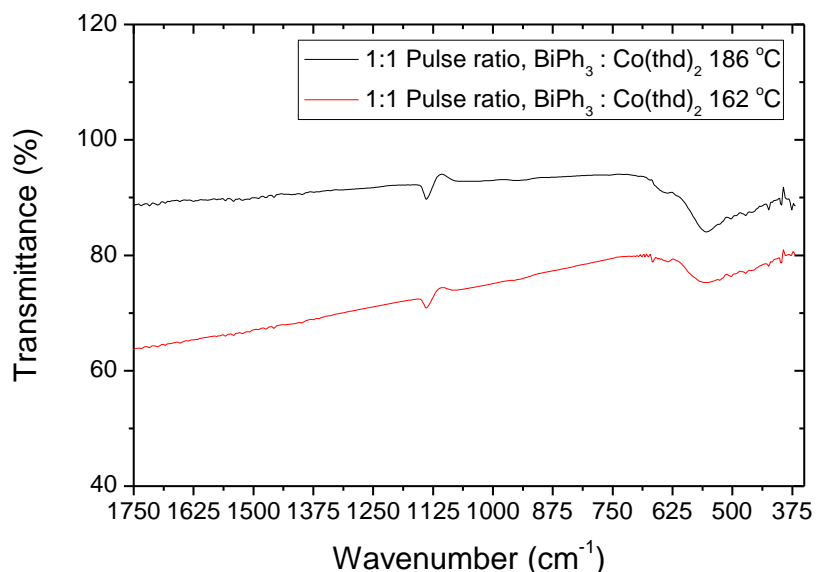


Figure 4-29. The FT-IR spectrums for two films deposited from $\text{BiPh}_3/\text{H}_2\text{O}$ and $\text{Co}(\text{thd})_2/\text{O}_3$ at 162 and 186 °C on Si(111). Both films were deposited from a 1:1 pulsing ratio between $\text{BiPh}_3/\text{H}_2\text{O}$ and $\text{Co}(\text{thd})_2/\text{O}_3$.

In Ref. [127] it is reported that phenyl groups has absorption in the area 650-700 cm^{-1} with strong absorption peaks around 675 cm^{-1} and 725 cm^{-1} . The spectra given in *Figure 4-29* shows a broad band and small absorptions in the area 625-669 cm^{-1} and 625-708 cm^{-1} for the sample deposited at 186 and 162 °C, respectively. The sample deposited at 162 °C shows a small absorption peak at 666 cm^{-1} . Incorporated phenyl groups might cause this absorption peak, however, as none of the samples shows any absorption in the area around 725 cm^{-1} , this is unlikely. In addition, Co_3O_4 has an absorption peak at 661 cm^{-1} which could also be responsible for the observed peak at 666 cm^{-1} . There seems to be no indication of any carbonate contamination as neither film has absorption peaks in the 1400 cm^{-1} area.

4.3.2 Thin films based on $\text{Bi}(\text{thd})_3 / \text{H}_2\text{O}$ and $\text{Co}(\text{thd})_2 / \text{O}_3$

As mentioned earlier the investigation of the $\text{Bi}(\text{thd})_3$ precursor was performed in two rounds. The results obtained from the investigation of the Bi-Co-O system from these two rounds are given below.

4.3.2.1 From the first round of investigation

The $\text{Bi}(\text{thd})_3$ precursor used in the first round of investigation was synthesized, as described in the patent by Baum et al. in Ref. [105], by Dr. Mohammed A. K. Ahmed.

Some preliminary depositions were done in order to obtain an indication whether depositions in the Bi-Co-O system from the two precursors $\text{Bi}(\text{thd})_3$ and $\text{Co}(\text{thd})_2$ would be facile. Two films were deposited at 162 and 186 °C from a 1:1 pulse ration between $\text{Co}(\text{thd})_2$ and $\text{Bi}(\text{thd})_3$. The resulting atomic composition, obtained by XRF, and the measured thickness and density, obtained by XRR, are presented below in *Table 4-17*.

The preliminary results was promising as both samples showed high bismuth content, and an almost perfect 50/50 atomic composition was obtained in KBG1005. The deposited films were also uniform with a good coverage of the substrates. Based on the preliminary results it was decided to deposit a 100 nm thick film, using the same parameters as used for KBG1005, to be studied in a transmission electron microscope (TEM). A complete XRF-series at both 162 and 186 °C was also made. However, the resulting XRF-series, shown in *Figure 4-30*, and the thick film studied with TEM (Appendix 9.3) contained almost no bismuth.

Table 4-17. Growth parameters for KBG1004 and KBG1005, together with measured thickness and roughness by XRR, and measured composition by XRF.

| Sample | KBG1004 | KBG1005 |
|---|---------|---------|
| Temperature (°C) | 186 | 162 |
| Pulse ratio Bi/Co | 50/50 | 50/50 |
| Metal cycles | 4000 | 4000 |
| Thickness (nm) | 35.3 | 31.1 |
| Density (g/cm ³) | 6.5 | 5.9 |
| Weight % Bi ₂ O ₃ | 78.59 | 74.55 |
| Weight % Co ₃ O ₄ | 21.41 | 25.45 |
| Atomic % Bi | 55.77 | 50.15 |
| Atomic % Co | 44.23 | 49.85 |

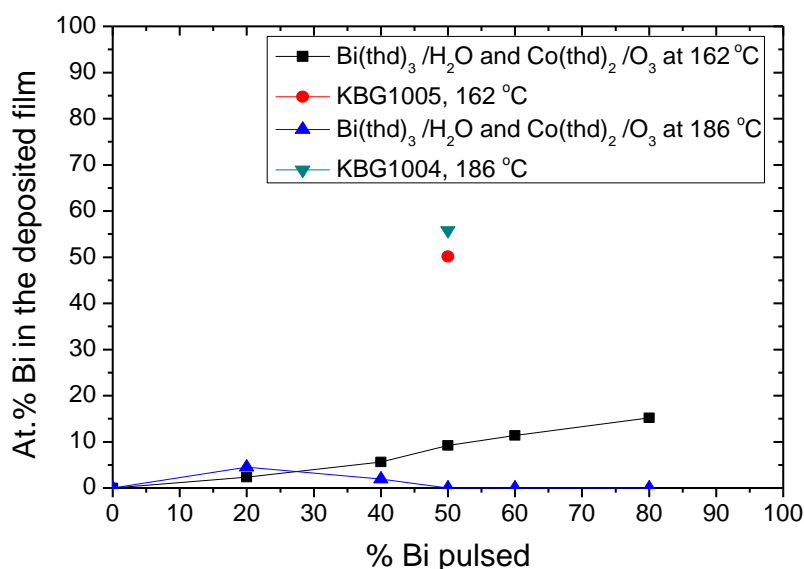


Figure 4-30. XRF series from $\text{Bi}(\text{thd})_3/\text{H}_2\text{O}$ and $\text{Co}(\text{thd})_2/\text{O}_3$ deposited at 162 °C (black line, squares) and at 186 °C (blue line, triangles). Measured atomic percentage of bismuth in KBG1004 (dark cyan mark, triangle) and KBG1005 (red mark, circle) displayed for comparison.

From the suddenly decrease in bismuth content it was suggested that the $\text{Bi}(\text{thd})_3$ precursor was sensitive for exposure to air/moisture, which resulted in reduced thermal properties. This assumption was further strengthened by Baum et al. in Ref. [105], where they describe that the monomeric $\text{Bi}(\text{thd})_3$

precursor transforms completely into a dimeric compound after 96 hours of exposure to air/moisture. Based on these findings it was decided that for further investigation of the $\text{Bi}(\text{thd})_3$ precursor, a new and fresh precursor had to be synthesized.

4.3.2.1.1 XRD study on Bi-Co-O thin film system

As KBG1004 and 1005 both showed a high and almost ideal composition for the BiCoO_3 phase, the crystal structure of these samples was studied with XRD. As θ - 2θ measurements showed no reflections, GIXRD was used, the obtained diffractograms are presented in *Figure 4-31*.

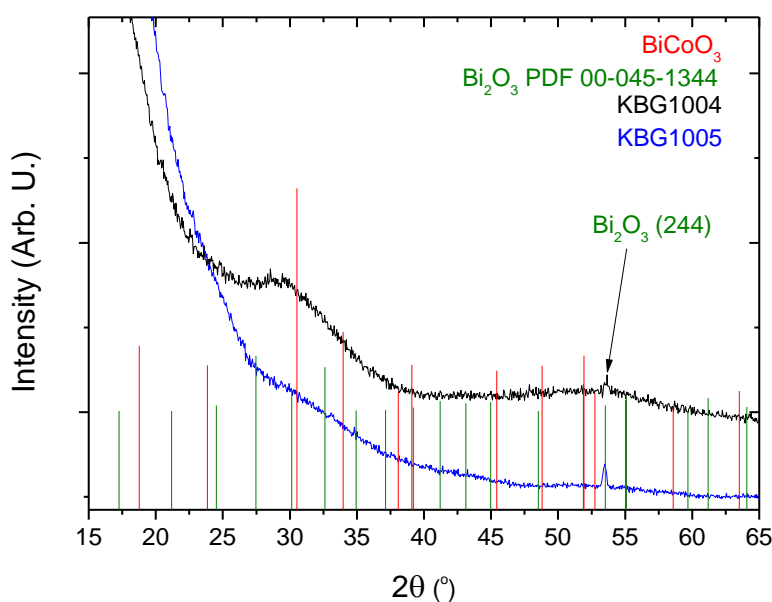


Figure 4-31. The obtained diffractograms, by GIXRD, of films containing almost 1:1 atomic composition of bismuth and cobalt (KBG1004 and KBG1005). The simulated diffractogram for the multiferroic phase BiCoO_3 is given (red lines), green lines are the diffractogram for the cubic phase of Bi_2O_3 (PDF 00-045-1344).

In *Figure 4-31* the observed peak at 53.521° in both diffractograms does not correspond with reflections from neither the Co_3O_4 phase nor the $\alpha\text{-Bi}_2\text{O}_3$ phase. Nor does it correspond with any of the reported Bi-Co-O phases. Although it was highly unlikely that the BiCoO_3 phase was formed in these depositions, a diffractogram for BiCoO_3 was simulated based on the information given in Ref. [27], and checked against the observed peak. As can be seen from *Figure 4-31* the observed peak could not be indexed as the BiCoO_3 phase either. However, the peaks could be identified as a cubic phase of Bi_2O_3 , space group $I23$. This may indicate that both the deposited samples contained the cubic Bi_2O_3 phase, nevertheless, no conclusion can be drawn as the obtained diffractograms presents only one peak. This is an interesting result however, as in Ref. [128] it is reported that the transformation from the monoclinic $\alpha\text{-Bi}_2\text{O}_3$ phase to the cubic Bi_2O_3 phase, which takes place at 650°C for powder samples under vacuum, is essential for the formation of the multiferroic compound BiFeO_3 . The possible obtained cubic Bi_2O_3 phase in KBG1004 and KBG1005 could therefore be assumed to also be important for the formation of the multiferroic compound BiCoO_3 .

4.3.2.1.2 Heat treatment of the Bi-Co-O thin film

In an attempt to obtain more crystalline samples for further study with XRD, KBG1004 and KBG1005, were both heat treated at 400°C under O_2 atmosphere for two hours. Although it was highly unlikely that the BiCoO_3 phase was present in any of the samples, it was chosen to use a relatively low temperature and instead increase the heat treatment time. BiCoO_3 decomposes to a sillenite-like phase and Co_3O_4 at temperatures higher than 467°C [27]. The resulting diffractograms obtained by GIXRD are presented in *Figure 4-32*.

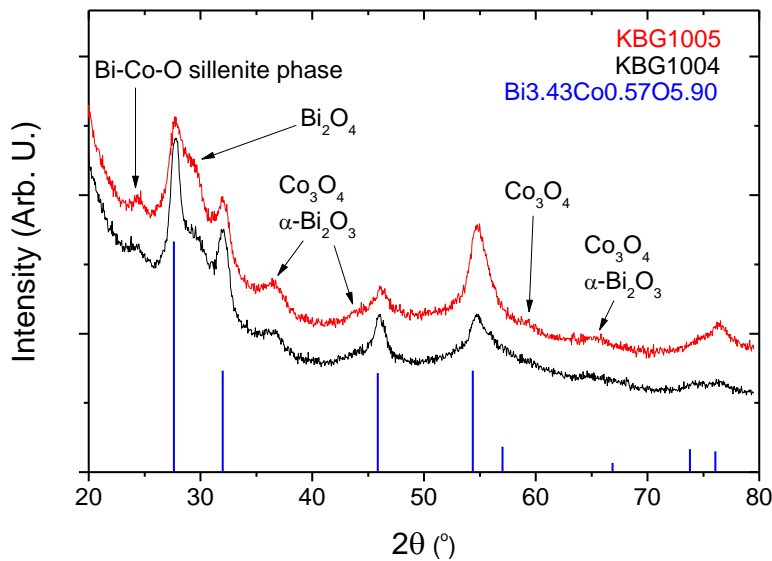


Figure 4-32. The obtained diffractograms, by GIXRD, of two thin films containing almost 1:1 at% Bi:Co, heat-treated at 400 °C for two hours under O₂ atmosphere. Bi_{3.43}Co_{0.57}O_{5.90} given by PDF 00-050-0369.

Figure 4-32 shows that the obtained diffractograms are similar for the two heat-treated samples. The diffractograms indicates that both films contain some sillenite-like phase, where the phase Bi_{3.43}Co_{0.57}O_{5.90} was found to correspond well with most of the observed large peaks. Sillenite phases of other compositions has lesser match, however, most of them did match the peak at 25°. Suggesting that a phase of another composition than what is suggested in Figure 4-32 might be present, either together or instead of the displayed phase. If the latter is true then this phase is likely to be unreported in the literature.

The possible peak at 29° labeled as Bi₂O₄ could not be fitted to other Bi-O, Co-O nor Bi-Co-O phases, except some oxygen poor Bi-O phases which is unlikely given the heat treatment was carried out in an oxygen atmosphere. However, it is also unlikely that the Bi₂O₄ phase has been formed during the heat treatment. In the only reported investigation carried

out on this phase, it is reported that it transformed to Bi_2O_3 at temperatures higher than $300\text{ }^\circ\text{C}$ [129]. However, in this transformation, as Bi^{5+} is reduced to Bi^{3+} , oxygen is released, thus the oxygen atmosphere during heat treatment may have influenced this transformation.

4.3.2.1.3 AFM study on Bi-Co-O films

AFM was used in order to study the roughness and topography of the as deposited films KBG1004 and KBG1005. The measured roughness in RMS is given below in *Table 4-18*.

Table 4-18. *The deposition parameters for the mixed oxide films, and the measured roughness, in RMS, obtained by AFM.*

| Sample | Roughness |
|---------|-----------|
| | nm |
| KBG1004 | 0.91 |
| KBG1005 | 1.09 |

The measured topography of KBG1004 and KBG1005 are given below in *Figure 4-33* and *Figure 4-34*, respectively.

The measured roughness of the sample deposited at $162\text{ }^\circ\text{C}$ is slightly higher than the sample deposited at $186\text{ }^\circ\text{C}$, and as can be seen from the measured topography in *Figure 4-33* and *Figure 4-34* the sample deposited at $162\text{ }^\circ\text{C}$ also has thinner and sharper grains. An explanation for the observed difference might be due to less surface reconstructions during the deposition at $162\text{ }^\circ\text{C}$, due to lower thermal energy.

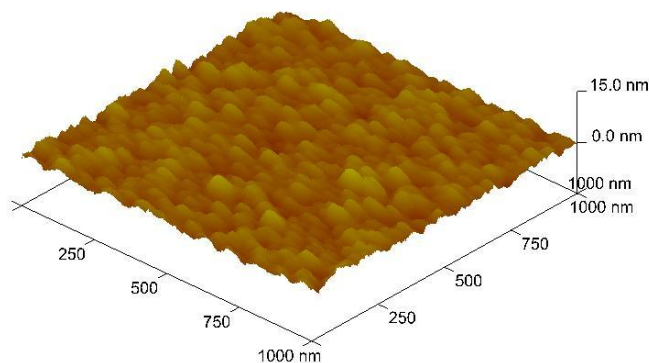


Figure 4-33. Topography of KBG1004, obtained by AFM. Deposited from 4000 cycles on Si(111) at 186 °C.

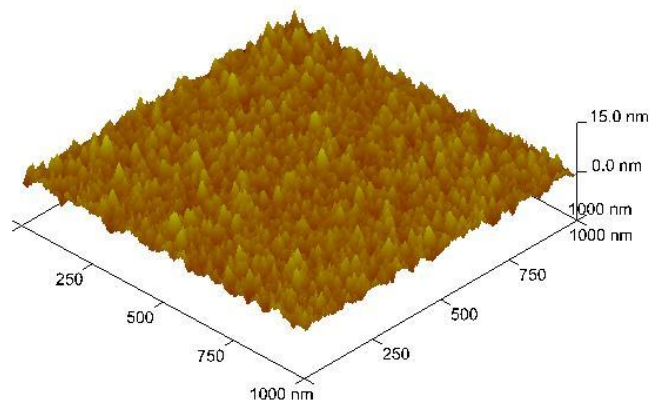


Figure 4-34. Topography of KBG1005, obtained by AFM. Deposited from 4000 cycles on Si(111) at 162 °C.

4.3.2.2 From the second round of investigation

In the second round of investigation the Bi(thd)₃ precursor named W, see Table 4-8 on page 107, was used to deposit an XRF series together with Co(thd)₂. All the deposited films showed large gradients in the flow direction, and the resulting XRF data, see Table 4-19, showed that the deposited films contained almost no cobalt.

Table 4-19. The atomic composition of films deposited from $\text{Bi}(\text{thd})_3 / \text{H}_2\text{O}$ and $\text{Co}(\text{thd})_2 / \text{O}_3$.

| Sample | Temperature (°C) | Bi/Co pulse ratio (%) | At. % | |
|---------|---------------------|--------------------------|-------|-------|
| | | | Bi | Co |
| KBG1111 | 235 | 80/20 | 100 | 0 |
| KBG1109 | 235 | 60/40 | 99,78 | 0,216 |
| KBG1107 | 235 | 50/50 | 100 | 0 |
| KBG1108 | 235 | 40/60 | 97,17 | 2,83 |
| KBG1110 | 235 | 20/80 | 100 | 0 |

4.3.2.2.1 In-situ QCM analysis of $\text{Bi}(\text{thd})_3$ on Co_3O_4 surfaces

An in-situ QCM measurement was carried out at 235 °C in order to try to obtain a better understanding for why almost no cobalt could be detected in the deposited Bi-Co-O films. It was suggested that the $\text{Bi}(\text{thd})_3$ precursor likely etched the Co_3O_4 surface, based on the observed large gradients in the films together with the obtained XRF data. To check for any possible dissimilarity on different surfaces in the QCM measurement, a 20s $\text{Bi}(\text{thd})_3$ pulse was applied to both a Al_2O_3 and a Co_3O_4 surface, deposited using 30 cycles of TMA and H_2O and 50 cycles of $\text{Co}(\text{thd})_2$ and O_3 respectively. The obtained results are given in *Figure 4-35*.

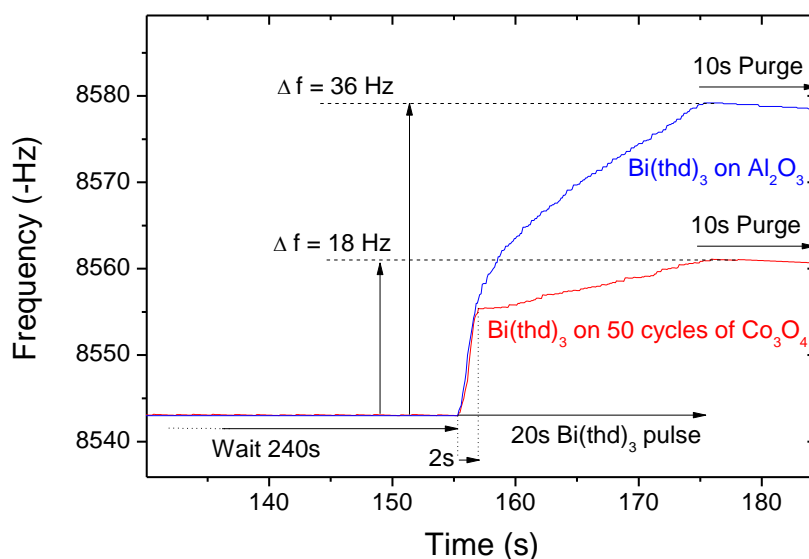


Figure 4-35. In-situ QCM measurement performed at 235 °C, showing the change in frequency when a 20s Bi(thd)₃ pulse is applied to a Co₃O₄ surface (red line) and a Al₂O₃ surface (blue line).

The QCM result in *Figure 4-35* indicates that for a pulse time of 2 seconds of Bi(thd)₃, the change in frequency is the same for both surfaces studied. However, after the first two seconds, one can see that the difference quotient changes for the two surfaces. The registered increase in mass is much larger for the Al₂O₃ surface, than the Co₃O₄ surface. This may indicate that an etching process of the Co₃O₄ surface takes place simultaneously as Bi₂O₃ is deposited.

However, one could argue that maybe the density of surface reactive sites is higher on the Al₂O₃ surface than the Co₃O₄ surface, and thus more mass is deposited on Al₂O₃. In addition as the quartz crystal may slightly change its response during the measurement, the values of the difference in frequency changes, given in *Figure 4-35*, when Bi(thd)₃ are deposited on the Co₃O₄ surface and the Al₂O₃ surface, are not absolute, as the two measurements are

separated in time. However, the change in frequency for one TMA/H₂O cycle was roughly 13 Hz during the whole measurement, indicating that the values given in *Figure 4-35* are comparable. Nevertheless, when the obtained in-situ QCM measurements are coupled with the obtained XRF results and the observed gradients of the deposited films, it is likely that some sort of etching process of the Co₃O₄ surface takes place by the Bi(thd)₃ precursor.

5 Discussion

In this chapter the work conducted will be discussed in a larger picture. A comparison will be given of the three investigated cobalt precursor combinations. The different bismuth precursors investigated will be evaluated for the use in the ALD process, where the main focus is on the applicability for deposition of BiCoO₃. In the evaluation of depositions in the Bi-Co-O system possible combinations with the cobalt precursors will also be discussed. In addition, some interesting results will be looked at in more detail.

5.1 Cobalt precursors

The two similar growth systems Co(thd)₃/O₃ and Co(thd)₂/O₃ do show some clear differences when compared, *Table 5-1*. Because the investigated films based on Co(thd)₂/O₃ show large deviations in certain areas from what is reported in the literature, the literature values are also taken into consideration in the comparison.

Cobalt is the only reported transition metal where stable thd-complexes can be obtained as both Co(thd)₂ and Co(thd)₃ [106], therefore a comparison of these two similar growth systems are interesting.

Table 5-1. A comparison of the $\text{Co(thd)}_2/\text{O}_3$ and $\text{Co(thd)}_3/\text{O}_3$ growth systems. Roughness values and the crystallites height is compared for ca. 100 nm thick films.

| Precursor combination | Unit | $\text{Co(thd)}_2/\text{O}_3$ | | $\text{Co(thd)}_3/\text{O}_3$ |
|---|-----------|-------------------------------|--------------|-------------------------------|
| | | This work | Ref.[13, 14] | This work |
| ALD temperature window | °C | - | 114-307 | 162 - 259 |
| Growth rate/cycle | pm /cycle | 15-18 | 20±1 | 6 |
| Decomposing temperature of precursor | °C | 300 | 310 | 430 |
| Reactive towards H_2O | | yes | - | no |
| Orientation on Si at 186 °C | - | (100) weak (111) | (100) | (111) |
| Carbonate contamination | - | No | No | No |
| Roughness on Si deposited at 186 °C | nm | 0.22 | 2.1 | 5.57 |
| Roughness on silica glass deposited at 186 °C | nm | - | 2.8 | 4.73 |
| Height of crystallites at 200 °C | nm | 47.4 | - | 25.4 |

One of most noteworthy differences between the two systems is the growth rate, which is 70% lower for the $\text{Co(thd)}_3/\text{O}_3$ precursor combination when compared to the $\text{Co(thd)}_2/\text{O}_3$ system. When compared further, the ALD temperature window is also 49% smaller in range for the for the $\text{Co(thd)}_3/\text{O}_3$ system. The ALD temperature window and growth rate is discussed more in detail later in this section.

Another interesting observation is that the film deposited from $\text{Co(thd)}_3/\text{O}_3$ has a much higher surface roughness, when compared to the films deposited from $\text{Co(thd)}_2/\text{O}_3$, both in this work and in Ref. [14]. This could suggest that films with a higher crystallinity are deposited from the $\text{Co(thd)}_3/\text{O}_3$ combination than the $\text{Co(thd)}_2/\text{O}_3$ combination. However, the calculated crystallite heights, from the measured FWHM values, indicates that the film deposited from $\text{Co(thd)}_2/\text{O}_3$ consists of taller crystallites. As

these two observations are somewhat contradictory, there might be another explanation for this difference in roughness. By comparing the measured topography of a 74 nm thick film deposited from Co(thd)_3 , given in *Figure 4-19* on page 123, with a 60 nm thick film deposited from $\text{Co(thd)}_2/\text{O}_3$ in Ref.[14] large differences are observed. The crystallites on the film deposited from $\text{Co(thd)}_2/\text{O}_3$ are more uniformly distributed on the surface, indicating that the $\text{Co(thd)}_2/\text{O}_3$ precursor combination has higher nucleation density on silicon than the $\text{Co(thd)}_3/\text{O}_3$ combination. In addition, the observed growth orientation for these two systems are different, where $\text{Co(thd)}_3/\text{O}_3$ shows (111)-oriented growth at 186 °C while $\text{Co(thd)}_2/\text{O}_3$ shows (100)-oriented growth.

The observed decomposition temperature for the $\text{Co(thd)}_3/\text{O}_3$ process at 283 °C is surprisingly low when compared to fact that the precursor was measured to be stable up to 430 °C. No decomposition could be observed in the precursor supply tube, even for depositions carried out at 332 °C. Which may indicate that the Co_3O_4 surface might lower the decomposition temperature of the Co(thd)_3 precursor through a catalytic effect. Catalytic effects of a ZrO_2 surface has also been suggested for the observed decomposition of $\text{Zr}[\text{OC}(\text{CH}_3)_3]_4$ at 250 °C, even though the precursor molecule should be stable at this temperature [130]. An alternative explanation may be that the chemisorbed precursor molecule on the surface has a lower thermal stability than the precursor molecule in the gas phase. This mechanism where the chemisorbed precursor molecule on the surface exhibit different thermal stability than the gas phase molecule, is also a suggested explanation in Ref.[73] for the observed increase in the decomposition temperature of Mn(thd)_3 when used on surfaces that also contained Ca or La atoms.

For further discussion and comparison the $\text{Co(thd)}_2/\text{H}_2\text{O}$ system will be included as well.

Before these three systems are discussed, it should be noted that the observed reactivity of the Co(thd)_2 precursor towards water is rather peculiar, as the synthesis of this compound is carried out in aqueous ethanol. However, it is obvious that the reactivity is highly temperature dependant. Nevertheless, the comparison of Co-O films deposited from $\text{Co(thd)}_2/\text{O}_3$ and $\text{Co(thd)}_2/\text{H}_2\text{O}$ precursor combinations presents a rather unique opportunity, as there are only a few other thd-complexes reported deposited from both O_3 and H_2O . Related ALD processes reported in the literature are $\text{Ni(thd)}_2/\text{H}_2\text{O}$ for deposition of NiO [131, 132] and $\text{Ni(thd)}_2/\text{O}_3$ for deposition of LaNiO_3 [133]. $\text{Ca(thd)}_2/\text{H}_2\text{O}$ has been proven by in-situ QCM measurements to grow films of CaO [134] and $\text{Ca(thd)}_3/\text{O}_3$ has been used for deposition of in the La-Ca-Mn-O system [135].

However, none of the two precursors mentioned above has been used to deposit the same system from both O_3 and H_2O , consequently comparing thin films of the same material system deposited from the same precursor with both O_3 and H_2O , as given here, is the first of its kind for thd-complexes. However, it should be noted that large differences should be expected for the two systems $\text{Co(thd)}_2/\text{O}_3$ and $\text{Co(thd)}_2/\text{H}_2\text{O}$, as one uses a highly oxidizing agent while the other is not.

For a simple comparison of the $\text{Co(thd)}_2/\text{O}_3$, $\text{Co(thd)}_2/\text{H}_2\text{O}$ and $\text{Co(thd)}_3/\text{O}_3$ growth systems, the growth rate as a function of the temperature of these three systems is presented in *Figure 5-1*.

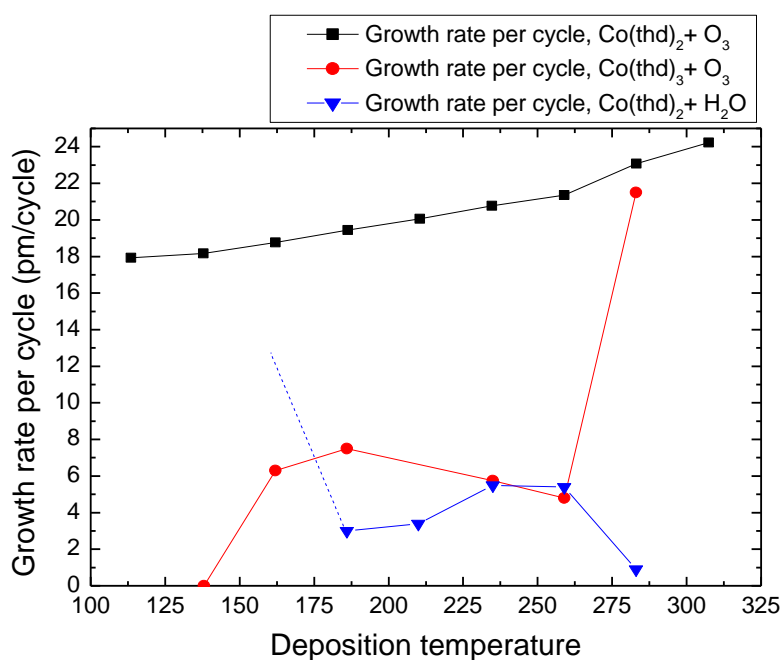
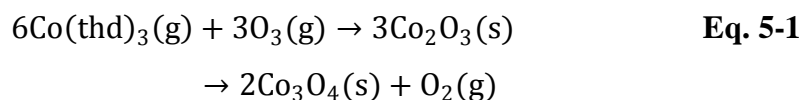


Figure 5-1. The growth rate of $\text{Co}(\text{thd})_2/\text{O}_3$ from [14] (black line, squares), $\text{Co}(\text{thd})_2/\text{H}_2\text{O}$ (blue line, triangles) and $\text{Co}(\text{thd})_3/\text{O}_3$ (red line, dots) as a function of deposition temperature. The blue stippled line indicates increased growth rate at lower temperatures.

Both novel precursor combinations reported in this work has a relatively small ALD window compared to the already know $\text{Co}(\text{thd})_2/\text{O}_3$ precursor combination. However, there is no reason why the $\text{Co}(\text{thd})_2/\text{H}_2\text{O}$ process should show a lower decomposition temperature than the $\text{Co}(\text{thd})_2/\text{O}_3$ process. The $\text{Co}(\text{thd})_2$ precursor used in this work was observed to decomposed before it entered the reaction chamber when deposited at 283 °C during investigation of the $\text{Co}(\text{thd})_2/\text{H}_2\text{O}$ ALD temperature window. The conditions in the precursor tube of $\text{Co}(\text{thd})_2$ should be the same as for deposition of the $\text{Co}(\text{thd})_2/\text{O}_3$ system. Based on that $\text{Co}(\text{thd})_2$ is reported to be stable up to 307 °C [13, 14], it is likely that the precursor used in this work might have been contaminated or hydrated, resulting in slightly lower decomposition temperature. As a consequence, if the $\text{Co}(\text{thd})_2$ precursor

used in this work would have been stable up to the reported value of 307 °C the upper limit of the ALD window may also have been extended likewise. Nevertheless, the limited range in ALD temperature window for the two new cobalt precursors combinations, makes them less flexible for use together with other precursors. Although they both have an ALD temperature window that are in an area where most other systems also show ALD growth. One can see that both new precursor systems have roughly a 70% lower growth rate than the Co(thd)₂/O₃ system. For the Co(thd)₃/O₃ system a decrease in growth rate would be expected, as the Co(thd)₃ molecule is more bulky than the Co(thd)₂ molecule. The bulkyness of the Co(thd)₃ molecule may also be the reason for why this precursor does not react with H₂O, as the crowded environment around the metal atom denies a nucleophilic attack from the H₂O molecule. However, the formation of Co₃O₄ from Co(thd)₃ and O₃ is surprising due to the need of a reduction. The formation of Co₃O₄ from Co(thd)₃ can be visualized as given in *Eq. 5-1*.



It should be noted though, that the given reaction in *Eq. 5-1* is highly unlikely as there exist little evidence for the Co₂O₃ phase in the literature. However, it does display the concept of that in order to obtain the Co₃O₄ phase oxygen has to be removed by some mechanism.

On the other hand, the low growth rate of Co(thd)₂ and H₂O may be due to limited reactivity. As mentioned earlier β-diketonato complexes are generally regarded as stable towards H₂O.

However, the rather uncharacteristic ALD temperature window observed for the Co(thd)₂/H₂O growth system deserves a closer examination using thermodynamics, see *Figure 5-2*.

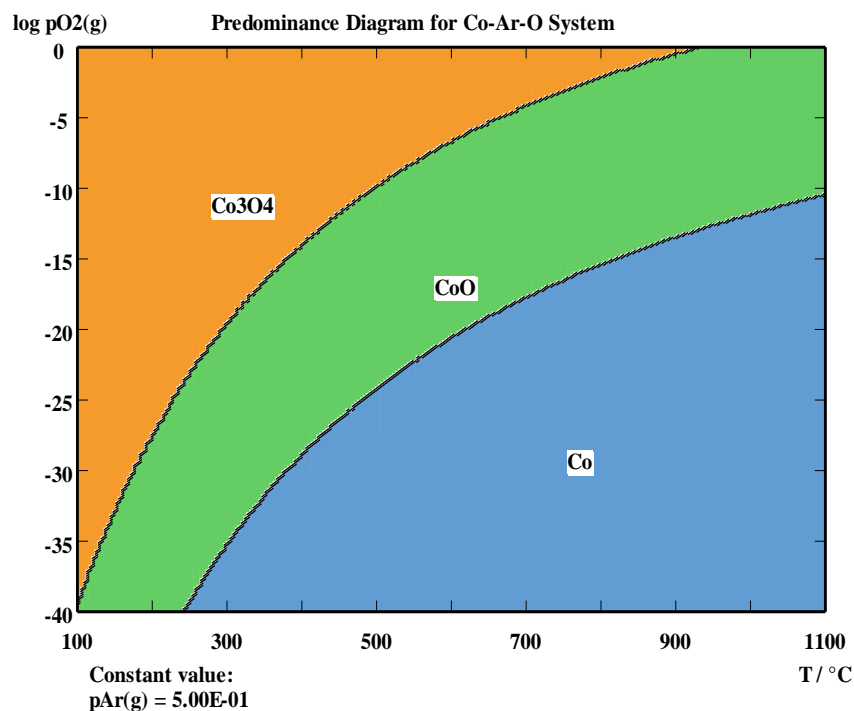


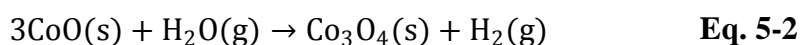
Figure 5-2. Predominance diagram noting the stable phase as a function of temperature and oxygen pressure, calculated by HSC Chemistry for Windows 4.1 [136].

For the ALD depositions carried out in this work it would be appropriate to assume that the log pO₂ pressure was in the area between -5 and -10 in *Figure 5-2*.

By reference to *Figure 5-1*, the growth rate at the lower end of the ALD temperature window for the Co(thd)₂/H₂O process, is lower than the growth rate at higher temperature. Based on this observation one could assume that CoO is deposited at the lower end, because a lower growth rate can be suggested. The volume per cobalt atom roughly is 19 Å³ and 66 Å³ in the CoO and Co₃O₄ structure, respectively. Hence if the same amount of material was deposited over the whole temperature range, a sudden increase in growth rate could be expected for the temperatures where the Co₃O₄ phase is deposited. Secondly, by reference to *Figure 5-2*, however, the CoO

phase is not stable until relatively high temperatures are reached, even under a very low vapor pressure of O₂. As CoO is the only phase detected at 186 °C, this suggests that a kinetic barrier is present to prevent formation of Co₃O₄.

When the deposition temperature is raised to 210 °C the Co₃O₄ phase is the only phase detected, suggesting that this limited increase in temperature is sufficient for decomposition of CoO. In addition, as the observed growth rate is only slightly higher than at 186 °C, this may suggest that the CoO phase is the as-deposited phase, with its given growth rate, whereupon CoO transforms to Co₃O₄. Regarding possible oxygen sources for the excess oxygen in Co₃O₄, the only known sources are H₂O and the thd-ligand. Raising the question, which one of them is more likely to be reduced? As the reduction of H₂O by CoO, given in *Eq. 5-2*, has a $\Delta G = 95.77$ kJ/mol at 200 °C, this reaction is not likely occurring.



In order to suggest if the thd-ligand can act as an oxygen source, we can look at the literature. It has been reported previously that when films of La₂S₃ is deposited from La(thd)₃ and H₂S, the phase La₂O₂S is formed during annealing [137]. The observed oxygen was suggested to be residual in the deposited films and stem from the thd-ligands, suggesting that the thd-ligand can act as an oxygen source at some given conditions.

Hence, when the two oxygen sources present, H₂O and thd, are compared, it is more likely that the thd-ligand is reduced and donates oxygen to the CoO phase in order for it to form the stable Co₃O₄ phase.

As the temperature is raised to 235 °C the kinetics may be high enough for the Co²⁺ ion to reduce the thd-ligand as it is deposited, and thus Co₃O₄ may be deposited directly with its respective growth rate. Note that

the growth rate at this temperature is almost the same as the one for the deposition of Co_3O_4 from $\text{Co}(\text{thd})_3/\text{O}_3$.

By further increasing the temperature, both obtained phases are apparently stable as a mixture of the CoO and Co_3O_4 phase, which results in a slight decrease in the observed growth rate. By reference to *Figure 5-2* this would mean that the deposition would have to be carried out in the area around $-20 \log p\text{O}_2$, which is not likely. However, the calculated diagram given in *Figure 5-2* does only serve as a guideline, suggesting that the proposed mechanisms discussed above could be an explanation for this step like-growth. Nevertheless, it is rather amazing that all this can be observed in the relatively limited temperature window examined and alternative explanations should also be sought.

5.2 Bismuth precursors

As can be seen from the investigations carried out in the prior art and in this work, identifying a suitable bismuth precursor for the ALD process seems to be a challenging task indeed. However, some promising results was obtained by the use of $\text{Bi}(\text{thd})_3$ as precursor, this compound will therefore be discussed in more detail in this section. The different behavior and phases obtained of $\text{Bi}(\text{thd})_3$ in this work indicates that this system is complex and not completely understood in the literature. It is clear that the synthesized $\text{Bi}(\text{thd})_3$ precursor in this work can be used for deposition of bismuth oxide, however, it cannot be used for deposition of the wanted phase BiCoO_3 , most likely due to some sort of etching process of the Co_3O_4 surface. This etching process will be the topic for discussion later in this section.

However, before the $\text{Bi}(\text{thd})_3$ precursor is discussed, the BiPh_3 and H_2O precursor will be discussed as a potential bismuth precursor for ALD.

BiPh_3 is not suited for depositions of BiO_x as it does not yield films when deposited together with either H_2O or O_3 . As shown in this work it does not grow on its own surface. It can however be used for deposition in the Bi-Co-O system, although the obtained bismuth content is relatively low. A possible explanation for this is that the cobalt surface either presents surface reactive sites that the BiO_x surface lacks, and/or that the Co_3O_4 surface has a catalytic effect on the process.

By reference to *Figure 4-23* on page 128, the decrease in the deposited mass after 3 $\text{BiPh}_3/\text{H}_2\text{O}$ cycles may indicate that most of the reactive sites on the cobalt surface is covered, as it is not likely that one monolayer of Bi_2O_3 is deposited with only a measured decrease in frequency of 2.85 Hz. One TMA/ H_2O cycle for comparison gave a decrease in frequency of 7.5 Hz and if one TMA/ H_2O cycle is assumed to have a growth rate of 0.15 nm, an approximation for the deposited thickness of the Bi_2O_3 layer can be made. The density of Al_2O_3 and Bi_2O_3 is 3950 kg/m^3 and 8900 kg/m^3 , respectively, which would result in a thickness of 0.25 \AA of Bi_2O_3 , if deposited uniformly on the surface. As 0.25 \AA is less than the thickness of one monolayer of Bi-O, this suggests that the growth stops while there are still some exposed Co_3O_4 surface. This means that the Co_3O_4 surface is likely to have some favorable reaction sites, which may or may not act catalytically towards the deposition of BiPh_3 .

However, when BiPh_3 is deposited on an Al_2O_3 surface at $200 \text{ }^\circ\text{C}$ there is a decrease in frequency of 3 Hz after 9 cycles of $\text{BiPh}_3/\text{H}_2\text{O}$ [1], for comparison in the same measurement 1 cycle of TMA/ H_2O resulted in a decrease in mass of 17 Hz, which means that there are close to no deposition of Bi_2O_3 on an Al_2O_3 surface. This observation may suggest that a catalytically active surface is needed. As mentioned in the prior art, BiPh_3 could also be used for deposition in the Bi-Ti-O system [8]. In Ref. [8]

bismuth content as high as 61 at.% bismuth was achieved in the Bi-Ti-O system. However, it should be noted that the deposition temperature used for this achievement was 300 °C, which is higher than the decomposition temperature found for BiPh₃ in this work. That a decomposition reaction is the reason for the high bismuth content obtained in Ref. [8] is further backed up by the observed drop to only 7 at.% Bi in the deposited films, for a 80% pulsing of BiPh₃, when the deposition temperature was below 240 °C. The obtained 7 at.% Bi from a 80/20 pulsing ratio between Bi/Ti is roughly in the same range as what was obtained from a 80/20 pulsing ratio between Bi/Co in this work. However, both TiO₂ and Co₃O₄ may be active catalytic materials while Al₂O₃ apparently is not. This also suggests that it is more likely that a catalytic process is needed for the deposition of BiPh₃ with ALD. From a practical point, BiPh₃ is easy to handle and yields uniform films that do not contain notable carbonate nor phenyl groups when deposited together with Co(thd)₂/O₃. Nevertheless, this precursor seems like it is not suitable for deposition of BiCoO₃ with neither of the cobalt precursors investigated in this work.

For the successful use of Bi(thd)₃ in the ALD process there are some challenges that need to be solved. Firstly, more knowledge is necessary regarding the different phases and chemistry of Bi(thd)₃. Secondly, the effect of the synthesis parameters on the obtained phases should be investigated, in order to control better the synthesis.

The high bismuth content obtained in the deposited films during the first round of investigation of Bi(thd)₃ in this work, indicates that at least one phase of Bi(thd)₃ exists and can be used in the Bi-Co-O system. In order to gain more knowledge about the Bi(thd)₃ system an attempt to identify the unknown phase obtained in the performed syntheses will be given below.

If all the obtained diffractograms of the synthesized $\text{Bi}(\text{thd})_3$ compounds in this work are compared a likely suggestion for an unknown phase of $\text{Bi}(\text{thd})_3$ can be made. The diffractogram obtained from the finger during the purification of *D* showed almost no resemblance to the reported phase Armelao1, given in *Table 4-6* page 105. When the diffractograms of the reported phase Armelao1 and the obtained compound *D_finger* was compared with the products obtained from the syntheses in this work, given in *Table 4-3* on page 98, it became clear that all the other synthesized compounds could be identified as various mixtures of these two phases. An example of this is given in *Figure 5-3*.

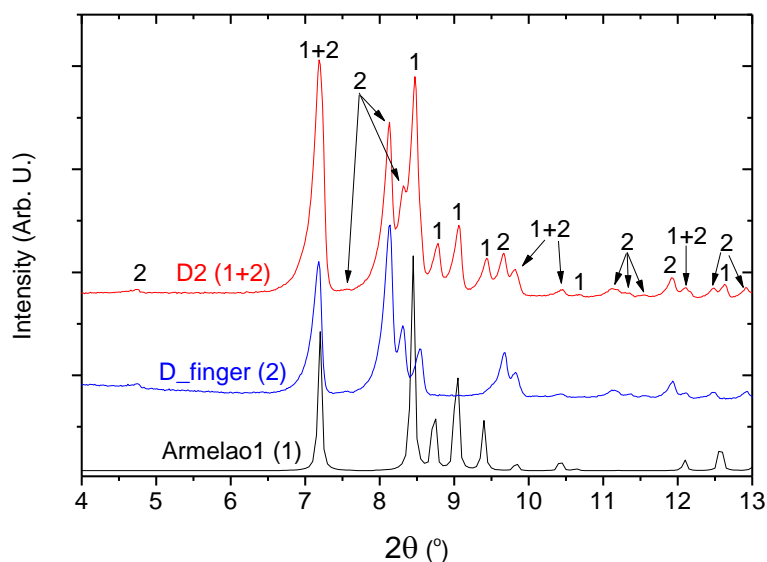


Figure 5-3. Diffractograms obtained by XRD, showing that the red diffractogram from D2 can be identified as a mixture of the reported phase Armelao1 (marked 1), and a unknown $\text{Bi}(\text{thd})_3$ phase (marked 2).

With this new knowledge the syntheses performed in this work can be identified as having small or large amounts of this new $\text{Bi}(\text{thd})_3$ phase. In addition the syntheses conditions can be backtracked, thus obtaining an

indication on which parameters during the syntheses yielded large amounts of one of these two phases.

By reference to *Table 4-4*, *Figure 4-8* and *Figure 4-9* some suggestions for the effect of the syntheses parameters on the obtained phase composition can be given:

- Exposure to air yields large amounts of Armelao1.
- Dried solvents yields large amounts of the new Bi(thd)₃ phase.
- If the synthesized compound is sublimed two times the first sublimation yields more of the new phase, the second more of Armelao1.
- By comparing *D* and *E* the use of a commercially bough powder of NaOMe instead of home-made NaOMe seems to yield larger amounts of the new phase. As the use of home-made NaOMe is more likely to give more water contamination than the exchange of BiCl₃ with BiI₃.

Based on these observations, and that the samples where the new phase was present in large amounts was more sticky and also melted during X-ray measurements, this may indicate that the new phase contains less crystal water than the reported phase Aremelao1. As crystal water stabilizes the structure, the compound would be expected to display a lower melting point when crystal water is removed. This assumption is also strengthened by the obtained liquid from the complexation with tetraglyme in this work, and the lowering of the melting points of hydrated thd-complexes by complexation with tetraglyme reported in Ref [138].

It should also be noted that both Armelao [121] and Fukin [103] synthesized $\text{Bi}(\text{thd})_3$ by reacting BiPh_3 with $\text{H}(\text{thd})$, where Armelao obtained two monomeric compound with various amounts of crystal water and Fukin obtained a dimeric compound with crystal water. The patented synthesis route by Baum et al. [105], where $\text{Na}(\text{thd})$ is reacted with BiCl_3 in an aprotic solvent, which the syntheses in this work is based on, is claimed to yield monomeric anhydrous $\text{Bi}(\text{thd})_3$. From this, two observations can be made. Firstly, commercially $\text{Bi}(\text{thd})_3$ are most likely synthesized by reacting BiPh_3 with $\text{H}(\text{thd})$, as this route is not patented. This may explain why there is no previously reported deposition of Bi_2O_3 from $\text{Bi}(\text{thd})_3$ by ALD. As the dimeric compound obtained by Fukin does have poorer thermal properties than the monomeric compound, as described by Baum et al. In addition, it may also be likely that the phases obtained by Armelao shows poor behavior in the ALD process, otherwise one would assume that ALD deposition from $\text{Bi}(\text{thd})_3$ was already reported in the literature. Secondly, this also suggests that the new phase obtained phase from the syntheses carried out in this work may be the monomeric anhydrous compound. However, Baum et al. claims that the monomeric anhydrous compound had a melting temperature of 139 °C, which is higher than the melting temperature for the dimeric compound with crystal water synthesized by Fukin [103]. This does not seem to fit the assumption that less incorporated crystal water destabilizes the structure and thus results in a lower melting point.

However, as the deposited $\alpha\text{-Bi}_2\text{O}_3$ films showed evidence of carbonate contamination by FT-IR measurements it might suggest that maybe some decomposition of the precursor also occurs in addition to the suggested reaction with the crystal water. One would assume that if the growth only occurred through the ligand exchange reaction between H_2O and the $\text{Bi}(\text{thd})_3$ precursor that little to none carbonate contaminations

should be incorporated into the film. However, the observed carbonate contamination can also be due to the decomposition of the Armelao1-phase which was present in all the samples synthesized. Or it might be that the carbonate was formed during storage in air.

5.3 Etching of Co_3O_4 by $\text{Bi}(\text{thd})_3$

There is no reported etching of cobalt surfaces by thd-complexes in the literature. As mentioned in the prior art, cobalt has been deposited together with other thd-complexes such as $\text{Fe}(\text{thd})_3$ and $\text{La}(\text{thd})_3$ in the Fe-Co-O system [15] and La-Co-O system [32], respectively. Hence, it is unlikely that the cobalt surface is particularly unstable towards other thd-complexes. Indicating that the suggested etching is probably due to some properties of the $\text{Bi}(\text{thd})_3$ precursors synthesized in this work. However, in both Ref. [15, 32] O_3 was used for deposition for both metal precursors, which may suggest that reacting thd-complexes with H_2O , as done in this work, may result in corrosive by-products, as $\text{H}(\text{thd})$. Etching of SrO surfaces by $\text{H}(\text{thd})$ has previously been observed in the $\text{Sr}(\text{thd})_2/\text{H}_2\text{O}$ system [139]. Other β -diketonates ligands such as $\text{H}(\text{hfac})$ has been shown to etch surfaces of CuO, PbO, ZnO, ZnS, V_2O_5 [140]. It is therefore likely that the reaction between $\text{Bi}(\text{thd})_3$ with H_2O , either from the incorporated crystal water in the precursor or the applied water pulse, has resulted in the formation of $\text{H}(\text{thd})$ vapor which in turn has etched the Co_3O_4 surface as observed in this work, and the Fe_2O_3 surface as observed in Ref. [1]. The etching process of Fe_2O_3 is discussed in detail in Ref. [1] and the most likely mechanism suggested was that the $\text{Bi}(\text{thd})_3$ precursor reacted with its own crystal water, resulting in $\text{H}(\text{thd})$ which thus caused etching.

Based on this it is likely to assume that the $\text{Bi}(\text{thd})_3$ precursor that yielded films containing almost 50/50 at.% bismuth and cobalt, form

Bi(thd)₃/H₂O and Co(thd)₂/O₃ process, did not contain any crystal water. As the surface is saturated by Bi(thd)_x complexes before water is pulsed in, the resulting H(thd) ligands should be less likely to etch away the underlying Co₃O₄ surface, as a Bi(OH)₂ terminated surface is most likely formed in the same step. An alternative explanation may be that the precursor contained some crystal water, but at the deposition temperature used, 162 and 186 °C, the Co₃O₄ surface was stable towards the H(thd) vapour.

It should be noted that the suggested etching process observed by in-situ QCM in Ref. [1] for the Fe(thd)₃ + Bi(thd)₃ system seems to take place in another manner than the suggested etching process observed for the Co₃O₄ surface in this work. In Ref. [1] when a 20s Bi(thd)₃ pulse was applied to the Fe₂O₃ surface, an increase in mass up to a pulse length of 2.5 seconds was observed, before a large decrease in mass occurred, whereupon the growth continued as on the Al₂O₃ surface. This suggests that Al₂O₃ surfaces are not prone to etching, which is also likely given the results in this work. The reason for this observed difference in the etching mechanisms can be due to different stability of the Co₃O₄ and Fe₂O₃ surfaces. Or it can be due to the use of a precursor with small or large amounts of crystal water. As the precursor used in Ref. [1] that resulted in the etching of Fe₂O₃ surfaces was the precursor labeled *B* in this work. As *Figure 4-8* on page 106 shows, this precursor contains large amounts of the Armelao1 phase. However, the precursor *W* used in this work which showed etching of the Co₃O₄ surface contained very little of the armelao1 phase (*Figure 4-9*), this could explain the differences observed between the two surfaces.

However, as the Co(thd)₂/H₂O precursor combination is found to yield uniform films in this work, and the likely mechanism for growth is a ligand exchange reactions between the Co(thd)₂ and H₂O, yielding a Co(OH)

surface complex and H(thd). This might point to that H(thd) ligands are not responsible for the etching of the Co_3O_4 surfaces observed in this work. However, as mentioned earlier the Al_2O_3 surface is likely to be stable towards etching, a question arises as to what property does the Al_2O_3 surface have, which the Fe_2O_3 and Co_3O_4 surfaces lacks? One likely suggestion may be that both the Fe_2O_3 and Co_3O_4 surfaces were deposited from O_3 , yielding an oxygen terminated surface, while Al_2O_3 was deposited from H_2O , yielding an OH terminated surface. As there are not many other likely reasons for why an Al_2O_3 surface is stable towards etching while a Co_3O_4 and Fe_2O_3 surface is not, the key for avoiding etching might be an OH terminated surface. If H(thd) ligands are the cause for the etching, this will also explain why no etching is observed in the $\text{Co}(\text{thd})_2/\text{H}_2\text{O}$ process by the formed H(thd) ligands. But it is observed in the Bi-Co-O process where $\text{Co}(\text{thd})_2$ was used with O_3 , which results in an oxygen terminated surface. As a consequence it would be interesting to deposit Co_3O_4 from $\text{Co}(\text{thd})_2/\text{H}_2\text{O}$ and then investigate if etching occurs when a $\text{Bi}(\text{thd})_3$ pulse is applied. On the other hand etching may take place, however, as $\text{Co}(\text{thd})_2$ reacts with H_2O there might be a redeposition of Co_3O_4 . This might also be the reason why the etching process appears different for a Co_3O_4 surface and a Fe_2O_3 surface. However, as almost no cobalt is detected in the deposited films by XRF, this is probably not likely. If not on the other hand the etching process is much faster than the redeposition process.

However, if the formation of the H(thd) vapor which is suggested to cause etching is not a result from the reaction between the precursor and its crystal water, but instead is a result of the reaction with the applied H_2O pulses. Another solution to the etching problem could be to exchange H_2O with O_3 for the deposition with $\text{Bi}(\text{thd})_3$. On the other hand if O_3 is used instead of H_2O it is more likely that carbonate contaminations may be

formed in the deposited films. This might be a small price to pay however, if this turns out to be the only way to avoid etching.

5.4 The Bi-Co-O films

Based on that the peak observed around 53.5° in the as deposited films, as shown in *Figure 4-31* disappeared when the samples were subject to mild heat treatment at 400°C , indication of a meta-stable cubic Bi_2O_3 in the as deposited films from $\text{Bi}(\text{thd})_3$ and $\text{Co}(\text{thd})_2$ is strengthened. If this phase was present in the as-deposited films, it most likely formed the sillenite phase during heat treatment. The deposition of this meta stable cubic phase is also observed in the as deposited films of Bi_2O_3 by MOCVD from BiPh_3/O_2 at 450°C [127]. Confirming that this phase can be obtained at temperatures lower than 650°C , which is the temperature where this cubic phase is formed from $\alpha\text{-Bi}_2\text{O}_3$ powder under vacuum conditions.

In addition as both films contained almost a 1:1 ratio between bismuth and cobalt, by reference to the phase diagram given in *Figure 1-3* in section 1.2.1 on page 6 and that the suggested formed sillenite phase $\text{Bi}_{3.43}\text{Co}_{0.57}\text{O}_{5.90}$ has a surplus of bismuth compared to cobalt, it is likely that the peaks labeled as both Co_3O_4 and $\alpha\text{-Bi}_2\text{O}_3$ in *Figure 4-32* are caused by Co_3O_4 .

6 Conclusion

The main goal of this work was to deposit the multiferroic material BiCoO_3 . In order to achieve this goal a number of precursor pairs for both cobalt and bismuth were investigated for ALD growth. The motivation has been to find a mutual compatible precursor pair for deposition of both cobalt and bismuth. The precursor pairs under investigation have been $\text{Co}(\text{thd})_2/\text{O}_3$, $\text{Co}(\text{thd})_2/\text{H}_2\text{O}$, $\text{Co}(\text{thd})_3/\text{O}_3$, $\text{Co}(\text{thd})_3/\text{H}_2\text{O}$, $\text{Bi}(\text{t-OBu})_3/\text{H}_2\text{O}$, BiPh_3/O_3 , $\text{BiPh}_3/\text{H}_2\text{O}$ and $\text{Bi}(\text{thd})_3/\text{H}_2\text{O}$.

An ALD temperature window was found for depositions in the range 162 – 259 °C, with an average growth rate of 6 pm/cycle for the novel $\text{Co}(\text{thd})_3/\text{O}_3$ precursor combination. The deposited films consisted of Co_3O_4 , where a (111)-orientation was found on Si(111) at 186 °C. No deposited film could be detected from the $\text{Co}(\text{thd})_3/\text{H}_2\text{O}$ precursor combination at the investigated temperatures 186 and 235 °C.

For the $\text{Co}(\text{thd})_2/\text{H}_2\text{O}$ precursor combination, an ALD temperature window was found in the range 186 – 259 °C, which showed a step-like growth rate of 3.2 pm/cycle at 186 – 210 °C, while a growth rate of 5.4 pm/cycle was obtained in the range 235 – 250 °C. For the lower temperature range single phase films of CoO was obtained, while a mixture of Co_3O_4 and CoO was deposited in the higher temperature range.

$\text{Bi}(\text{t-OBu})_3$ proved not to be suitable as a bismuth precursor in an ALD process, as it was found to decompose already at 65 °C.

BiPh_3/O_3 and $\text{BiPh}_3/\text{H}_2\text{O}$ does not yield films of bismuth oxide, however, $\text{BiPh}_3/\text{H}_2\text{O}$ may be used for deposition in a limited range of the Bi-Co-O

system with ALD. It was not possible to obtain high enough concentrations of bismuth to deposit the desired phase BiCoO_3 . The highest obtained Bi content was 22.8 at.%, with respect to metal content, at 175 °C.

A new phase of the $\text{Bi}(\text{thd})_3$ precursor which proves suitable for ALD depositions has been identified in this work. An ALD temperature window was found in the temperature range 206 – 283 °C for the $\text{Bi}(\text{thd})_3/\text{H}_2\text{O}$ process. Uniform films were deposited with an average growth rate of 16 pm/cycle in the whole range. Crystalline films of $\alpha\text{-Bi}_2\text{O}_3$ has for the first time been deposited with ALD. The films showed a (012)-preferred orientation on Si(111) for depositions in the range 235 – 283 °C.

The application of $\text{Bi}(\text{thd})_3$ for deposition in the Bi-Co-O system yielded varying results. Indications for that the $\text{Bi}(\text{thd})_3$ precursor etches the Co_3O_4 surface was found and a likely mechanism for the etching process has been suggested.

Heat treatment of thin films with a composition near 50:50 at.% Bi:Co resulted in multiple phases where none was BiCoO_3 .

7 Further work

There is still a lot of interesting and exciting work to be carried out on the different systems investigated in this work.

The step-like growth, observed for the $\text{Co}(\text{thd})_3/\text{O}_3$ system, as a function of the O_3 pulse length needs a closer examination. An indication whether the proposed mechanism is likely or not can be obtained relatively easy by investigating pulse lengths of i.e. 4-5 and 7 seconds. In addition, analysis of the exhaust gas of the process by mass spectrometry (MS) might shed some new light on the mechanism involved. This system should also be investigated further with respect to deposited crystal phases and compared to the similar $\text{Co}(\text{thd})_2/\text{O}_3$ system.

The new $\text{Co}(\text{thd})_2/\text{H}_2\text{O}$ precursor combination should be investigated further with respect to crystallinity and orientation of the deposited films. The enormous increase in growth rate observed at 162 °C should be reproduced and verified as ALD growth. In addition, further investigations of the uncharacteristic ALD temperature window should be carried out to verify the mechanism behind the observed stepped growth. To verify the suggested mechanism in this work an in-situ QCM measurement should be carried out at 210 °C. An increase in mass should be expected observed after each cycle, as more oxygen is needed when CoO transform into Co_3O_4 .

In order to obtain better knowledge of the $\text{Bi}(\text{thd})_3$ chemistry, the structure of the newly identified phase of $\text{Bi}(\text{thd})_3$ should be solved. The easiest way would probably be to obtain single crystals for XRD analysis by recrystalliation from dry hexane or by sublimation. The crystals would have to be encapsulated in i.e. epoxy in order to be protected from air, and

cooling should be applied during the measurement in order to avoid melting. If the obtained phase is shown to be anhydrous, in situ QCM-measurements should be carried out in order to measure if this precursor show self-limiting growth or not.

Further studies should also be carried out on reacting different $\text{Bi}(\text{thd})_3$ phases containing crystal water with tetraglyme. By performing capillary XRD analysis of the oily sample cooled by i.e. liquid nitrogen, it might be possible to solve the crystal structure. In addition the sublimation temperature and thermal stability of the oily product should also be carried out. If these results are promising, the compound should be tested for use in the ALD process. Given the ALD behavior is satisfactory, a new and less tiresome synthesis of $\text{Bi}(\text{thd})_3$ might be developed. The unpatented and simple reaction between BiPh_3 and $\text{H}(\text{thd})$ in hexane, which is shown to be able to yield monomeric phases with crystal water[121], could then be used and the resulting crystal water removed with tetraglyme.

The suggested etching reaction observed from $\text{Bi}(\text{thd})_3$ can be studied further by simultaneously carry out an in-situ QCM analysis while the products released through the exhaust is investigated by MS. In addition it would also be interesting to verify if a Co_3O_4 surface, deposited from $\text{Co}(\text{thd})_2$ and H_2O , is stable towards $\text{Bi}(\text{thd})_3$. In addition, the $\text{Bi}(\text{thd})_3/\text{O}_3$ process should be investigated for ALD growth. If ALD growth is obtained it would be interesting to examine whether this precursor combination also causes etching of Co_3O_4 surfaces when deposited in the Bi-Co-O system.

There exists yet another bismuth precursor which could also be interesting for depositions by ALD, namely $\text{Bi}(\text{Me}_2(\text{dmp}))$. In this work, it was chosen not to proceed with the synthesis and characterization of this precursor due

to the limited timeframe. As mentioned before, this precursor is reported to be stable towards water, liquid at room temperature with a high vapor pressure and that it decomposes at 230 °C [96, 100]. The decomposing temperature is a bit low, however, it is not extremely low and in the same temperature range as BiPh₃. XPS measurements of the deposited films by MOCVD also showed no evidence of nitrogen contamination in the deposited films [96, 100].

The observed huge increase in growth rate of the Co(thd)₂/H₂O precursor combination, and why only Bi₂O₃ was detected on the single crystal substrates when the BiPh₃/H₂O process was added, should be reproduced and investigated further. A simultaneous in-situ QCM and MS measurement should shed some light on a possible mechanism.

Finally, if control is obtained over the Bi-Co-O system by ALD, the phases deposited at various compositions at different temperatures should be investigated closer. In addition, the ultimate goal would be to obtain the multiferroic phase BiCoO₃ by utilizing strain engineering on a suitable single crystal substrate. As it is shown previously in the literature, that utilizing epitaxial thin film growth can give access to high pressure and temperature phases, that are not easily accessible by traditional bulk synthesis techniques [61].

If a high purity sample of BiCoO₃ is obtained, the magnetic and ferroelectric properties should be investigated. This would hopefully give an answer to whether this material exhibits the proposed exciting and novel coupling between the magnetic and the ferroelectric properties.

Another aspect which could also prove to be extremely interesting would be to investigate whether any of the physical properties of this material can be altered or improved by varying the thickness of the deposited films.

8 References

1. Østreng, E., *Tynne filmer av multiferroisk BiFeO₃*, in *Chemistry Department*. 2009, University of Oslo: Oslo.
2. Hill, N.A., *Why are there so few magnetic ferroelectrics?* J. Phys. Chem. B, 2000. **104**(29): p. 6694-6709.
3. Fiebig, M., *Revival of the magnetoelectric effect*. J. Phys. D: Appl. Phys, 2005. **38**(8): p. R123-R152.
4. Lottermoser, T., et al., *Magnetic phase control by an electric field*. Nature, 2004. **430**(6999): p. 541-544.
5. Kimura, T., et al., *Magnetic control of ferroelectric polarization*. Nature, 2003. **426**(6962): p. 55-58.
6. Hur, N., et al., *Electric polarization reversal and memory in a multiferroic material induced by magnetic fields*. Nature, 2004. **429**(6990): p. 392-395.
7. Ikeda, N., et al., *Ferroelectricity from iron valence ordering in the charge-frustrated system LuFe₂O₄*. Nature, 2005. **436**(7054): p. 1136-1138.
8. Schuisky, M., et al., *Atomic layer CVD in the Bi-Ti-O system*. Chemical Vapor Deposition, 2000. **6**(3): p. 139-145.
9. Vehkamäki, M., et al., *Bismuth precursors for atomic layer deposition of bismuth-containing oxide films*. Journal of Materials Chemistry, 2004. **14**(21): p. 3191-3197.
10. Vehkamäki, M., et al., *Atomic layer deposition of ferroelectric bismuth titanate Bi₄Ti₃O₁₂ thin films*. Chem. Mater, 2006. **18**(16): p. 3883-3888.
11. Harjuoja, J., et al., *Crystallization of bismuth titanate and bismuth silicate grown as thin films by atomic layer deposition*. Journal of Crystal Growth, 2006. **286**(2): p. 376-383.
12. Klepper, K.B., O. Nilsen, and H. Fjellvåg, *Epitaxial growth of cobalt oxide by atomic layer deposition*. Journal of Crystal Growth, 2007. **307**(2): p. 457-465.
13. Klepper, K.B., *Growth of thin films of Co₃O₄ by atomic layer deposition*. Thin Solid Films, 2007. **515**: p. 7772-7781.
14. Klepper, K.B., *Tynne filmer av Co₃O₄ framstilt med ALCVD*, in *Chemistry Department*. 2005, University of Oslo: Oslo.
15. Lie, M., et al., *Growth of iron cobalt oxides by atomic layer deposition*. Dalton Transactions, 2008. **2008**(2): p. 253-259.
16. Vanderah, T.A., et al., *Phase Formation and Properties in the System Bi₂O₃: 2CoO_{1-x}: Nb₂O₅*. EUROPEAN JOURNAL OF INORGANIC CHEMISTRY, 2006. **2006**(23): p. 4908.

17. Yasui, S., et al., *Crystal structure and electrical properties of {100}-oriented epitaxial BiCoO₃-BiFeO₃ films grown by metalorganic chemical vapor deposition*. Japanese Journal of Applied Physics, 2008. **47**(9): p. 7582-7585.
18. Tomashpol'Skii, Y.Y., E.V. Zubova, and K.P. Bordina, *XRay investigation of new perovskites formed at high pressures*. Soviet Phys Crystallography, 1969. **13**(6): p. 859.
19. Vasudevan, S., et al., *Studies on BiCoO₃ and BiCo_{1-x}Fe_xO₃*. Mater. Res. Bull, 1979. **14**: p. 451.
20. Rozaj-Brvar, A., M. Trontely, and D. Kolar, *The Bi₂₄CoO₃₇ Compound and the Bi₂O₃-CoO System*. J. Less-Common Met., 1979. **68**(1): p. 7-14.
21. Ramanan, A., J. Gopalakrishnan, and C.N.R. Rao, *Ternary bismuth oxides Bi_{26-x}M_xO_{40-y} (M = Mg, Al, Co and Ni) related to [alpha] - Bi₂O₃*. Materials Research Bulletin, 1981. **16**(2): p. 169-174.
22. Dance, J.-M., et al., *Etude par rpe du fer trivalent et du cobalt trivalent dans des phases de structure sillenite*. Materials Research Bulletin, 1982. **17**(4): p. 473-479.
23. Gorashchenko N.G., K.Z.S., Maier A.A., and Balashov V.A., *Abstracts of Papers*. VI Vsesoyuznaya konferentsiya po rostu kristallov (VI All-Union Conf. on Crystal Growth), Tsakhkadzor, p.84, 1985.
24. Gopalakrishnan, J. *Synthesis and Structure of Some Interesting Oxides of Bismuth*. 1986.
25. MARY, T., et al., *Crystal structure of Bi_{12.7}Co_{0.3}O_{19.35}*. European journal of solid state and inorganic chemistry, 1996. **33**(4): p. 285-293.
26. Kargin, Y., V. Voevodskii, and V. Skorikov, *Reactions of Bi~ 2O~ 3 with Cobalt Oxides*. RUSSIAN JOURNAL OF INORGANIC CHEMISTRY C/C OF ZHURNAL NEORGANICHESKOI KHIMII, 1998. **43**: p. 1946-1949.
27. Belik, A.A., et al., *Neutron powder diffraction study on the crystal and magnetic structures of BiCoO₃*. Chemistry of Materials, 2006. **18**(3): p. 798-803.
28. Zhang, Y., et al., *Synthesis and magnetic properties of nanoporous Co₃O₄ nanoflowers*. Microporous and Mesoporous Materials, 2008. **114**(1-3): p. 257-261.
29. T. Oguchi, T.S., and Y. Uratani, *First-Principles Study of Multiferroic Oxides*. ISSP Activity Report, 2007: p. 49-50.
30. Azuma, M., et al., *Rhombohedral-Tetragonal Phase Boundary with High Curie Temperature in (1-x) BiCoO₃-xBiFeO₃ Solid Solution*. Japanese Journal of Applied Physics, 2008. **47**(9): p. 7579.

-
31. Yasui, S., et al., *Crystal structure analysis of epitaxial BiFeO₃-BiCoO₃ solid solution films grown by metalorganic chemical vapor deposition*. Japanese Journal of Applied Physics Part 1-Regular Papers Brief Communications & Review Papers, 2007. **46**(10B): p. 6948-6951.
 32. Seim, H., et al., *Growth of LaCoO₃ thin films from β -diketonate precursors*. Applied Surface Science, 1997. **112**: p. 243-250.
 33. Rooth, M., E. Lindahl, and A. Harsta, *Atomic Layer Deposition of Co₃O₄ Thin Films Using a CoI₂/O₂ Precursor Combination*. CHEMICAL VAPOR DEPOSITION-WEINHEIM-, 2006. **12**(4): p. 209.
 34. Backman, L., et al., *Effect of support and calcination on the properties of cobalt catalysts prepared by gas phase deposition*. Applied Catalysis A, General, 2000. **191**(1-2): p. 55-68.
 35. Rautiainen, A., et al., *Preparation of silica-supported cobalt catalysts through chemisorption of cobalt (ii) and cobalt (iii) acetylacetonate*. Physical Chemistry Chemical Physics, 2002. **4**(11): p. 2466-2472.
 36. Puurunen, R., T. Zeelie, and A. Krause, *Cobalt (III) Acetylacetonate Chemisorbed on Aluminum-Nitride-Modified Silica: Characteristics and Hydroformylation Activity*. Catalysis Letters, 2002. **83**(1): p. 27-32.
 37. Milt, V., M. Ulla, and E. Lombardo, *Cobalt-containing catalysts for the high-temperature combustion of methane*. Catalysis Letters, 2000. **65**(1): p. 67-73.
 38. Backman, L., et al., *A novel Co/SiO₂ catalyst for hydrogenation*. Catalysis Today, 1998. **43**(1-2): p. 11-19.
 39. Backman, L., et al., *Characterisation of Co/SiO₂ catalysts prepared from Co (acac) ₃ by gas phase deposition*. Applied Catalysis A, General, 2001. **208**(1-2): p. 223-234.
 40. Milt, V., M. Ulla, and E. Lombardo, *Zirconia-Supported Cobalt as a Catalyst for Methane Combustion*. Journal of Catalysis, 2001. **200**(2): p. 241-249.
 41. Milt, V., E. Lombardo, and M. Ulla, *Stability of cobalt supported on ZrO₂ catalysts for methane combustion*. Applied Catalysis B, Environmental, 2002. **37**(1): p. 63-73.
 42. Lim, B., A. Rahtu, and R. Gordon, *Atomic layer deposition of transition metals*. Nature Materials, 2003. **2**(11): p. 749-754.
 43. Terajima, H. and S. Fujiwara. *Surface Diffusion Distance of Bi Adatoms on Mica Surface*. 1974.
 44. Hwang, G.W., et al., *Dielectric Science and Materials-Characteristics of Amorphous Bi₂Ti₂O₇ Thin Films Grown by*
-

-
- Atomic layer Deposition for Memory Capacitor Applications*. Journal of the Electrochemical Society, 2006. **153**(1): p. 20.
45. Cho, Y.J., et al., *Atomic Layer Deposition (ALD) of Bismuth Titanium Oxide Thin Films Using Direct Liquid Injection (DLI) Method*. Integrated Ferroelectrics, 2003. **59**(1): p. 1483-1489.
 46. Jain, R., V. Gupta, and K. Sreenivas, *Sintering characteristics and properties of sol gel derived Sr_{0.8}Bi_{2.4}Ta_{2.0}O₉ ceramics*. Materials Science & Engineering B, 2000. **78**(2-3): p. 63-69.
 47. Harjuoja, J., et al., *New approach to the ALD of bismuth silicates: Bi(CH₂SiMe₃)₃ acting as a precursor for both bismuth and silicon*. Chemical Vapor Deposition, 2005. **11**(8-9): p. 362-367.
 48. Ravindran, P., et al., *Magnetic-instability-induced giant magnetoelectric coupling*. Advanced Materials, 2008. **20**(7): p. 1353-+.
 49. Uratani, Y., et al., *First-Principles Predictions of Giant Electric Polarization*. JAPANESE JOURNAL OF APPLIED PHYSICS PART 1 REGULAR PAPERS SHORT NOTES AND REVIEW PAPERS, 2005. **44**(9B): p. 7130.
 50. Cai, M.Q., et al., *First-principles study of structural, electronic, and multiferroic properties in BiCoO₃*. Journal of Chemical Physics, 2007. **126**(15): p. -.
 51. Tilley, R., *Understanding solids*. 2004: Wiley. 593.
 52. Vonsovskii, S.V., *Magnetism*. 1974.
 53. Ben G. Streetman, S.K.B., *Solid state electronic devices*. 2006: Pearson. 581.
 54. Bussmann-Holder, A. and H. Böttner, *Ferroelectricity in oxides*. 1992.
 55. Cohen, R.E., *Origin of ferroelectricity in perovskite oxides*. 1992.
 56. Hill, N.A., P. Battig, and C. Daul, *First principles search for multiferroism in BiCrO₃*. J. Phys. Chem. B, 2002. **106**(13): p. 3383-3388.
 57. Hill, N.A. and K.M. Rabe, *First-principles investigation of ferromagnetism and ferroelectricity in bismuth manganite*. Physical Review B, 1999. **59**(13): p. 8759-8769.
 58. Neaton, J.B., et al., *First-principles study of spontaneous polarization in multiferroic BiFeO₃*. Physical Review B, 2005. **71**(1): p. 14113.
 59. Ramesh, R. and N.A. Spaldin, *Multiferroics: progress and prospects in thin films*. Nature Materials, 2007. **6**(1): p. 21-29.
 60. Eerenstein, W., N.D. Mathur, and J.F. Scott, *Multiferroic and magnetoelectric materials*. Nature, 2006. **442**(7104): p. 759-765.
-

-
61. Martin, L.W., et al., *Multiferroics and magnetoelectrics: thin films and nanostructures*. Journal of Physics: Condensed Matter, 2008. **20**(43): p. 434220.
 62. Hill, N.A., *Density functional studies of multiferroic magnetoelectrics*. Annual Review of Materials Research, 2002. **32**: p. 1-37.
 63. Spaldin, N.A., *Magnetic Materials, Fundamentals and Device Applications*. 2003: Cambridge University Press.
 64. Suntola, T. and J. Hyvarinen, *Atomic layer epitaxy*. Annual Review of Materials Science, 1985. **15**(1): p. 177-195.
 65. Suntola, T., *Thin Solid Films*. 1992.
 66. Suntola, T. and J. Antson, *US Pat.* 1977, NO Patent 4,058,430.
 67. Nishizawa, J., H. Abe, and T. Kurabayashi, *Molecular Layer Epitaxy*. Journal of the Electrochemical Society, 1985. **132**(5): p. 1197-1200.
 68. Usui, A. and H. Sunakawa, *Gaas Atomic Layer Epitaxy by Hydride Vpe*. Japanese Journal of Applied Physics Part 2-Letters, 1986. **25**(3): p. L212-L214.
 69. Suntola, T., *In: Hurle DTJ (ed) Handbook of crystal growth, vol 3*. 1994, Elsevier, Amsterdam.
 70. Ritala, M. and M. Leskela, *Atomic Layer Deposition*, in *Handbook of Thin Film Materials*, H.S. Nalwa, Editor. 2002, Academic Press: San Diego, CA. p. 103-159.
 71. Puurunen, R., *Surface chemistry of atomic layer deposition: A case study for the trimethylaluminum/water process*. Journal of Applied Physics, 2005. **97**: p. 121301.
 72. Ritala, M. and M. Leskelä, *Deposition and processing of thin film materials*. Handbook of Thin Film Materials, 2002. **1**.
 73. O.Nilsen, *Growth of thin films of functional oxides with the ALCVD method*, in *Department of Chemistry, Faculty of Mathematics and Natural Sciences*. 2003, University of Oslo: Norway.
 74. Suntola, T., *Atomic Layer Epitaxy*, ed. M. Simposon. 1990, Glasgow, London: Blackie and Son.
 75. Earnshaw, A. and N. Greenwood, *Chemistry of the Elements*. 1997: Elsevier.
 76. Nilsen, O., H. Fjellvåg, and A. Kjekshus, *Growth of calcium carbonate by the atomic layer chemical vapour deposition technique*. Thin Solid Films, 2004. **450**(2): p. 240-247.
 77. Puurunen, R.L., *Surface chemistry of atomic layer deposition: A case study for the trimethylaluminum/water process*. Journal of Applied Physics, 2005. **97**: p. 121301.

-
78. Foss, S., et al., *Structure determination of MnO₂ films grown on single crystal alpha-Al₂O₃ substrates*. Philosophical Magazine, 2005. **85**(23): p. 2689-2705.
 79. Puurunen, R., et al., *Island growth in the atomic layer deposition of zirconium oxide and aluminum oxide on hydrogen-terminated silicon: Growth mode modeling and transmission electron microscopy*. Journal of Applied Physics, 2004. **96**: p. 4878.
 80. Nilsen, O., et al., *Simulation of growth dynamics in atomic layer deposition. Part I. Amorphous films*. Thin Solid Films, 2007. **515**(11): p. 4527-4537.
 81. Nilsen, O., et al., *Simulation of growth dynamics in atomic layer deposition. Part II. Polycrystalline films from cubic crystallites*. Thin Solid Films, 2007. **515**(11): p. 4538-4549.
 82. Nilsen, O., et al., *Simulation of growth dynamics in atomic layer deposition. Part III. Polycrystalline films from tetragonal crystallites*. Thin Solid Films, 2007. **515**(11): p. 4550-4558.
 83. Nilsen, O., et al., *Effect of substrate on the characteristics of manganese (IV) oxide thin films prepared by atomic layer deposition*. Thin Solid Films, 2004. **468**(1-2): p. 65-74.
 84. Färm, E., et al., *Selective-Area Atomic Layer Deposition Using Poly (methyl methacrylate) Films as Mask Layers*. 2008.
 85. Leskelä, M. and M. Ritala, *ALD precursor chemistry: Evolution and future challenges*. JOURNAL DE PHYSIQUE 4, 1999. **9**: p. 837-852.
 86. Vehkamäki, M., et al., *Process for producing oxide films*. 2003, Google Patents.
 87. Mehrotra, R.C. and A.K. Rai, *Bismuth alkoxides*. Indian J. Chem, 1966. **4**: p. 537.
 88. Tyholt, F., *Chemical solution deposition of piezoelectric Pb(Zr,Ti)O₃ and multiferroic BiFeO₃ thin films*, in *Faculty of Mathematics and Natural Sciences 2008*, University of Oslo: Oslo.
 89. Evans, W.J., J. Hain, and J.W. Ziller, *Synthesis and first X-ray crystal structure of a Bi (OR)₃ complex: tris (2, 6-dimethylphenoxo) bismuth*. Journal of the Chemical Society. Chemical communications, 1989(21): p. 1628-1629.
 90. Massiani, M.C., et al., *Molecular precursors of bismuth oxides;-diketonates and alkoxides. Molecular structure of [Bi₂(2, 1-OC₂H₄OMe)₄(1-OC₂H₄OMe)₂] and of Bi(OSiPh₃)₃(THF)₃*. Polyhedron, 1991. **10**(4-5): p. 437-445.
 91. Haaland, A., et al., *Molecular structure of a monomeric bismuth trisalkoxide by gas electron diffraction*. Acta chemica scandinavica(Copenhagen. 1989), 1993. **47**(10): p. 1043-1045.
-

-
92. Otway, D.J. and W.S. Rees, *Group 2 element -diketonate complexes: synthetic and structural investigations*. Coordination Chemistry Reviews, 2000. **210**(1): p. 279-328.
 93. Kang, S.W. and S.W. Rhee, *Growth of bismuth oxide films by direct liquid injection-metal organic chemical vapor deposition with Bi(tmhd)3 (tmhd: 2, 2, 6, 6-tetramethyl-3, 5-heptanedione)*. Thin Solid Films, 2004. **468**(1-2): p. 79-83.
 94. Jones, A.C., *Molecular design of improved precursors for the MOCVD of electroceramic oxides*. Journal of Materials Chemistry, 2002. **12**(9): p. 2576-2590.
 95. Sanderson, R.T., *A Comparative Study of Methyl Compounds of the Elements*. Journal of the American Chemical Society, 1955. **77**(17): p. 4531-4532.
 96. Furukawa, T., et al., *PROPERTIES OF A NOVEL BISMUTH PERCURSOR FOR MOCVD*. Integrated Ferroelectrics, 2006. **84**(1): p. 197-202.
 97. Aaltonen, T., et al., *Ruthenium thin films grown by atomic layer deposition*. Chemical Vapor Deposition, 2003. **9**(1).
 98. Niinistö, J., et al., *Advanced cyclopentadienyl precursors for atomic layer deposition of ZrO₂ thin films*. Journal of Materials Chemistry, 2008. **18**(28): p. 3385-3390.
 99. Lorberth, J., et al., *Synthesis and crystal structure of EO Fischer's "red crystalline modification of tris-cyclopentadienylbismuth, (1h-C₅H₅)₃Bi"*. Journal of Organometallic Chemistry, 1995. **485**(1-2): p. 149-152.
 100. Furukawa, T., N. Oshima, and H. Funakubo, *Development of a Novel Bismuth Precursor for MOCVD*. Tosoh Research & Technology Review, 2006. **50**: p. 41-44.
 101. Leonard, J., B. Lygo, and G. Procter, *Advanced practical organic chemistry*. 1998: CRC.
 102. Komiya, S., *Synthesis of Organometallic Compounds: A Practical Guide*. 1997: John Wiley and Sons Ltd.
 103. Fukin, G.K., et al., *Crystal and molecular structure of bismuth dipivaloylmethanate*. Russian journal of inorganic chemistry, 1993. **38**(7): p. 1118-1123.
 104. Hammond, G.S., D.C. Nonhebel, and C.H.S. Wu, *Chelates of -Diketones. V. Preparation and Properties of Chelates Containing Stereically Hindered Ligands*. Inorganic Chemistry, 1963. **2**(1): p. 73-76.
 105. Baum, T.H., G. Bhandari, and M. Chappuis, *Anhydrous mononuclear tris (. beta.-diketonate) bismuth compositions for deposition of bismuth-containing films, and method of making the same*. 1999, Google Patents.
-

-
106. Ahmed, M.A.K., et al., *Syntheses, Structures, and Polymorphism of β -Diketonato Complexes-Co (thd) 3 Dedicated to Professor Rudolf Hoppe on the Occasion of his 85th Birthday*. Zeitschrift für anorganische und allgemeine Chemie, 2008. **634**(2).
 107. Flewitt, P.E.J. and R.K. Wild, *Physical methods for materials characterisation*. 2003: Institute of Physics Publishing.
 108. Kittel, C., *Introduction to solid state physics*. 8 ed. 2005: John Wiley & Sons, Inc.
 109. Birkholz, M., *Thin film analysis by x-ray scattering*. 2006: Wiley-VCH.
 110. Johnson, A.W., *Invitation to organic chemistry*. 1999: Jones & Bartlett Publishers.
 111. Uniquant. <http://www.uniquant.com/introduction.html>. [cited 16.03.09].
 112. Butt, H., B. Cappella, and M. Kappl, *Force measurements with the atomic force microscope: Technique, interpretation and applications*. Surface Science Reports, 2005. **59**(1-6): p. 1-152.
 113. Bubert, H. and H. Jenett, *Surface and thin film analysis*. 2002: Wiley-VCH Weinheim.
 114. Nilsen, O., H. Fjellvåg, and A. Kjekshus, *Inexpensive set-up for determination of decomposition temperature for volatile compounds*. Thermochemica Acta, 2003. **404**(1-2): p. 187-192.
 115. Sauerbrey, G., *The use of quartz oscillators for weighing thin layers and for microweighing*. Z. Phys, 1959. **155**: p. 206–222.
 116. Aicha **Elshabini-Riad**, F.D.B., *Thin Film Technology Handbook*. 1997: McGraw-Hill Professional.
 117. Thompson, M., et al., *Thickness-Shear-Mode Acoustic-Wave Sensors in the Liquid-Phase - a Review*. Analyst, 1991. **116**(9): p. 881-890.
 118. Lu, C. and A.W. Czanderna, *Application of Piezoelectric Quartz Crystal Microbalances Amsterdam*. The Netherlands, 1984.
 119. Alnes, M.E., *Syntese av Li-holdige filmer med ALCVD*, in *Department of Chemistry*. 2008, University of Oslo.
 120. Cotton, F.A., et al., *Trapping Tetramethoxyzincate and-cobaltate (II) between Mo²⁴⁺ Units*. Inorg. Chem, 2003. **42**(15): p. 4619-4623.
 121. Armelao, L., et al., *Synthesis, X-ray structure and bonding of tris (2, 2-6, 6-tetramethylheptane-3, 5-dionato) bismuth (III)*. Inorganica Chimica Acta, 1998. **275**: p. 340-348.
 122. Drake, S.R., et al., *Lanthanide -diketonate glyme complexes exhibiting unusual co-ordination modes*. Journal of the Chemical Society. Dalton transactions, 1993(15): p. 2379-2386.
 123. Tang, C.W., C.B. Wang, and S.H. Chien, *Characterization of cobalt oxides studied by FT-IR, Raman, TPR and TG-MS*. Thermochemica Acta, 2008. **473**(1): p. 68-73.
-

-
124. Tsyganova, E.I. and L.M. Dyagileva, *The reactivity of metal -diketonates in the thermal decomposition reaction*. Russian Chemical Reviews, 1996. **65**(4): p. 315-328.
 125. Narang, S.N., N.D. Patel, and V.B. Kartha, *Infrared and Raman Spectral Studies and Normal Modes of α -Bi₂O₃*. J. Mol. Struct, 1994. **327**(1): p. 221–35.
 126. Taylor, P., S. Sunder, and V.J. Lopata, *Structure, spectra, and stability of solid bismuth carbonates*. Canadian Journal of Chemistry, 1984. **62**(12): p. 2863-2873.
 127. Bedoya, C., et al., *MOCVD of Bismuth Oxides: Transport Properties and Deposition Mechanisms of the Bi (C₆H₅)₃ Precursor*. Chem. Mater, 2004. **16**(16): p. 3176-3183.
 128. Thrall, M., et al., *An in situ study of the formation of multiferroic bismuth ferrite using high resolution synchrotron X-ray powder diffraction*. Journal of the European Ceramic Society, 2008. **28**(13): p. 2567-2572.
 129. Kumada, N., et al., *Crystal Structure of Bi₂O₄ with -Sb₂O₄-Type Structure*. Journal of Solid State Chemistry, 1995. **116**(2): p. 281-285.
 130. Kukli, K., M. Ritala, and M. Leskela, *Low-Temperature Deposition of Zirconium Oxide-Based Nanocrystalline Films by Alternate Supply of Zr [OC (CH₃)₃]₄ and H₂O*. Chemical Vapor Deposition, 2000. **6**(6).
 131. Lindahl, E., et al., *Epitaxial NiO (100) and NiO (111) films grown by atomic layer deposition*. Journal of Crystal Growth, 2009. **311**(16): p. 4082-4088.
 132. Lindahl, E., M. Ottosson, and J.O. Carlsson, *Atomic Layer Deposition of NiO by the Ni (thd)₂/H₂O Precursor Combination*. Chem. Vap. Deposition, 2009. **15**: p. 186-191.
 133. Seim, H., et al., *Deposition of LaNiO₃ thin films in an atomic layer epitaxy reactor*. Journal of Materials Chemistry, 1997. **7**(3): p. 449-454.
 134. Aarik, J., et al., *Precursor properties of calcium -diketonate in vapor phase atomic layer epitaxy*. Applied Surface Science, 1994. **75**(1-4): p. 33-38.
 135. Nilsen, O., et al., *Growth of La_{1-x}Ca_xMnO₃ thin films by atomic layer deposition*. Journal of Materials Chemistry, 2007. **17**(15): p. 1466-1475.
 136. Roine, A., *HSC Chemistry® for Windows 4.1 Chemical Reaction and Equilibrium Software with Extensive Thermochemical Database*. Outokumpu Research OY, Pori, Finland, 1997.

137. Kukli, K., et al., *Deposition of lanthanum sulfide thin films by atomic layer epitaxy*. Journal of Alloys and Compounds, 1998. **275**: p. 10-14.
138. Drake, S.R., et al., *The synthesis and X-ray structure characterisation of the volatile complexes [Sr (thd) 2 {Me (OCH 2 CH 2) 3 OMe}] and [Sr 2 (thd) 4 {Me (OCH 2 CH 2) 2 OMe} 2 (μ-H 2 O)](Hthd= 1, 1, 1, 6, 6, 6-hexamethylheptane-2, 4-dione)*. Journal of the Chemical Society, Chemical Communications, 1993. **1993**(5): p. 478-480.
139. Aarik, J., et al., *In situ study of a strontium -diketonate precursor for thin-film growth by atomic layer epitaxy*. Journal of Materials Chemistry, 1994. **4**(8): p. 1239-1244.
140. Rousseau, F., et al., *Low-temperature dry etching of metal oxides and ZnS via formation of volatile metal -diketonate complexes*. Journal of Materials Chemistry, 1992. **2**(8): p. 893-894.

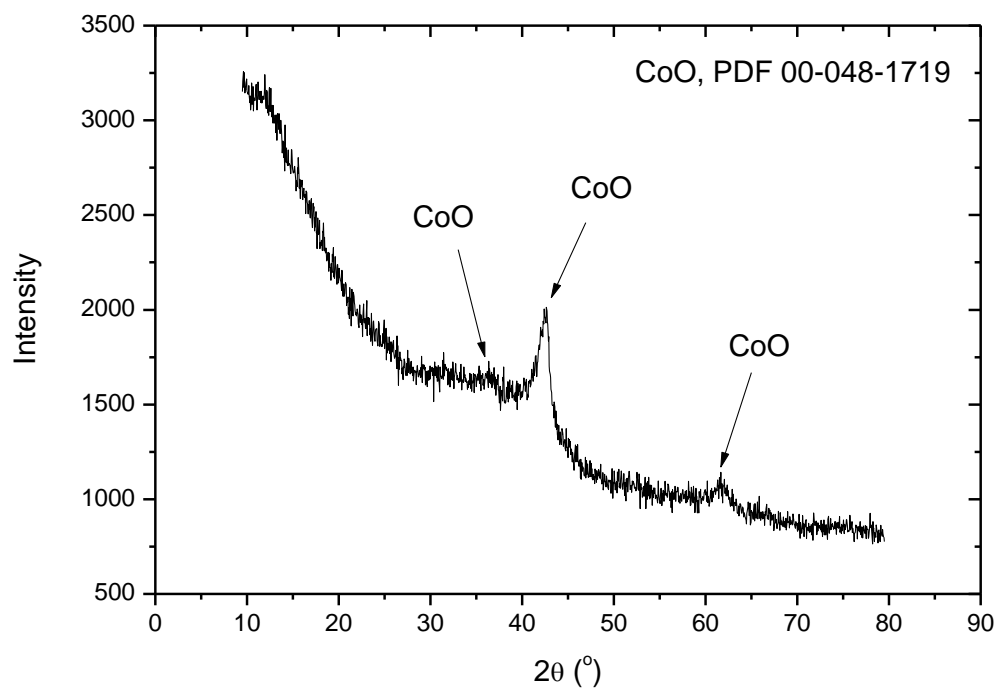
9 Appendix

9.1 Bi(thd)₃ synthesis sample names

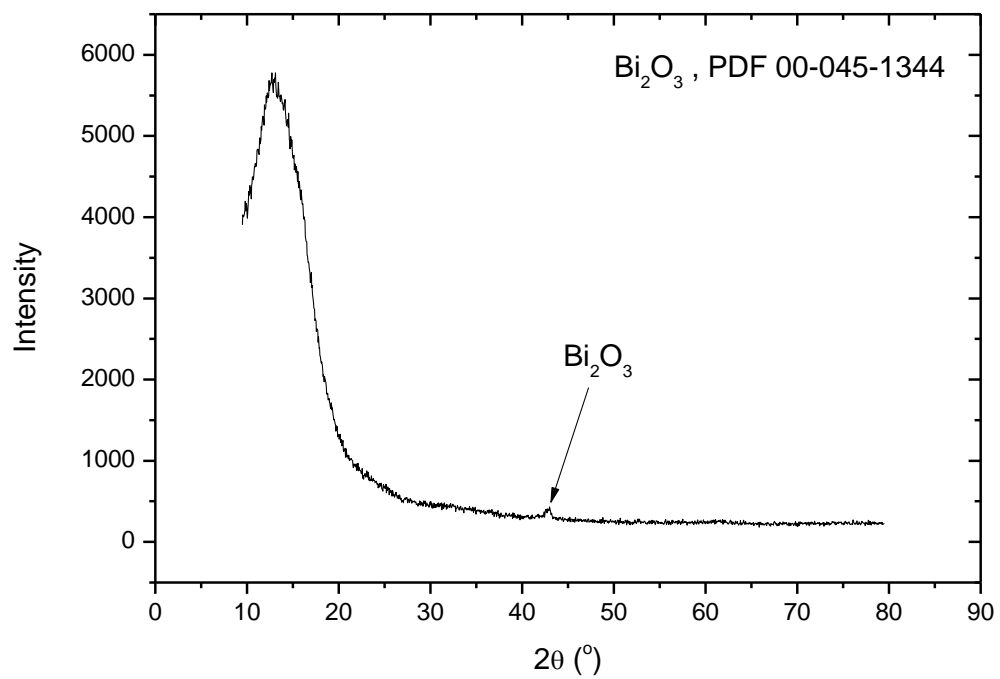
| Abbreviations used for Bi(thd)₃ compounds synthesized in this work | |
|--|-----------------------------------|
| Labeld in this thesis | Name used during this work |
| A | EØ_Bithd_290908 |
| B | KBG_Bithd_200109 |
| C | KBG_Bithd_120209 |
| D | EØ_Bithd_240209 |
| E | KBG_Bithd_250809 |

9.2 KBG1117

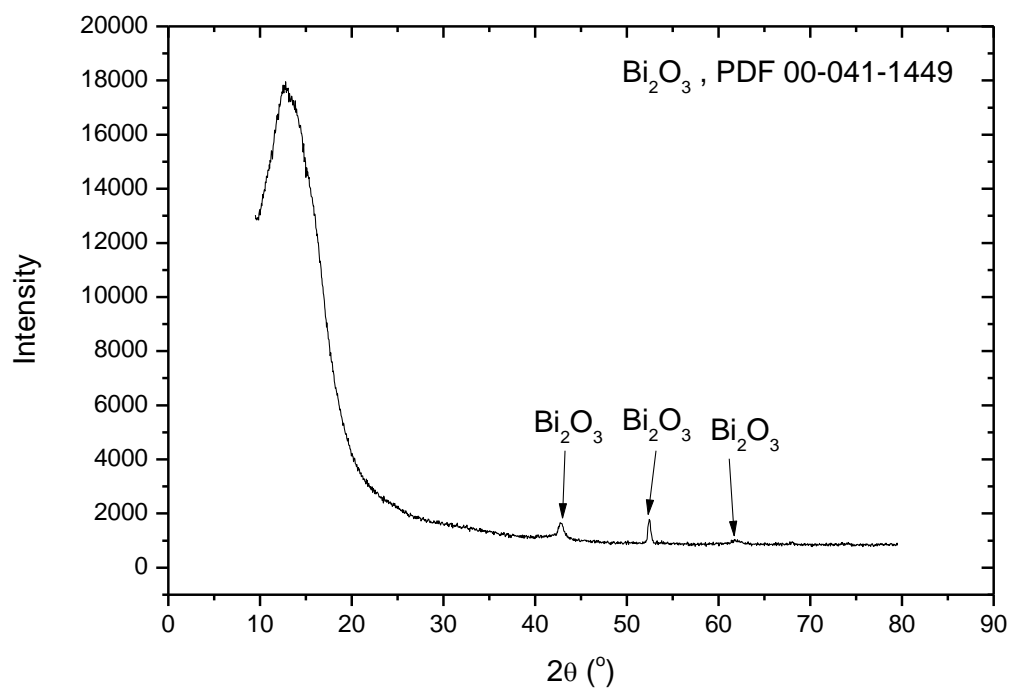
GIXRD on Si(111):



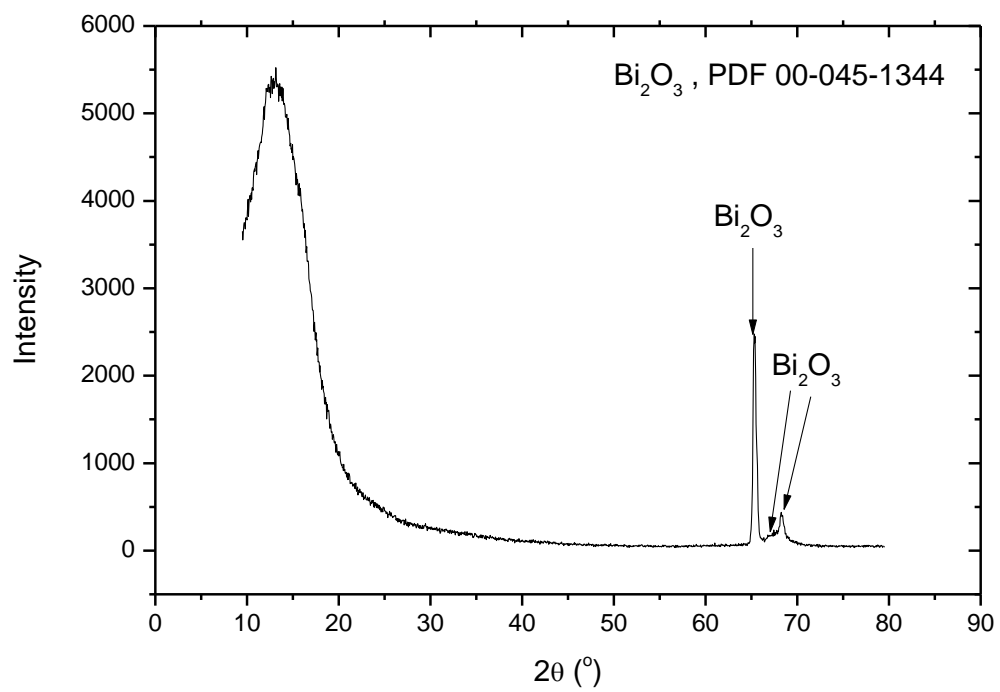
MgO(100):



SrTiO₃(100):



$\text{Al}_2\text{O}_3(1102)$:



9.3 TEM of KBG1008

Obtained data from TEM:

3 at.% Bi / 97 at.% Co, main phase Co_3O_4

Obtained pictures from TEM:

